A STUDY OF GRAIN REFINEMENT OF AZ91E AND Mg-9 wt.% Al ALLOYS USING ZINC OXIDE

by

Subrata Kumar Saha

Bachelor of Technology (Honours)

Indian Institute of Technology (IIT)-Kharagpur, India, 1996

A thesis
presented to Ryerson University
in partial fulfillment of the
requirements for the degree of

Master of Applied Science

in the Program of
Mechanical and Industrial Engineering

Toronto, Ontario, Canada, 2014

© Subrata Kumar Saha 2014

Author's Declaration

I hereby declare that I am the sole author of this thesis. This is a true copy of the thesis, including any required final revisions, as accepted by my examiners.

I authorize Ryerson University to lend this thesis to other institutions or individuals for the purpose of scholarly research.

I further authorize Ryerson University to reproduce this thesis by photocopying or by other means, in total or in part, at the request of other institutions or individuals for the purpose of scholarly research.

I understand that my thesis may be made electronically available to the public.

Abstract

A STUDY OF GRAIN REFINEMENT OF AZ91E AND Mg-9 wt.% Al ALLOYS USING ZINC OXIDE

Master of Applied Science, 2014
Subrata Kumar Saha

Mechanical and Industrial Engineering
Ryerson University

Grain refinement is a proven method to improve mechanical properties of Mg alloys. In this research, the influence of ZnO on the microstructure of selected magnesium alloys was investigated. For graphite mold casting with an addition of 0.75 wt.% ZnO, the grain size of the AZ91E alloy decreased from 217 μm to 108 μm. For the binary alloy (Mg-9 wt.% Al), the grain size reduced from 288 μm to 93 μm with an addition of 3 wt.% ZnO. No significant fading of ZnO grain refiner was observed for both the alloys.

In permanent mold casting process, with an addition of 0.5 wt.% ZnO, the grain size of the AZ91E alloy decreased from 133 μm to 79 μm with significant improvements in mechanical properties. Cleavage type fracture was dominant in the base alloy while alloys refined with 0.5 wt.% ZnO showed more quasi-cleavage type fracture.

Acknowledgements

Dedication

To Subhra, Sulagna and Sucheta

-my love, my dream

Table of Contents

List of Tables

List of Figures

List of Appendices

Nomenclature

A. English

c_0	Initial Concentration of Alloy	wt.%
c_{oi}	Initial Concentration of Element i	wt.%
d	Average Grain Size	μm
D_l	Diffusion Coefficient of the Solute in the Liquid	m^2/sec
EMV	Electromagnetic Vibration	
ΔG	Free Energy of Formation	cal
ΔG_T	Total Free Energy Change	J
G_l	Temperature Gradient in the Liquid Ahead of Solid-Liquid Interface	K/m
ΔG_v	Free Energy Change per Unit Volume	J/m^3
GRF	Growth Restriction Factor	K
ΔH	Heat of Formation	cal
H_f	Latent Heat of Fusion per Unit Volume	J/m^3
HRE	Hardness, Rockwell E	
HSC	Hot Tearing Susceptibility Coefficient	
HV	Vickers Hardness	
k	Distribution Coefficient	wt.%/wt.%
k_i	Distribution Coefficient of Element i	wt.%/wt.%
k_y	Stress Concentration Factor	$Nm^{-5/2}$
m_L	Liquidus Slope in Phase Diagram	K/wt.%
m_{li}	Slope of the Liquidus Line of Element i	K/wt.%
M_m	Mass of the Sample	g

M_{m+w}	Mass of Water with Sample	g
OR	Orientation Relationship	
r	Radius of Nucleant	m
r^*	Critical Radius of Nucleant	m
R	Growth Rate of Solid Liquid Interface	m/sec
ΔS	Entropy of Reaction	cal/deg
T	Temperature	˚C
ΔT	Undercooling	˚C
T_E	Equilibrium Solidification Temperature	˚C
T_F	Freezing Temperature	˚C
T_G	Growth Temperature	˚C
T_L	Liquidus Temperature	˚C
T_m	Equilibrium Solidification	K
T_N	Nucleation Temperature	˚C
T_o	Ambient Temperature	˚C
T_S	Solidus Temperature	˚C
UST	Ultrasonic Treatment	

B. Greek

σ_{sl}	Surface Free Energy of Solid-Liquid Interface	J/m^2
σ_{SL}	Surface Free Energy of Substrate-Liquid Interface	J/m^2
σ_{SC}	Surface Free Energy of Substrate-Cluster Interface	J/m^2
σ_{LC}	Surface Free Energy of Liquid-Cluster Interface	J/m^2
θ	Wetting Angle	
σ_y	Yield Strength	MPa
σ_0	Friction Stress (Experimental Constant)	MPa
ρ_s	Theoretical Density of Sample	g/cm^3
ρ_w	Density of Water at Room Temperature	g/cm^3

C. Elements

Mg	Magnesium
Al	Aluminum
Zn	Zinc
RE	Rare earth
Mn	Manganese
Zr	Zirconium
Fe	Iron
Ni	Nickel
Si	Silicon
Sn	Tin
Ca	Calcium
Cu	Copper
Ge	Germanium
Sc	Scandium
Sr	Strontium
Ce	Cerium
Yb	Ytterbium
Y	Yttrium
Pb	Lead
Li	Lithium

Chapter 1: Introduction

The demand for reduced carbon emissions and increased fuel economies has necessitated the need for new light weight materials to be used in automotive and aerospace applications. Magnesium (Mg) which is 85% lighter than iron and 35% lighter than aluminum (Al) is considered as a potential alternative to Al in the automotive industry to reduce component weights and reduce emissions. Magnesium also has a high strength-to-weight ratio and a high impact resistance. The AZ91 series of alloys are the most popular and widely used cast Mg alloys in the industry. However, some of the major drawbacks like their inadequate mechanical properties and poor workability have maintained the use of Mg-Al alloys to a marginal level in comparison to those of Al alloys. Increasing the mechanical properties of Mg-Al alloys will increase their use for more demanding industrial applications.

Improving the mechanical properties of Mg-Al alloys will augment their use for more demanding industrial applications. Grain refinement can significantly improve the mechanical properties of Mg alloys through fine and uniform grain structure, as well as promoting a more uniform distribution of secondary phases [Vinotha et. al., 2009].

Over the past few years, a significant number of publications related to grain refinement of Mg-Al alloys have been produced. Studies suggest that carbon based grain refiners resulted in the most effective of grain refinement of Mg-Al alloys. However, environmental concern related to release of green house gases associated with these refiners has limited their use in the industry. Researchers have found some alternative potential environmentally friendly grain refiners for Mg-Al alloys. In spite of some success with these refiners, there is no universally accepted refiner for Mg-Al alloys that is effective as well as environment friendly. This warrants the development of alternative environmentally friendly effective grain refiners for Mg-Al alloys. In this study, grain refining potential of ZnO in 9 wt.% Al bearing Mg alloys was examined which is an ongoing quest towards improving Mg grain refinement, with cost effective approach.

Objective

The main objective of this study was to specifically examine the effectiveness of ZnO as a potential grain refiner in Mg alloys bearing 9 wt.% Al (AZ91E commercial alloys and Mg-9 wt.% Al binary alloys). In this regard, an extensive study of the influence of the effect of ZnO on the grain size, microstructure, hardness, and tensile properties of the alloys at ambient temperature were carried out. In addition, this study sought to determine the refining mechanism of ZnO in the Mg-Al alloys.

Chapter 2: Theoretical Background and Literature Review

This chapter begins with a discussion on magnesium alloys. Thereafter, there is a discussion of literature relevant to the process and mechanism of grain refinement in these alloys.

2.1 MAGNESIUM AND MAGNESIUM ALLOYS

Sir Humphrey Davy discovered magnesium (Mg) in 1808. It comprises 2.7% of earth's crust and 0.13% of world's ocean water [Avedesian et. al., 1999]. Magnesium is the lightest structural metal and is 85% lighter than iron and 35% lighter than aluminum (Al). Being the lightest structural metal, Mg and its alloys are potential candidates to replace denser metals such as cast iron, steel, copper base alloys and even aluminum alloys in automotive applications [Mordike et. al., 2001]. Magnesium also has a high strength-to-weight ratio and a high impact resistance [Elsayed et. al., 2014]. Magnesium, in its alloyed form with other metals, has the most use in engineering application.

Magnesium is mainly alloyed with Al, zinc (Zn), manganese (Mn), rare earths (RE) and zirconium (Zr) to improve strength or corrosion resistance. A summary of the major effects of common alloying elements in Mg are as follows [Avedesian et. al., 1999]:

(i) Aluminum has the most favourable effect on Mg of all other alloying elements. It improves strengths and hardness, widens freezing range and improves castability. Commercial Mg alloys generally contain up to 10 wt.% of Al.

(ii) Zinc is the second most favourable alloying element next to Al. It helps overcome the corrosive effects of iron and nickel impurities. When combined with Al it improves room temperature strength.

(iii) Iron (Fe) is a harmful impurity in Mg alloys that greatly reduces corrosion resistance even at small concentration. For maximum resistance to corrosion, 0.005% is specified as the upper limit for the Fe content in Mg alloys.

(iv) Manganese improves the salt water resistance of Mg-Al and Mg-Al-Zn alloys by removing Fe. It also slightly increases yield strength.

(v) Nickel (Ni) is another harmful impurity in Mg alloys which greatly reduces corrosion resistance.

(vi)   Silicon (Si) increases fluidity of molten Mg. However, it decreases corrosion resistance in the presence of Fe.

(vii)   Rare earth metals increase the strength of Mg alloys at elevated temperatures. They also reduce weld cracking and porosity in castings as they narrow the freezing range of the alloys.

(viii)   Tin (Sn) increases ductility of Mg alloys and makes it more suitable for hammer forging.

(ix)   Zr is a powerful grain refiner for Mg alloys. However, it cannot be used with the alloys containing Al and Mn as they form stable compounds with these elements and thus removed from solid solution.

Since Al is the most preferred and common alloying element for Mg, Mg alloys can be generally classified in two groups- (i) Al free such as ZE41 and ZK60 and (ii) Al bearing such as AM50, AM60 and AZ91 [StJohn et. al., 2005]. The nomenclature for Mg alloy designations contains letters to identify the alloying elements and numbers to indicate the alloy concentration and will be discussed further in the next section.

2.1.1 ALLOY DESIGNATION

No international system has been developed for Mg alloy designation, but the naming method adopted by American Society for Testing and Materials (ASTM) in 1948 is being widely used. The standard is explained in Table 2.1.1 [ASM Handbook, Vol. 2, 1992].

For example, for the alloy AZ91E-T6, the first part of the designation, AZ, signifies two principal alloying elements are Al and Zn. The second part, 91, gives the rounded off weight percentage of Al and Zn respectively. The third part, E, indicates that this is the fifth alloy containing 9 wt.% Al and 1 wt.% Zn. The fourth part, T6, denotes that alloy is solution treated and artificially aged.

Table 2.1.1 Standard ASTM System for designation of Mg Alloys

[ASM Handbook, Vol. 2, 1992]

First Part	Second Part	Third Part	Fourth Part	
Indicates the two principal alloying elements	Indicates the amount of the two principal alloying elements	Distinguishes between different alloys with the same percentage of the two principal alloying elements.	Indicates condition (temper)	**Description**
Consists of two code letters representing the two main alloying elements arranged in order of decreasing percentage (or alphabetically if percentages are equal)	Consists of two numbers corresponding to rounded-off percentage of the two main alloying elements and arranged in same order as alloy designation in first part.	Consists of a letter of the alphabet assigned in order as composition become standard.	Consists of a letter followed by a number (separated from the third part of the designation by a hyphen).	**Representation**
A-aluminum B-bismuth C-copper D-cadmium E-rare earth F- iron G-magnesium H-thorium K-zirconium L-lithium M-manganese N-nickel P-lead Q-silver R-chromium S-silicon T-tin W-yttrium Y-antimony Z-zinc	Whole numbers	Letters of alphabet except I and O.	F-fabricated O-annealed H10 and H11-slightly strain hardened H23,H24 and H26- strained hardened and partially annealed T4-solution heat treated T5-artificially aged only T6-solution heat treated and artificially aged T8-solution heat treated, cold worked and artificially aged.	**Values**

The primary Mg alloy investigated in this thesis is AZ91E and the next section describes its physical properties and microstructure.

2.1.2 AZ91 Mg ALLOY

The AZ91 series of alloys are the most popular and preferred Mg alloys in the industry as they have the best combination of castability, mechanical strength and ductility [Celotto, 2000]. The density of AZ91 is 1.81 g/cm^3 which is slightly higher than that of pure Mg (1.738 g/cm^3) but much lower than that of pure Al (2.7 g/cm^3) [ASM Handbook, Vol. 2, 1992]. The liquidus and solidus temperatures of this alloy are 598°C and 468°C respectively which results in a very wide freezing range of 130°C and allows the alloys to be highly castable. The cast microstructure of this alloy consists of primary Mg (α-Mg) and intermetallic compound, β-$Mg_{17}Al_{12}$. Optical micrographs of as-cast and heat treated (solution treatment at 400°C for 24 hours and ageing at 200°C for 30 minutes) AZ91 alloy are shown in Fig. 2.1.1 [Suresh et. al., 2009] with levels identifying each phase. The solidification sequence starts with nucleation of α-Mg at 650 - 600°C and at the later stage, eutectic phase, β-$Mg_{17}Al_{12}$ forms at 437°C [Dahle et. al., 2001]. A Mg-Al equilibrium phase diagram is presented in Fig. A.1 (in Appendix-A1). During cooling under still ambient air the $Mg_{17}Al_{12}$ eutectic takes a completely divorced form [Avedesian et. al., 1999].
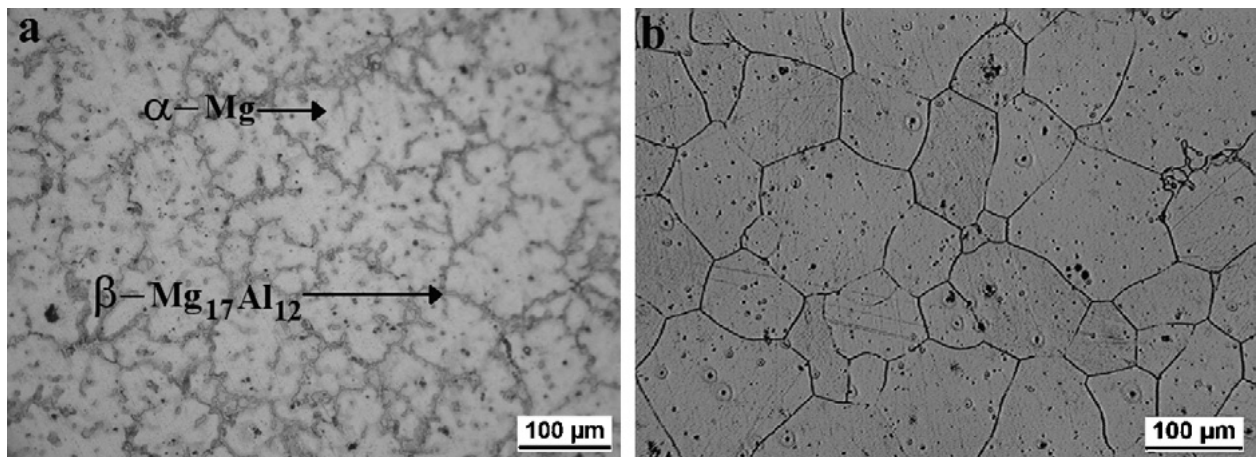
Fig. 2.1.1. Optical micrograph of AZ91 alloy (a) as-cast condition (b) heat treated condition [Suresh et. al., 2009].

However, some of the major drawbacks of Mg alloys (including AZ91E alloy) limiting their use in the automotive industry are their inadequate mechanical properties and poor workability relative to Al alloys [Liu et. al., 2010].

6

Since the AZ91E alloy series is the most popular among Mg alloys, it is important to develop an understanding regarding how to control its grain size and its effect on properties.

2.2 GRAIN REFINEMENT

Grain refinement is one of the best methods to improve the properties of an alloy. Some of the major advantages that can be achieved through grain refinement process are [Robert et. al., 1992]:

    (a) good porosity distribution into small non-interconnected holes

    (b) improvement in machinability

    (c) uniformity in mechanical properties

    (d) better distribution of secondary phase

    (e) improvement in the surface finish of the castings and in the subsequent machining

The larger grain boundary area associated with a smaller grain size effectively increases the yield strength of a material [Gruzleski, 2000] by impeding dislocation motion. The variation of yield strength with grain size follows the classic Hall-Petch relation (Equation 2.2.1) [Dieter, 1986].

$$\sigma_y = \sigma_0 + k_y d^{-\frac{1}{2}} \hspace{4cm} \text{Equation 2.2.1}$$

Where:

σ_y is the yield stress

σ_0 is the friction stress (an experimental constant)

k_y is the stress concentration factor (an experimental constant)

d is the average grain size.

Adding alloying elements during solidification process is one of the most effective ways to grain refine cast metals. However, issues related to understanding solidification of alloys, constitutional undercooling, solute effects and analysis of cooling curves are required for development of effective grain refiners for Mg-Al alloys and are discussed in the following sections.

2.3   SOLIDIFICATION OF ALLOYS

Solidification of alloys is the phase transformation process where non-crystallographic liquid turns into crystallographic solid. For alloys, solidification occurs over a range of temperatures and the temperature profile of an engineering alloy solidifying unidirectionally is schematically shown in Fig. 2.3.1 [Flemings, 1974]. The rate of solidification depends upon a driving force for nucleation, undercooling and heat removal efficiency from the system. The two basic phenomena associated with alloy solidification are nucleation and grain growth.
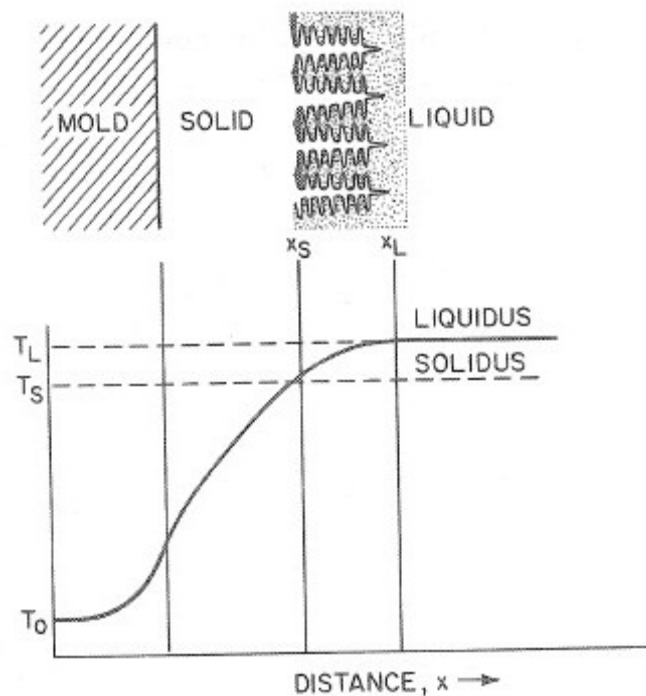
Fig. 2.3.1. Temperature profile of an engineering alloy solidifying unidirecionally [Flemings, 1974].

2.3.1 NUCLEATION

Nucleation is the primary process of solidification and can be defined as the formation of first nanocrystallities from molten material [Askeland et. al., 2010]. As the temperature of the liquid alloy goes below its liquidus temperature, a nucleating particle starts to form within the melt. The driving force associated with this change is the difference between the free energy of liquid and solid, ΔG_T. This energy change is the sum of volume free energy (ΔG_v) and surface free

energy (σ_{sl}) which for spherical nucleating particle of radius r can be written as [Askeland et. al., 2010] :

$$\Delta G_T = \frac{4}{3}\pi r^3 \Delta G_v + 4\pi r^2 \sigma_{sl} \qquad \text{Equation 2.3.1}$$

Where:

$\frac{4}{3}\pi r^3$ is the volume of spherical nucleating particle

$4\pi r^2$ is the surface area of spherical nucleating particle

ΔG_v is volume free energy and σ_{sl} is the surface free energy of the solid liquid interface

Fig. 2.3.2 shows the changes in volume free energy, surface free energy and resultant total free energy as a function of the radius of a nucleating particle, r [Gruzleski, 2000]. The total free energy reaches a maximum when r is equal to a critical value, r^*. Nuclei with $r > r^*$ are stable and begin to grow while those with $r < r^*$ remelt. As the nuclie grow, the total free energy decreases rapidly.
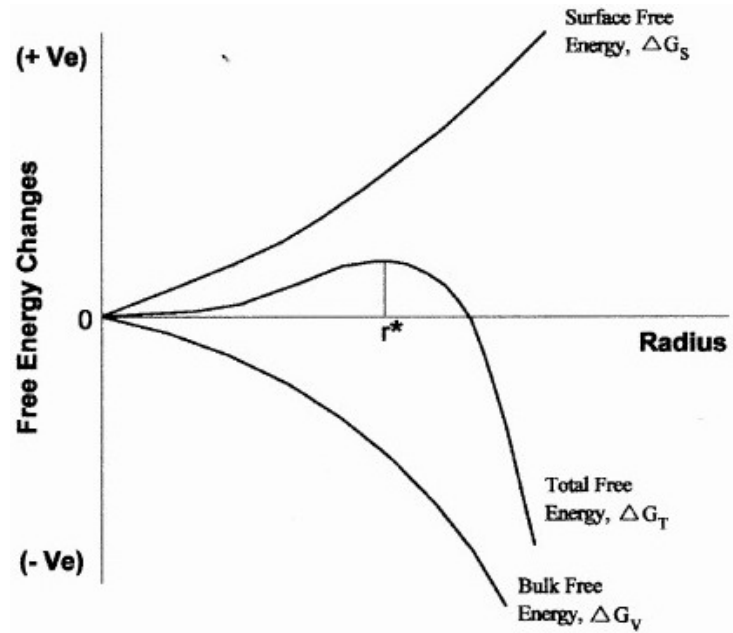
Fig. 2.3.2. Free energy changes of solid-liquid system as a function of radius of nucleating particle, r [Gruzleski, 2000].

Nucleation process can be broadly divided in two categories: homogeneous and heterogeneous nucleation.

2.3.1.1 Homogeneous Nucleation

In homogeneous nucleation, solid forms within its own melt without the aid of foreign materials. Nucleation in this way requires a large amount of driving force because of the relatively large contribution of surface energy to total free energy, ΔG_T, of very small particles [Flemings, 1974]. The critical radius, r^* of a spherical particle undergoing homogeneous nucleation due to undercooling ΔT is given by [Askeland et. al., 2010]:

$$r^* = \frac{2\sigma_{sl}T_m}{\Delta H_f \Delta T}$$

Equation 2.3.2

where ΔT is defined as $\Delta T = T_m - T$ with T_m and T being the melting point and melt temperature respectively. H_f is the latent heat of fusion per unit volume.

From Equation 2.3.2 it is evident that with the increase of undercooling the critical radius required for nucleation decreases. However, homogeneous nucleation rarely occurs in practice due to the presence of melt impurities and the mould wall. Nucleation under these effects is termed heterogeneous nucleation.

2.3.1.2 Heterogeneous Nucleation

Heterogeneous nucleation is nucleation on a pre-existing surface. Metals and most other liquids usually undercool by no more than a few degrees before crystallization begins. This crystallization originates on impurity particles such as nucleating agents or mold walls and thus can avoid very large thermodynamic barrier to homogeneous nucleation [Flemings, 1974]. A solid forming on an impurity needs a smaller increase in surface energy to reach the critical radius, r^*. Heterogeneous nucleation occurs more readily as the amount of undercooling required for r to be equal to r^* is lower than that for homogeneous nucleation and relatively fewer atoms are required to cluster together to form a stable nuclei. Heterogeneous nucleation largely depends upon the contact angle or wetting angle (θ) between the nucleating phase and nucleating surface. Fig. 2.3.3 shows schematic of the formation of a cluster on a substrate [Flemings, 1974].
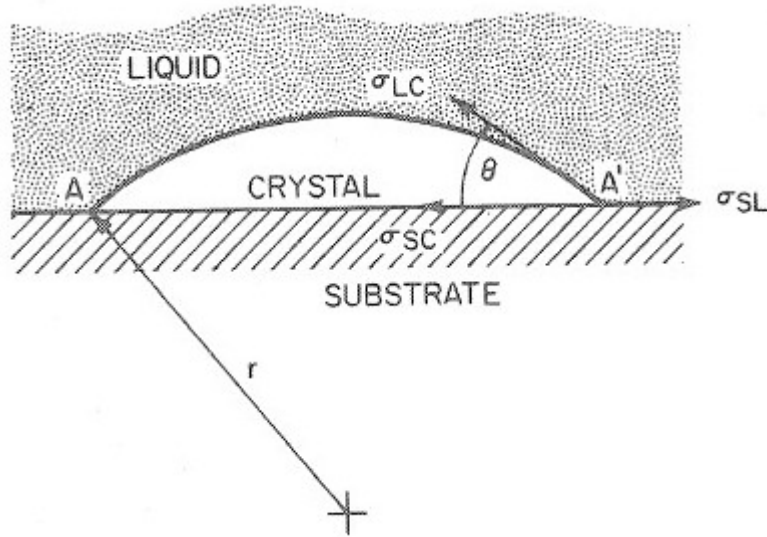
***Fig. 2.3.3. Schematic showing formation of a cluster on a substrate
[Flemings, 1974].***

Where:

σ_{SL} is the surface energy of the substrate-liquid interface

σ_{SC} is the surface energy of the substrate-cluster interface

σ_{LC} is the surface energy of the liquid-cluster interface

θ is the contact (or wetting) angle.

The equilibrium relationship of heterogeneous nucleation of a cluster shown in Fig. 2.3.3 can be modeled by the following equation [Flemings, 1974]:

$$\sigma_{SL} - \sigma_{SC} = \sigma_{LC} \cos \theta \qquad\qquad \text{Equation 2.3.3}$$

Solving equation 2.3.3 for $\cos \theta$ yields:

$$\cos \theta = \frac{\sigma_{SL} - \sigma_{SC}}{\sigma_{LC}} \qquad\qquad \text{Equation 2.3.4}$$

The most favourable condition of heterogeneous nucleation is when $\theta \rightarrow 0°$ or complete wetting occurs. In this condition the largest radius of curvature is created with the fewest number of

atoms. Contact angles exceeding 0˚ result in decreasing states of partial wetting, until θ= 180˚, when the situation has reverted to that of homogeneous nucleation. The various conditions of θ and r are illustrated in Fig. 2.3.4 [Gruzleski, 2000].

Liquid

θ Nucleus

Substrate

$\theta \longrightarrow 0^o$

$\cos \theta \longrightarrow 1$

Liquid

Nucleus

θ

Substrate

θ increases

$\cos \theta$ decreases

Nucleus   Liquid

Substrate

$\theta = 180^o$

$\cos \theta = -1$
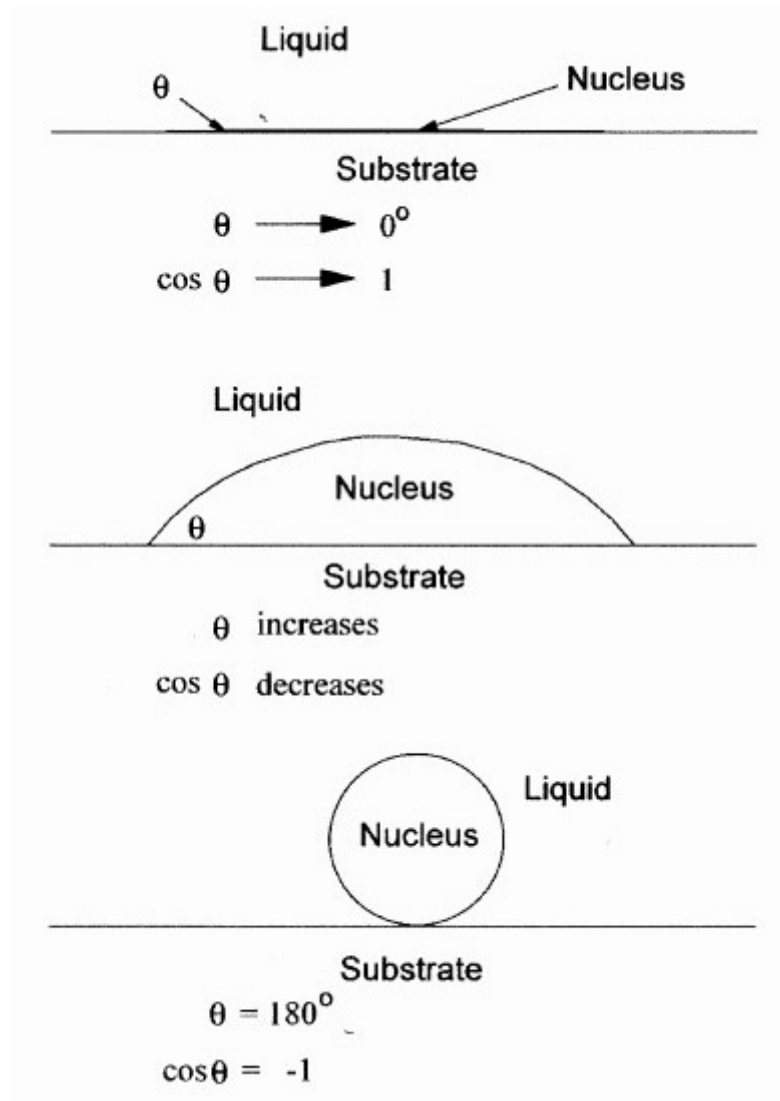
Fig. 2.3.4. Schematic representation showing the relationship between radius of curvature of a spherical cap and contact angle, θ [Gruzleski, 2000].

In commercial foundry practice, inoculants are added to molten alloys to promote heterogeneous nucleation, and thus to produce fine grained castings. From the above discussion it is evident that a good grain refiner (inoculants) should produce a small contact angle between the nucleating

substrate and the growing nucleus. Also, the nucleating substrate needs to be stable in the melt and not undergo other reactions that would destroy the active substrate [Gruzleski, 2000]. Some of the other characteristics of a good grain refiner can be summarized as follows [Murty et. al., 2002]:

1. It should have a higher melting point than the alloy being solidified.
2. It should be able to initiate freezing at very small undercooling.
3. A sufficient numbers of nucleating particles should be uniformly distributed.
4. The nucleating particles should be larger than a critical size, which depends on the undercooling of the melt.

Crystallographic similarity between nucleating agents and alloying elements also plays an important role for effective grain refinement and will be discussed in the subsequent section.

2.3.2 EFFECT OF CRYSTAL STRUCTURE ON GRAIN REFINEMENT

One of the basic requirements of good grain refiner is its crystal structure similarity to the material to be nucleated [Gruzleski, 2000]. The Edge-to-Edge Matching Model is a computer based program used to examine actual atom matching of two compounds of known crystallography across an interface between any two phases [Zhang et. al., 2005]. With the input data of crystal structures, lattice parameters and atom positions, it can predict an orientation relationship (OR) between any two phases (i.e., substrate and matrix). In this model, first closed packed or nearly closed packed rows of atoms between two phases are identified and then parallelism between one such rows in each phase is established. Next, closed packed planes containing these selected rows are identified in both the phases and a pair of these planes (one from each phase) are arranged to meet edge-to-edge. These matching planes are then rotated relative to one another and a value of rotation angle is established, where there is a maximum matching of atom rows in the interface between two phases. From these crystallographic manipulations the resulting OR and interface plane between the two phases can be identified [Kelly et. al., 2006]. Fig. 2.3.5 shows a schematic of the final edge-to-edge matching process between two phases [Kelly et. al., 2006]. Here, $(h_1k_1l_1)_A$ and $(h_1k_1l_1)_B$ planes of phase A and B are matched. These two planes are rotated by an angle φ so that closed packed parallel atom rows $[uvw]_A$ and $[uvw]_B$ of phase A and B, respectively, have a maximum match.
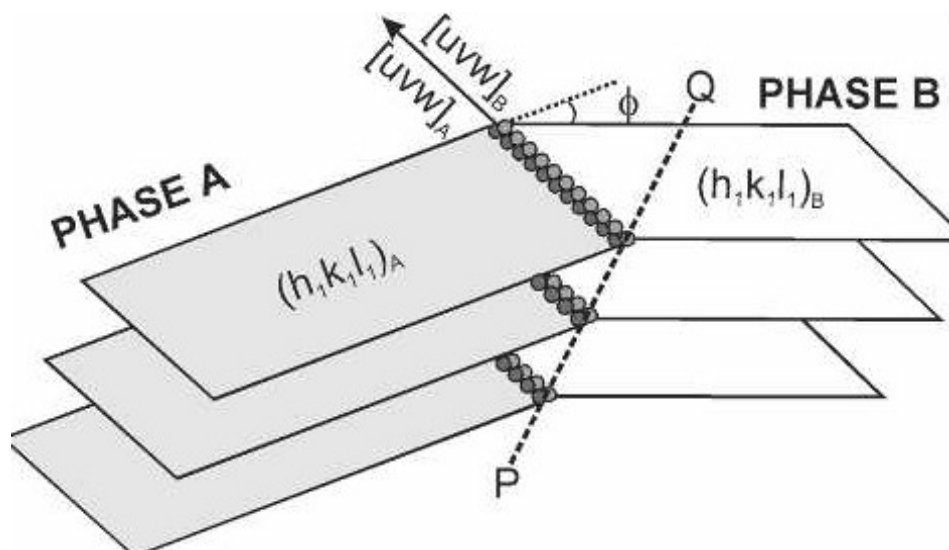
***Fig. 2.3.5. Schematic showing edge-to-edge matching model between two phases
[Kelly et. al., 2006].***

For a substrate to act as an effective nucleant it should have less than 10% inter-atomic misfits along the matching direction and d-value (inter-planer distance) mismatch between matching planes that contains these directions should be 6% or less [Zhang et. al., 2005].

It was found that Al_4C_3 or Al-C-O is the most reasonable mechanism for the grain refinement of Mg alloys through carbon inoculation processes [Qian et. al., 2005] using experimental technique and edge-to-edge model [Zhang et. al., 2005]. This is assumed to be due to crystallographic and lattice parameter similarity between α-Mg and Al-C-O based compounds [Bamberger, 2001]. Also, ZnO is one of the new potential nucleants which have very similar crystallographic structure with α-Mg. Both Mg and ZnO have hexagonal closed packed (HCP) crystal structure. The lattice parameters of Mg are a = 3.2029 Å, c = 5.2000 Å, c/a = 1.6235 and for ZnO are a = 3.2495 Å, c = 5.2069 Å and c/a = 1.602 [Pearson, 1964]. Using edge-to-edge matching model, the interplanar spacing (d-value) mismatch between matching planes and interatomic spacing misfit along matching directions are found to be 1.7 and 0.59% respectively [Fu et. al., 2008] for ZnO and Mg. With such crystallographic similarities, it is expected that ZnO would be an effective nucleant for α-Mg. There is a need to do experimental trials to confirm its performance in Mg alloys.

2.3.3 GRAIN GROWTH

Once nucleation takes place in an alloy, the next phase of solidification is grain growth. Fig. 2.3.6 shows the general grain structure of a casting consisting of an outer chill zone, an intermediate columnar zone and central equiaxed zone [Flemings, 1974]. The chill zone is a narrow brand of randomly oriented grains that occurs at the wall of the molds. As the heat is removed from the casting by the mold material, the grains in the chill zone grow in the direction opposite to that of the heat flow. This thin, elongated column like grains which are perpendicular to the mold wall form columnar zone. An equiaxed zone is frequently formed at the center of the casting. The equiaxed zone contains new, randomly oriented grains that can be promoted by a low pouring temperature, alloying elements or grain refining or inoculating agents [Askeland et. al., 2010]. More often, however, one or another of the zones is absent.

Columnar dendritic growth is the most common form of growth during solidification. In most commercial alloys, a highly branched columnar dendritic morphology can be seen [Flemings, 1974]. A fully developed dendritic structure may have primary, secondary or even higher order branches. Fig. 2.3.7 shows the growth of a dendrite growth in an alloy [Flemings, 1974]. Figures (a) through (d) show a fixed position at various stages of solidification. The growth of arms can be seen during the solidification process. Many smaller arms disappear while larger ones grow.
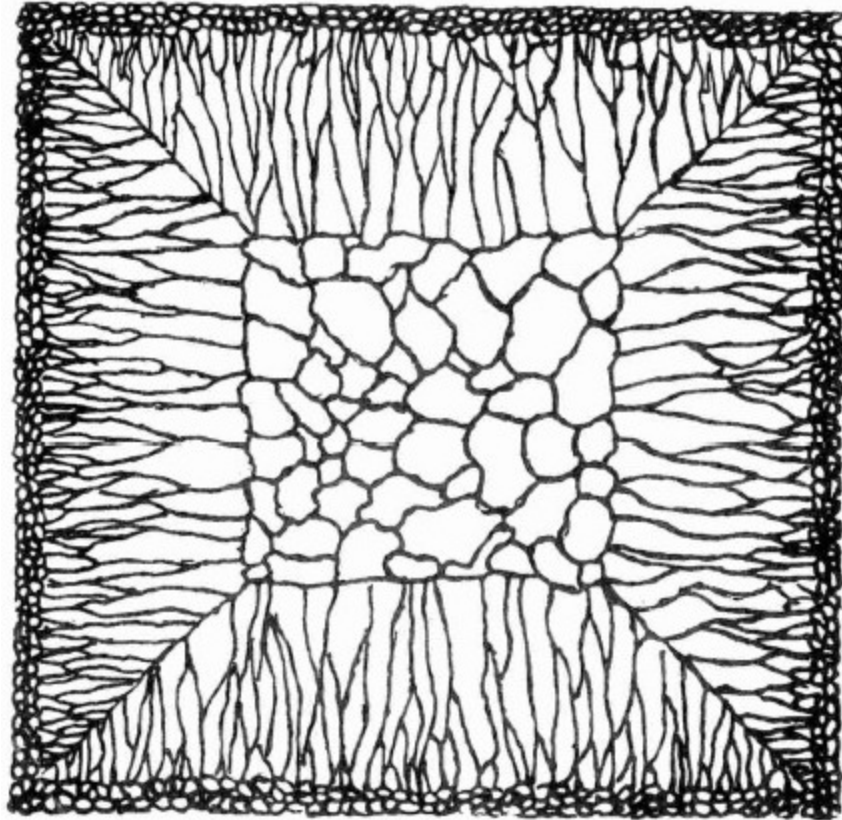
Fig. 2.3.6. Schematic showing chill zone, columnar zone and equiaxed zone in a casting [Flemings, 1974].
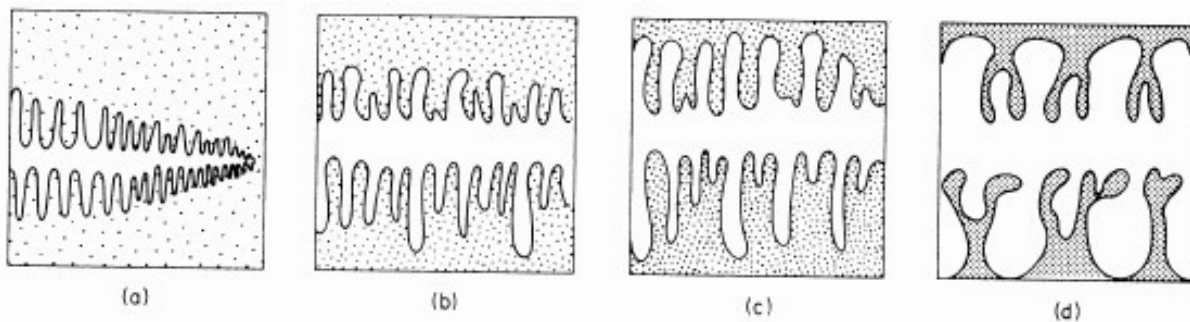
Fig. 2.3.7. (a-d) Schematic showing growth of dendrite in an alloy at various stages of solidification [Flemings, 1974].

Equiaxed grains grow in the same direction as that of heat flow towards the mold wall. These grains are characterized by having equal dimensions in all directions. Equiaxed grains are the result of copious nucleation throughout the body of the liquid, followed by free growth of the

16

individual grains until that growth is halted by grain impingement. Fig. 2.3.8 is a schematic of equiaxed grain growth [Gruzleski, 2000].
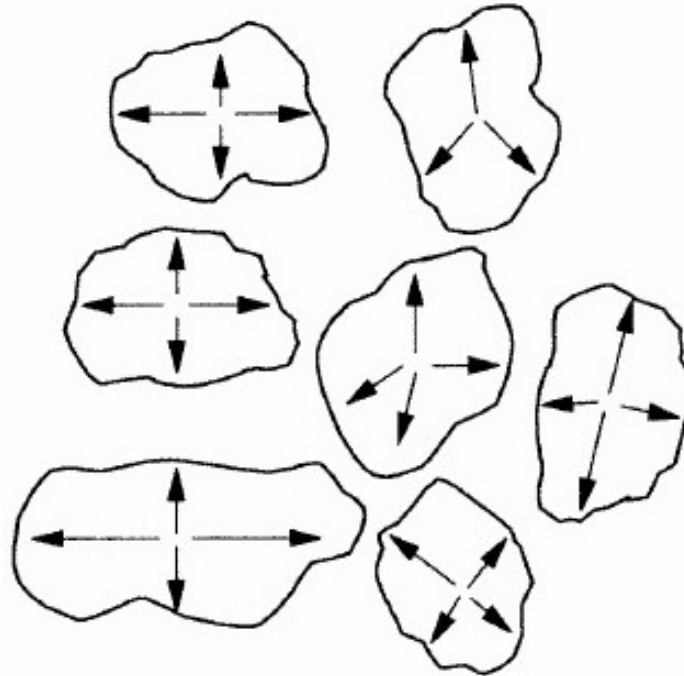
Fig. 2.3.8. Equiaxed grains grow almost equally in all directions [Gruzleski, 2000].

The constitutional undercooling plays a vital role in grain growth stage. Grain growth occurs when large amount of constitutional undercooling is present in the melt. Discussion on constitutional undercooling will be presented in the subsequent section.

2.4   CONSTITUTIONAL UNDERCOOLING

Constitutional undercooling is the driving force for crystal growth of alloys. During solidification, a solute-rich layer builds ahead of the solid-liquid interface. The liquid immediately in front of the solid-liquid interface is at a temperature below its equilibrium liquidus temperature. Therefore, it is undercooled. This undercooling arises due to changes in composition, not temperature, and results in instability of the solidification front since any protuberance forming on the interface would find itself in undercooled liquid and therefore would not remelt [Flemings, 1974]. At steady state conditions with no convection, the criterion for constitutional undercooling is given by [Flemings, 1974]:

$$\frac{G_l}{R} \geq -\frac{m_l c_0 (1-k)}{k D_l}$$
Equation 2.4.1

Where:

G_l is the actual temperature gradient in the liquid ahead of solid-liquid interface

R is the growth rate of solid liquid interface

m_l is the liquidus slope in the phase diagram

c_0 is the initial concentration of alloy

k is the distribution coefficient

D_l is the diffusion coefficient of the solute in the liquid.

Growth in practical alloy solidification conditions generate a large amount of constitutional undercooling far in excess of what can be eliminated by simple cellular solidification. This difficulty is handled by generating a dendritic structure [Gruzleski, 2000].

2.5   EFFECT OF SOLUTE ON GRAIN GROWTH

Solute elements play an important role in controlling grain growth and subsequent nucleation [Lee et. al., 2000]. Solute elements build up ahead of solid-liquid interface, providing constitutional undercooling and restricting grain growth. The growth restriction effect of an element can be quantified in terms of a growth restriction factor (GRF). The GRF indicates how susceptible solute elements are in producing a diffusion layer in front of the advancing solid-liquid interface which slows the grain growth. A higher GRF value means the solute has a higher efficiency of restricting grain growth resulting in smaller grain sizes. The common method of calculating GRF is to use the formula based on phase diagram features which is as follows [StJohn et. al., 2007]:

For a binary system,

GRF= $m_l c_0 (k-1)$ Equation 2.5.1

For alloys with i elements,

$$GRF = \sum_1^i m_{li} c_{0i} (k_i - 1)$$ Equation 2.5.2

where,

m_{li} is the slope of the liquidus line of element i

c_{oi} is the initial concentration of element i

k_i is the distribution coefficient of element i.

The GRF values of various alloying elements in Mg alloys determined through using binary phase diagrams are summarized in Table 2.5.1 [Lee et. al., 2000]. The GRF values of Zr, Ca and Si are the highest, followed by Ni, Zn and Cu. These elements have potentially high grain refining efficiency resulting from their high segregating potential at low addition levels in Mg alloys.

Along with the GRF values of elements analysis of cooling curve is useful for understanding of the solidification processes which includes nucleation and grain growth. Discussion on cooling curve analysis will be presented in the subsequent section.

Table 2.5.1 GRF Values of Different Alloying Elements in Mg [Lee et. al., 2000].

Element	System	GRF
Zr	Peritectic	38.29
Ca	Eutectic	11.94
Si	Eutectic	9.25
Ni	Eutectic	6.13
Zn	Eutectic	5.31
Cu	Eutectic	5.28
Ge	Eutectic	4.41
Al	Eutectic	4.32
Sc	Peritectic	3.96
Sr	Eutectic	3.51
Ce	Eutectic	2.74
Yb	Eutectic	2.53
Y	Eutectic	1.70
Sn	Eutectic	1.47
Pb	Eutectic	1.03

2.6 COOLING CURVE ANALYSIS

Cooling curves are the thermal fingerprint of material as it freezes. Proper interpretation of cooling curves can yield considerable information about solidification processes [Gruzleski, 2000]. Understanding of the cooling of a material is best explained using Fig. 2.6.1. Fig. 2.6.1. shows the changes in temperature of a pure material versus time for a case where undercooling is present. During solidification of an alloy, when no additional inoculants are present in the melt, the alloy does not begin to solidify immediately at the freezing, T_F [D' Elia, 2009] which is also called equilibrium solidification temperature. Instead, the liquid undercools to some minimum temperature, T_{Min} which is often equal to the nucleation temperature, T_N where nucleation occurs. With nucleation and crystal growth, latent heat is evolved and temperature starts rising again to the growth temperature, T_G. This reheating to growth temperature is known as recalescence. These temperatures are shown in Fig. 2.6.1.

As shown in Fig. 2.6.2, if sufficient inoculants are present no recalescence will be observed. In this case solidifications begins at the freezing temperature, T_F indicating that undercooling of liquid is not required to activate nucleating particles.
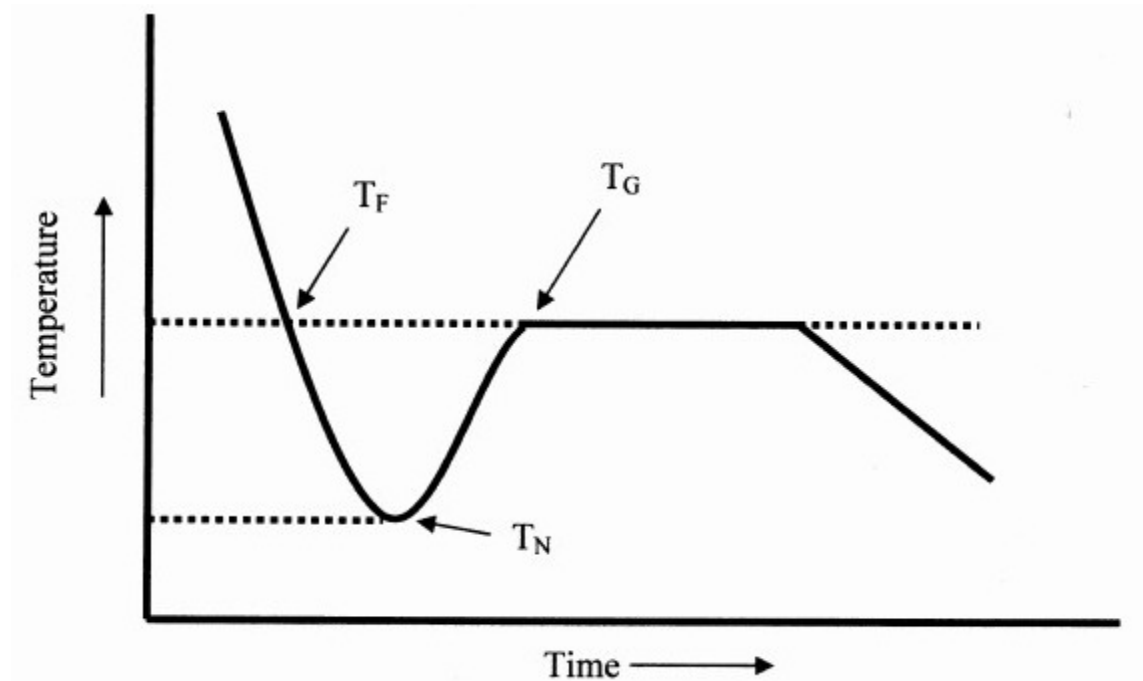
Fig. 2.6.1. Cooling curve of a pure material with undercooling present.
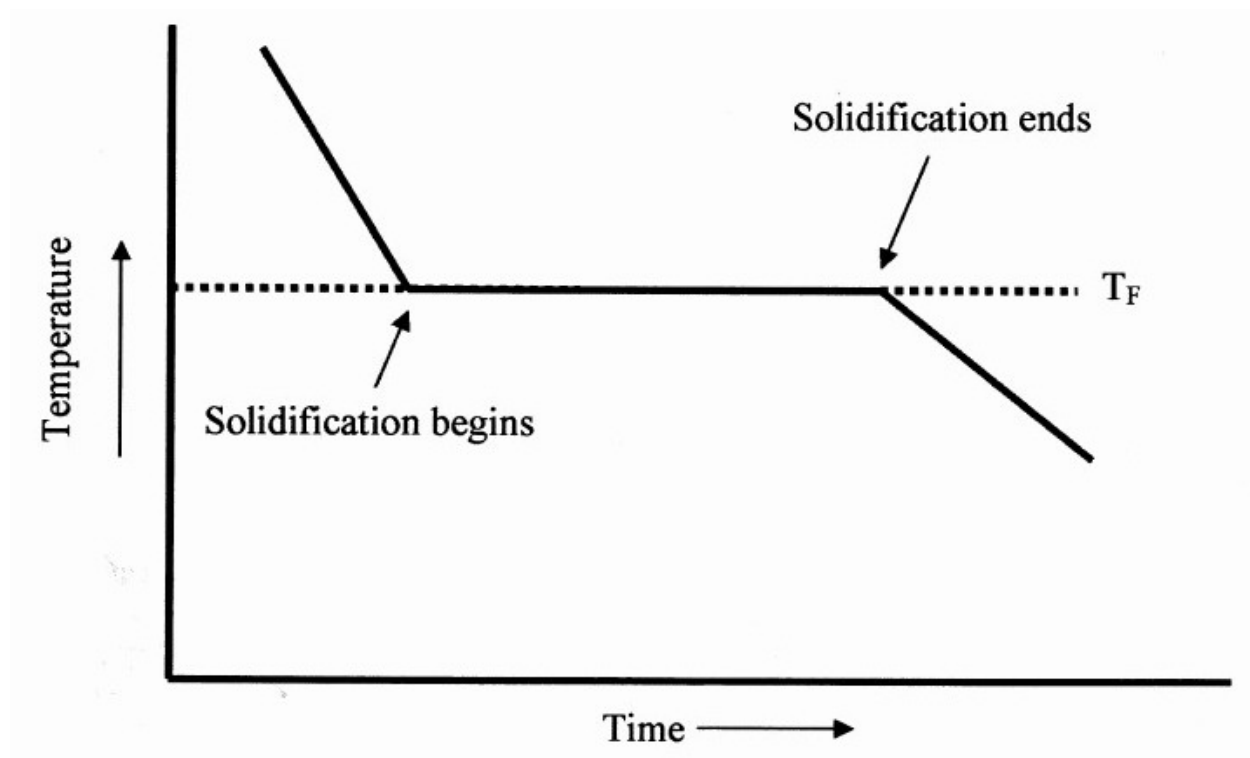
Fig. 2.6.2. Cooling curve of a pure material without undercooling.

The purpose of grain refinement is to provide suitable inoculants into molten alloys to ease the transition from liquid to solid during solidification. The following section describes some grain refinement techniques for Mg-Al alloys.

2.7   ROUTES FOR Mg-Al ALLOY GRAIN REFINEMENT

Grain refinement of Mg-Al alloys can be achieved through three major techniques:- (i) mechanical (ii) thermal and (iii) chemical. Agitation of melt during solidification is a typical example of a mechanical technique. Thermal techniques involve rapid cooling and superheating. On the other hand, addition of alloying elements and nucleating agents is classified as part of the chemical techniques for grain refinement. Due to its process simplicity and efficiency, chemical grain refinement techniques have become the most popular methods of grain refinement of Mg alloys in the casting industry.

Over the past few years, a significant number of publications related to grain refinement of Mg-Al alloys have been produced. The following discussion presents a summary of current methods (published) of grain refinement for Mg and its alloys. Special emphasis has been given to Al bearing Mg alloys, as they are the most commonly used alloys automotive applications.

2.7.1   MECHANICAL GRAIN REFINEMENT TECHNIQUES

Grain refinement through mechanical techniques can be achieved by applying mechanical motion (such as vibration or shaking) to the melt during solidification. Electromagnetic vibration (EMV) and ultrasonic treatment (UST) have been successfully applied for grain size reduction and distribution of AZ91 Mg alloy [Aghayani et. al., 2011]. Electromagnetic vibration is generated based on Fleming's left hand rule, which requires a perpendicular relation between the direction of the magnetic field and that of the flowing electric current [Li et. al., 2010]. Ultrasonic treatment uses an ultrasonic system to produce ultrasonic vibration during solidification. These applied vibrations break apart developing dendrites and refine the grain size.

In a recent study [Li et. al., 2010], EMV was utilized at frequencies from 50 to 5000 Hz to refine the grain size of AZ31 and AZ91D alloys. A significant reduction in grain size was observed at medium frequencies (f = 500 to 2000 Hz for AZ31 and f = 900Hz for AZ91D) for both the alloys as can be seen from Fig. 2.7.1 [Li et. al., 2010]. The average grain sizes were large at low frequencies and decrease with the increase of frequencies. The average minimum grain sizes were 53 μm for AZ31 and 57 μm for AZ91D alloys. A further increase of frequency led to the increase of grain size.
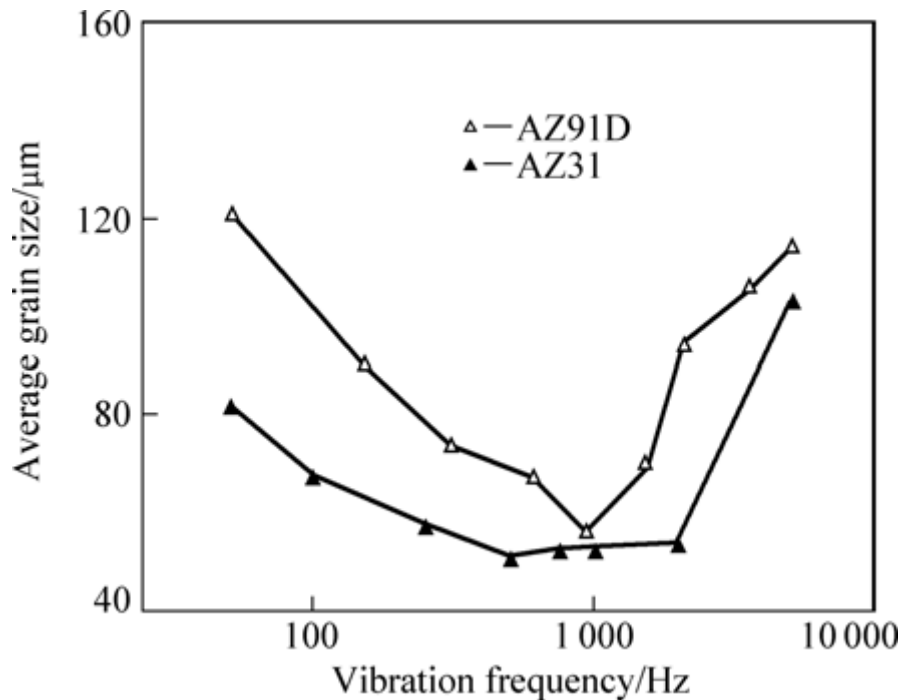
Fig. 2.7.1 Measured average grain size as a function of vibration frequency for AZ31 and AZ91D alloys [Li et. al., 2010].

Use of UST also revealed similar success with AZ91 Mg alloys [Aghayani et. al., 2011, Liu et. al., 2008]. Without UST, the alloy microstructure showed coarse dendrites of α-Mg; while under UST the alloy showed a fine and uniform grain structure. The microstructures of the AZ91D for with and without use of UST are shown in Fig. 2.7.2 [Liu et. al., 2008]. Without any UST applied, the coarse dendrites of the α-Mg were present; the grain size of which was in the range of few millimetres (Fig. 2.7.2-a). With UST applied during solidification (at temperatures

from 615°C to 580°C) fine and uniform grains of the primary α-Mg were produced (Fig. 2.7.2-b) with an average size of 195 µm.
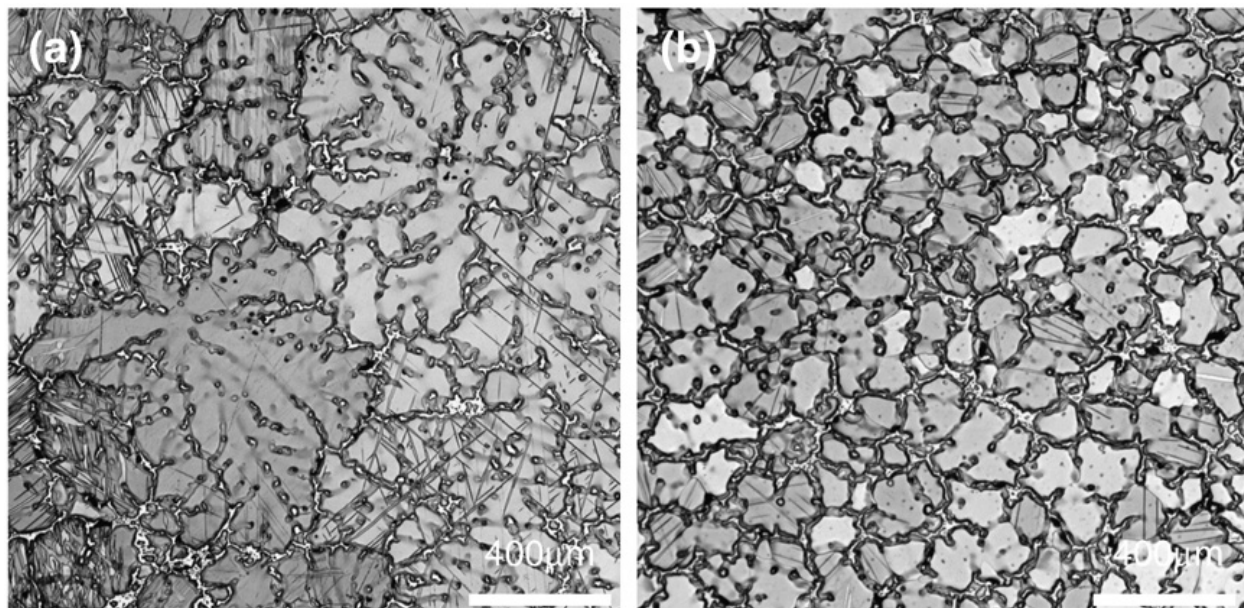
Fig. 2.7.2 Microstructure of AZ91D alloy (a) without UST (b) with UST [Liu et. al., 2008].

Aghayani et. al., 2011 reported that increasing applied ultrasonic power resulted in smaller; more rounded and better distributed grains and intermetallic particles of AZ91 alloy. Ultrasonic treatment also significantly improved tensile strength of the alloy. Tensile strength of the alloy without applying any UST was 94±2 MPa, whereas with 60% UST the tensile strength increased to 165±6 MPa.

The mechanism of grain refinement through agitation is not clear [Lee et. al., 2000]. Liu et. al., 2008 suggested that grain refinement was mainly attributed to the acoustic cavitation and flows induced by agitation through ultrasonic vibration; this made the most impurity particles active as nucleation centers. Some researchers showed that the grain refinement effect achieved for Mg alloys through agitation is more or less equivalent to the grain refinement obtained through superheating [Lee et. al., 2000]. At higher temperatures agitation increases the rate of nuclei phase formation resulting in grain refinement [Lee et. al., 2000].

Rameriz et. al., 2009 studied the role of solute in high-intensity ultrasonic grain refinement of Mg alloys. The study showed that the grain refinement exhibited was strongly dependant on the amount of solute present. The high-intensity ultrasonication has not changed the role of solute and the ultrasonic grain refinement arises from the effects of solute as well as ultrasonication.

Despite some success achieved with grain refinement of Mg alloys through agitation of the melt during solidification, these methods are not very popular in the casting industry owing to the complexity of adding additional equipment to the casting process incurring increased processing time and cost.

2.7.2 THERMAL TECHNIQUE-SUPERHEATING

A high temperature grain refinement technique for Al bearing Mg alloys is superheating [Vinotha et. al., 2009]. The superheating process involves heating a molten Mg-Al alloy to a temperature in the range of 180-300˚C above its liquidus, holding it at that temperature for a period of time, and then cooling rapidly to the required pouring temperature [Cao et. al., 2007]. Some of the major features of grain refinement through superheating, identified through a literature review are summarized below:

(i)   Superheating effect does not occur to a marked extent with any system other than Mg-Al alloys [Emley, 1966].

(ii)   Grain refinement through this process requires the presence of Fe and Mn and is significantly influenced by these elements [StJohn et. al., 2005].

(iii)   The required holding times decrease with increasing Al content and increasing maximum melt temperature and increases with crucible size and rate of heating [Emley, 1966].

(iv)   The refinement effect is suppressed by the presence of Be, Zr, Ti and excess Mn [Emley, 1966].

The exact mechanism of grain refinement through superheating is not clear with some conflicting results among researchers. In a research review [StJohn et. al., 2005], several hypotheses were identified for the mechanism of grain refinement through superheating. One of the hypotheses proposed is that Al-Fe or Al-Mn-Fe intermetallics precipitate from the melt and

act as nucleants [Emley, 1966]. This is supported by the observation that Mg-Al alloys exhibiting the superheating effect require the presence of Fe or Mn. Another hypothesis is the temperature-solubility theory [Achenbach et. al., 1939 as in StJohn et. al., 2005]. According to this theory, particles which are too large to act as nucleants at normal melting temperature will dissolve in the melt at high melting temperatures and then re-precipitate in larger number as fine nucleation sites upon cooling. Another hypothesis proposed is nucleation through Al_4C_3 particles based on the assumption that there is an uptake of carbon from the steel crucible walls at high superheating temperature [Emley, 1966]. Other researchers proposed nucleation on inclusions that formed (such as combination of particles composed of Mg, Al, O and C) during the superheating process [Tamura et. al., 2002].

Regardless of the mechanism, a marked degree of grain refinement is observed through this process for Mg-Al alloys. The effect of superheating on AZ91E alloy obtained by quenching from 600°C (873 K) is shown in Fig. 2.7.3 [Motegi, 2005]. In this research, melt was superheated to 850°C (1123 K) for 900 s and then cooled at 2.5 K/s to different temperatures (750°C/ 1023 K, 700°C/973 K, 650°C/923 K and 600°C/873 K) then immediately poured into two copper blocks. The superheated casting showed finer grain size than the untreated melt.

The major disadvantages associated with superheating are [StJohn et. al., 2005] the requirement of rapid cooling from treatment temperature to the pouring temperature and additional associated time and energy requirements; it is not very practical for large scale commercial melts. Because of the sometimes impractical requirements of superheating, alternative grain refinement techniques have been developed.
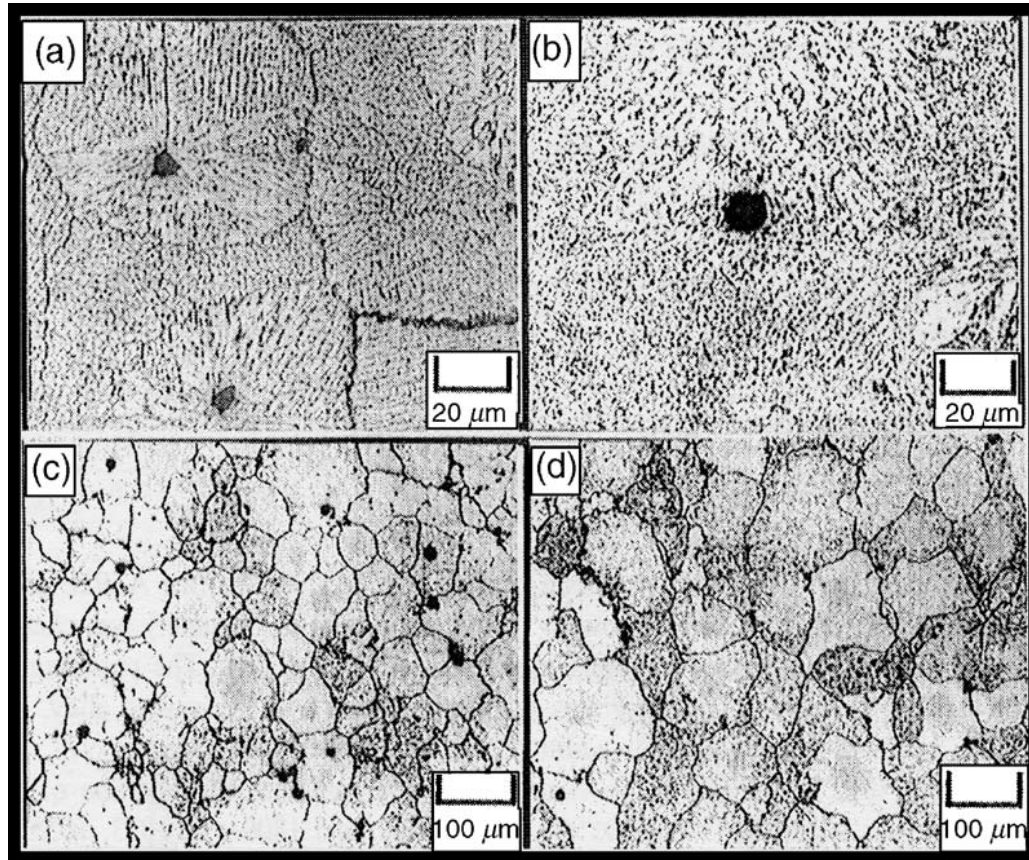
***Fig. 2.7.3. Grain structure of AZ91E alloys at different conditions. (a and b)
quenched sample (c and d) cast sample (a and c) Superheat treated (b and d)
non-superheat treated [Motegi, 2005].***

2.7.3 CHEMICAL GRAIN REFINEMENT TECHNIQUES

The addition of alloying elements and nucleating agents is classified as part of the chemical grain refinement techniques. Due to its process simplicity and efficiency, chemical grain refinement techniques have become the most popular methods of grain refinement for cast Mg alloys. Some of the methods that have achieved varying degrees of success in grain refining of Mg alloys are discussed in the following subsections.

2.7.3.1 Carbon Inoculation

Grain refinement through carbon inoculation is widely used means for grain refinement of Mg-Al alloys. Addition of different carbon containing agents (carbon inoculation) offers many

practical advantages like having lower operating temperature and lower tendency to fading [Dahle et. al., 2001] than many nucleating agents. Carbon can be effectively introduced to Mg-Al alloys in various forms, such as hexachloroethene (C_2Cl_6), hexachlorobenzene (C_6Cl_6), paraffin wax, lamp-black, carbonaceous gases, etc [Emley, 1966]. Different carbides like CaC_2 [Emley, 1966], Al_4C_3 [Nimityongskul et. al., 2010] [Lu et. al., 2005], SiC [Chen et. al., 2010] [Easton et. al., 2006] and carbonates like $MgCO_3$ [Chen et. al., 2011] [Gao et. al., 2010] have all been successfully used to refine Mg-Al alloys with C_2Cl_6, Al_4C_3 and SiC being the most effective.

In a recent study [Jin et. al., 2003] it was found that adding of 0.6 wt.% C_2Cl_6 to AZ31 alloy at 780˚C significantly decreased the grain size from approximately 400 μm (for base, as cast) to 120 μm as shown in Fig. 2.7.4 [Jin et. al., 2003]. Along with the grain refinement the use of C_2Cl_6 is also advantageous as it can be used for melt degassing (0.0025-0.1% of the metal charge at about 750˚C) [Emley, 1966]. However, use of C_2Cl_6 may cause environmental problems [StJohn et. al., 2005] due to the release of greenhouse gases. Therefore, alternative methods to grain refine without releasing greenhouse gases are necessary.
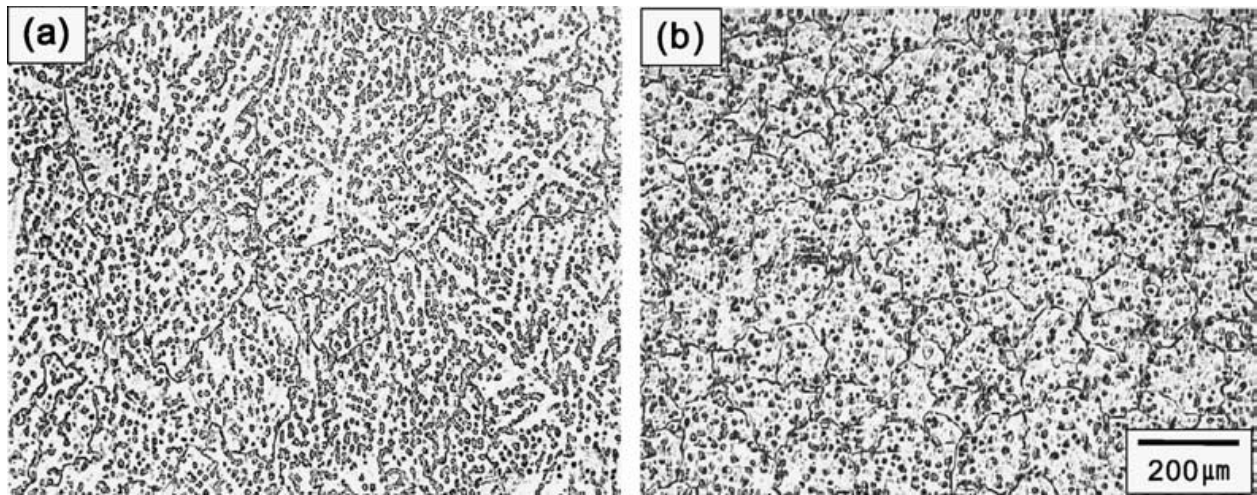
Fig. 2.7.4 Optical micrograph of as cast AZ31 Mg alloy (a) without C_2Cl_6 addition (b) with 0.6 wt.% C_2Cl_6 addition [Jin et. al., 2003].

Use of Al_4C_3 as grain refiner is considered as a more ecofriendly means of grain refinement for Mg-Al alloys than C_2Cl_6. In one study [Lu et. al., 2005], significant grain reduction was observed when freshly ground 1 wt.% Al_4C_3 powder was added to Mg-3wt.% Al alloy at 735°C and 785°C. At both addition temperatures, cast samples displayed similar equiaxed dendritic structure as can be seen in Fig. 2.7.5 and Fig. 2.7.6 [Lu et. al., 2005].

A similar grain refinement effect was also observed with the addition of 5 wt.% Al_4C_3 (particle size < 44 μm) to AM60B in an ultrasonic cavitation based solidification processing setup [Nimityongskul et. al., 2010]. The average grain size for the base AM60B at room temperature was 254 μm, which was reduced to 60 μm after addition of 5 wt.% Al_4C_3. At the same time, the mechanical properties were enhanced by the addition of Al_4C_3 to AM60B alloy.

Addition of SiC is another effective means of grain refinement for Al bearing Mg alloys. Chen et. al., 2010 added SiC in three compositions, such as, Al-33.3 wt.% SiC, Mg-33.3 wt.% SiC and (Mg+JDMJ reagent)-33.3 wt.% SiC in AZ91D alloy at different temperatures from 710°C to 770°C. JDMJ is a commercial degassing reagent for Mg alloys and it contains 43-45 wt.% $MgCl_2$, 20-30 wt.% KCl, 20-30 wt.% NaCl, 3-5 wt.% $CaCl_2$, 3-4.5 wt.% $BaCl_2$ and 1 wt.% foaming agent. Mg and JDMJ were added in equal amount in wt.%. The average grain size reduced from 311 μm for the base alloy to 71 μm with 0.2 wt.% addition of SiC added into the melt in the form of Mg-33.3 wt.% SiC 770°C. The melt was held for 10 min and rapidly cooled to 705°C then immediately poured. Huang et. al., 2011 investigated the effect of SiC in Mg-3 wt.% Al alloy. Silicon carbide with an average particle size of 2 μm was added to the melt in the form of an Al-SiC master alloy. After inoculation by SiC particles, the grain size of the Mg-3 wt.% Al decreased significantly and the grain size distribution was more homogeneous (Fig. 2.7.7). The grain size decreased from 417 μm for base alloy to 128 μm and 120 μm after adding 0.3 wt.% and 10 wt.% of SiC respectively. It is noticeable that SiC addition more than 0.3 wt.% has little influence on the grain size of Mg-Al alloys.
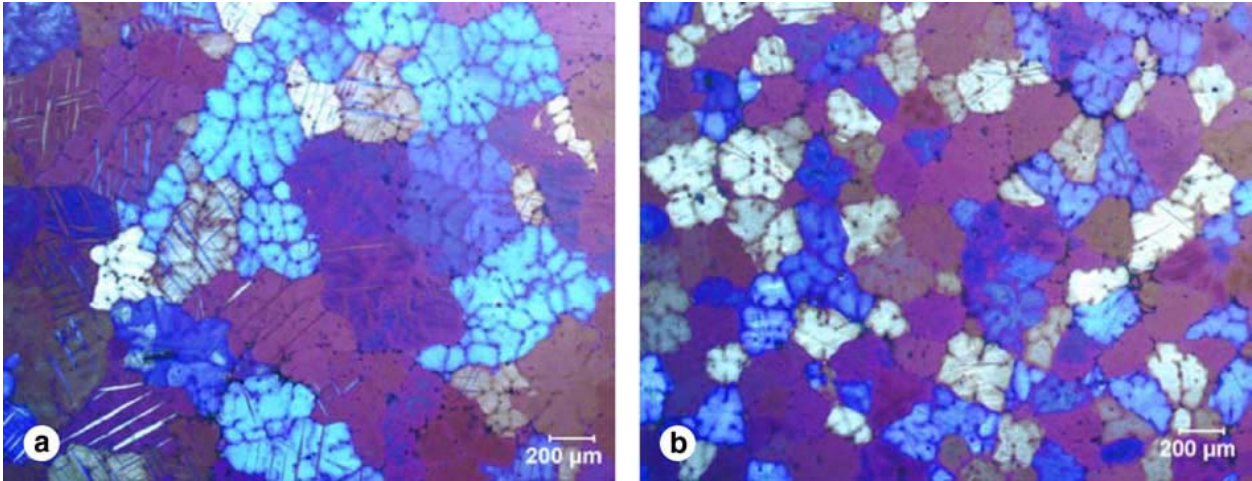
Fig. 2.7.5 Grain refinement efficiency of ground Al4C3 in Mg-3 wt.% Al at 735℃ (a) base alloy (b) 20 min after addition of Al_4C_3 [Lu et. al., 2005].
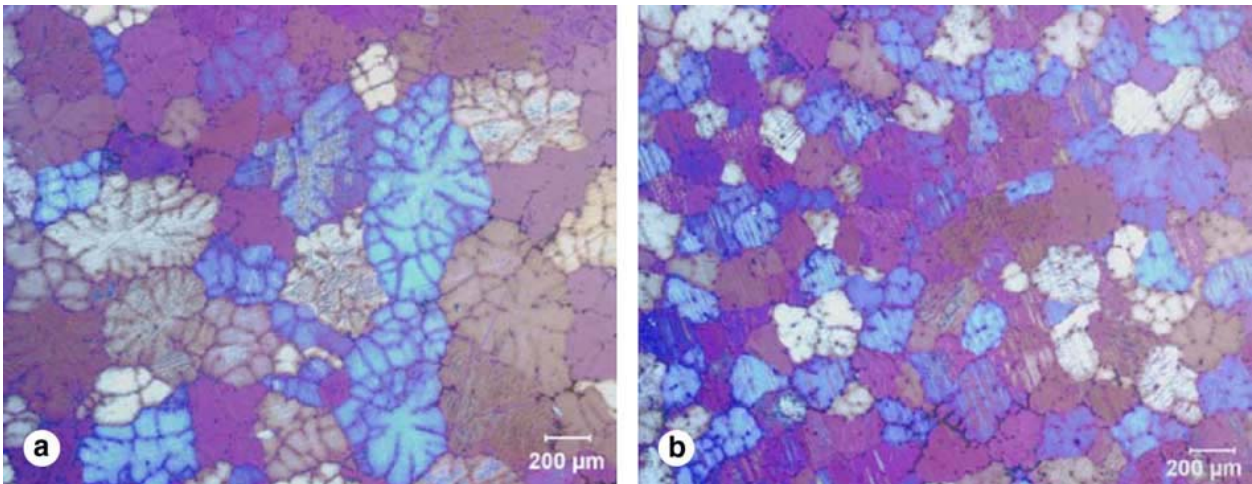
Fig. 2.7.6 Grain refinement efficiency of ground Al_4C_3 in Mg-3 wt.% Al at 785℃ (a) base alloy (b) 30 min after addition of Al_4C_3 [Lu et. al., 2005].
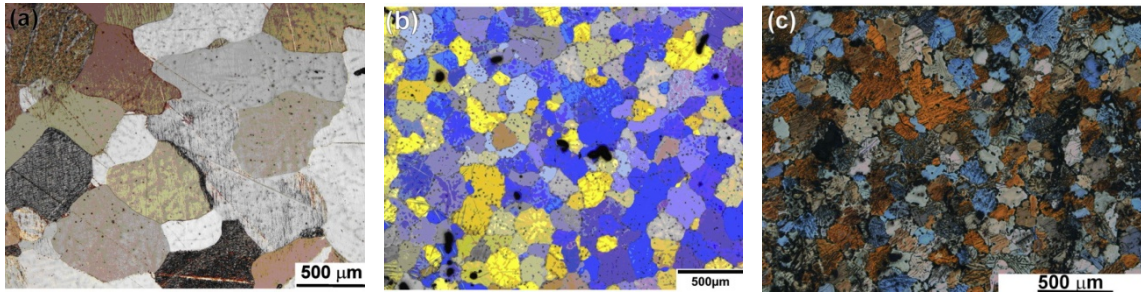
Fig. 2.7.7 Optical micrograph of as-cast alloys: (a) Mg-3 wt.% Al (b) Mg-3 wt.% Al-0.3 wt.% SiC (c) Mg-3 wt.% Al- 10 wt.% SiC [Huang et. al., 2011].

Chen et. al., 2010 found similar results with the addition of SiC to AM60B alloy. With 0.1 and 0.2 wt.% SiC additions significant refinement in primary Mg with fine equiaxed dendrites were found. When the addition level exceeded 0.2 wt.%, grain coarsening was observed. The quantitative change in grain size with SiC addition amount can be seen from Fig. 2.7.8 [Chen et. al., 2010].
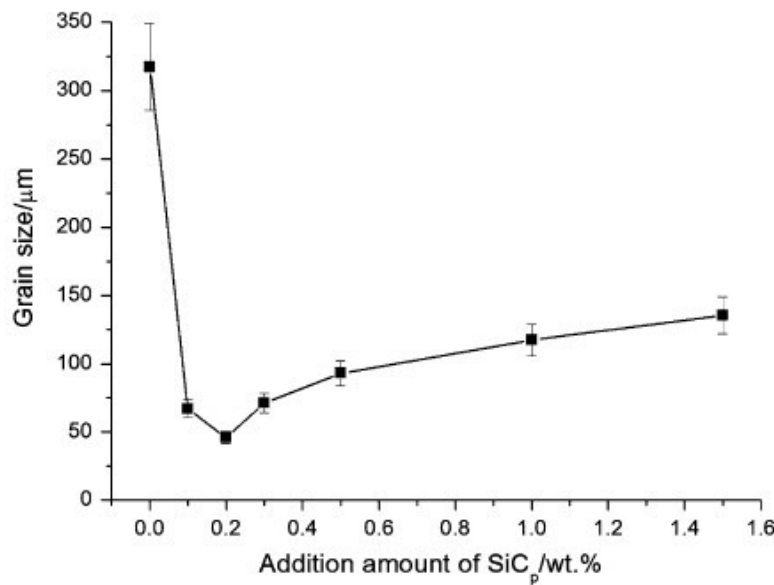
Fig. 2.7.8 Variation of grain size of AM60B alloy with SiC addition [Chen et. al., 2010].

Easton et. al., 2006 studied the potential of SiC particles as grain refiner to Mg-Al alloys with Al content range from 1 wt.% to 9 wt.%. Silicon carbide was introduced to the alloys in the form of Mg-SiC master alloy. The results suggested effective grain refinement of SiC in the range of Mg-Al alloys investigated. The greatest reductions in grain size were observed for the alloys with lower Al content. At higher Al content, such as 9 wt.% Al, grain refinement using SiC was relatively small. In the study, it was also observed that the addition of Mn poisoned the grain refining effect of SiC probably by forming less potent carbides containing Al, Mn and C.

There are number of hypothesizes that exist regarding the mechanism of grain refinement through carbon inoculation. The main hypothesis is nucleation through the formation of Al_4C_3 [Lu et. al., 2005], [Emley, 1966] or $AlN.Al_4C_3$ [Emley, 1966]. Yano et. al., 2001 detected Al-C-O based particles in Mg grains after carbon inoculation and proposed that Al-C-O particles are responsible for grain refinement. Although, Qian et. al., 2005 regarded the Al-C-O hypothesis as a modified version of the Al_4C_3 hypothesis. The strong segregation power of carbon is also believed to be responsible for grain refinement through carbon inoculation [Jin et. al., 2003]. According to this hypothesis, the segregation tendency of carbon element could greatly affect the constitutional undercooling and restrict the grain growth during the solidification process.

In spite of the contradictions over the grain refinement mechanism through carbon inoculation, it is an effective approach for grain refinement of Mg-Al alloys. However, these carbon based refiners may cause environmental problems due to harmful chlorine emissions [Zeng et. al., 2006]. Another major challenge with carbon inoculation is the existence of excess carbon left in the melt from a corrosion point of view [StJohn et. al., 2005].

2.7.3.2 The Elfinal Process
Grain refinement through the Elfinal process requires introduction of anhydrous $FeCl_3$ into the melt. This process was invented by a German company based on the hypothesis that iron particles could act as nucleation sites for Mg grains [StJohn et. al., 2005]. This process was observed to work fairly well with Mg-Al alloys at $750°C$ but this is not the case if Mn is absent in the alloy [Nelson, as in Emley, 1966]. Cao et. al., 2004 studied the grain refinement effect of $FeCl_3$ in high purity Mg-3 wt.% Al and Mg-9 wt.% Al alloys. The alloys were melted in a carbon

free aluminum titanite ($AlTi_2O_5$) crucible. The anhydrous $FeCl_3$ was introduced into the melt at 750°C. The results of the experiment are shown in Fig. 2.7.9 and Fig. 2.7.10 [Cao et. al., 2004]. The results indicate that anhydrous $FeCl_3$ has a significant grain refinement effect on Mg-3 wt.% Al and Mg-9 wt.% Al alloys respectively. The results also suggest that the Elfinal process is capable of grain refining high purity Mg-Al alloys that contain very low concentrations of Mn (<10 ppm), contrary to the observations by Nelson, as in Emley, 1966.
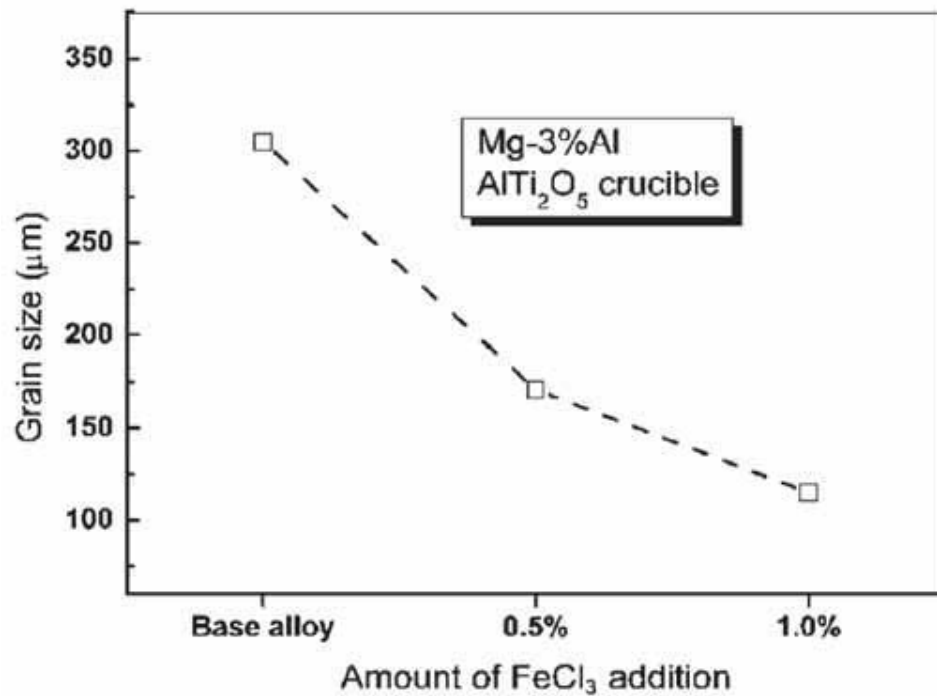
Fig. 2.7.9 Grain refinement of Mg-3 wt.% Al with FeCl₃ at 750°C [Cao et. al., 2004].
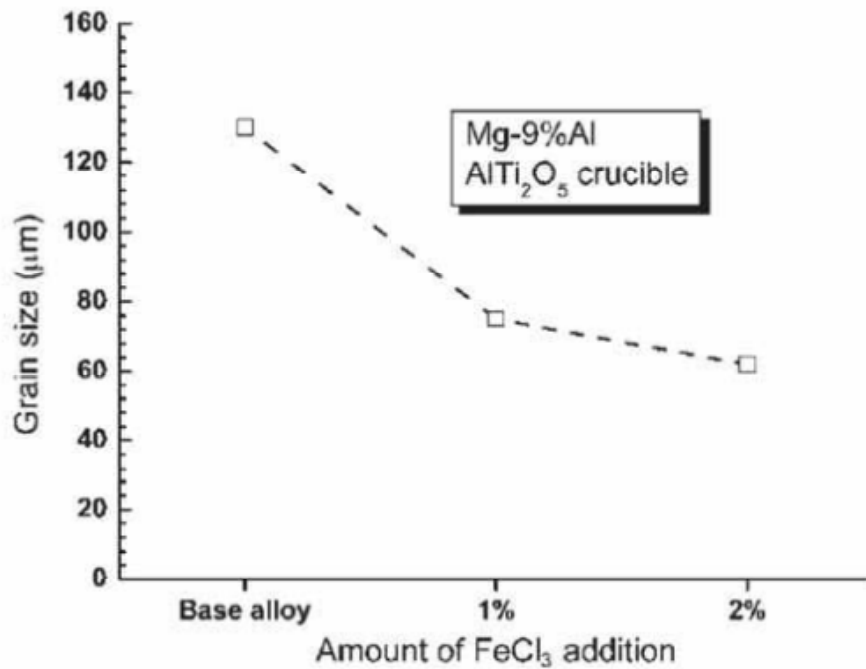
Fig. 2.7.10 Grain refinement of Mg-9 wt.% Al with FeCl₃ at 750°C [Cao et. al., 2004].

Cao et. al., 2004 observed the formation of many Fe- and Al-rich particles within Mg grains. With these observations they concluded that Fe- and Al-rich particles acted as nucleants for Mg grains and were responsible for grain refinement of Mg-Al alloys through the Elfinal process.

Although, the Elfinal process is an efficient grain refiner for Mg-Al alloys, it introduces Fe into the melt which is detrimental to the corrosion resistance of Mg-Al alloys. In addition, the release of Cl or HCl associated with use of $FeCl_3$ is another concern [StJohn et. al., 2005].

2.7.3.3 Native Grain Refinement

The native grain refinement of Mg-Al alloys is the process of grain refinement through control of impurity levels of Mg. Native grain size is the grain size that results in the alloy when high purity alloying elements are used. Accordingly, native grain refinement is the phenomenon where the native grain size is finer than that of the corresponding commercial purity alloy [Cao et. al., 2005]. Tamura et. al., 2002 investigated the effect of purity level on Mg-9 wt.% Al alloy prepared from commercial high-purity Al (99.99%) and distilled high-purity

Mg (<99.99%). A small amount of Fe and Mn were added to the alloy to see the influence of these impurities on grain sizes. It was observed that the grain sizes of the high-purity Mg-9 wt.% Al alloy refined naturally without using the grain refiner or superheat treatment were 40 μm and the grain size increased with increasing the Fe and Mn concentrations. The grain sizes of the alloy containing 0.01 wt.% Fe or 0.47 wt.% Mn were about 160 μm.

The native grain refinement phenomenon was further confirmed through the work done by Cao et. al., 2005. They identified that this approach of grain refinement is a unique characteristic of Mg-Al alloys. Other Mg alloy systems do not show the native grain refinement effect. Cao et. al., 2005 used high purity Al (Fe: 0.0001 wt.%, Si: 0.001 wt.%, Cu: 0.0015-0.003 wt.%, Zn: 0.001 wt.% and Ti: 0.001 wt.%) and Mg at two different purity levels- sublimed high purity Mg (99.98 wt.%) and commercial purity Mg (99.7 wt.%). One group of Mg-Al alloys were prepared by using high purity Mg and other group by using commercial purity Mg. For both the alloy groups, the Al content was varied in the range of 0.5-9 wt.%. It was found that at all levels of Al content; the high purity alloy consistently demonstrated finer grain size than commercial purity as can be seen from Fig. 2.7.11 [Cao et. al., 2005].

Tamura et. al., 2002 suggested that native grain refinement could be attributed to the heterogeneous nucleation of Mg on some combination of Al, O, and C particles. Cao et. al., 2005 assumed that probably Al_4C_3 nucleant particles were responsible for native grain refinement of Mg-Al alloys rather than Al-O-C particles. It was also identified that the presence of Fe and Mn in the alloy forms less potent nucleants through binding with effective nucleation substances and degrade the potency of Al_4C_3 [Tamura et. al., 2002].
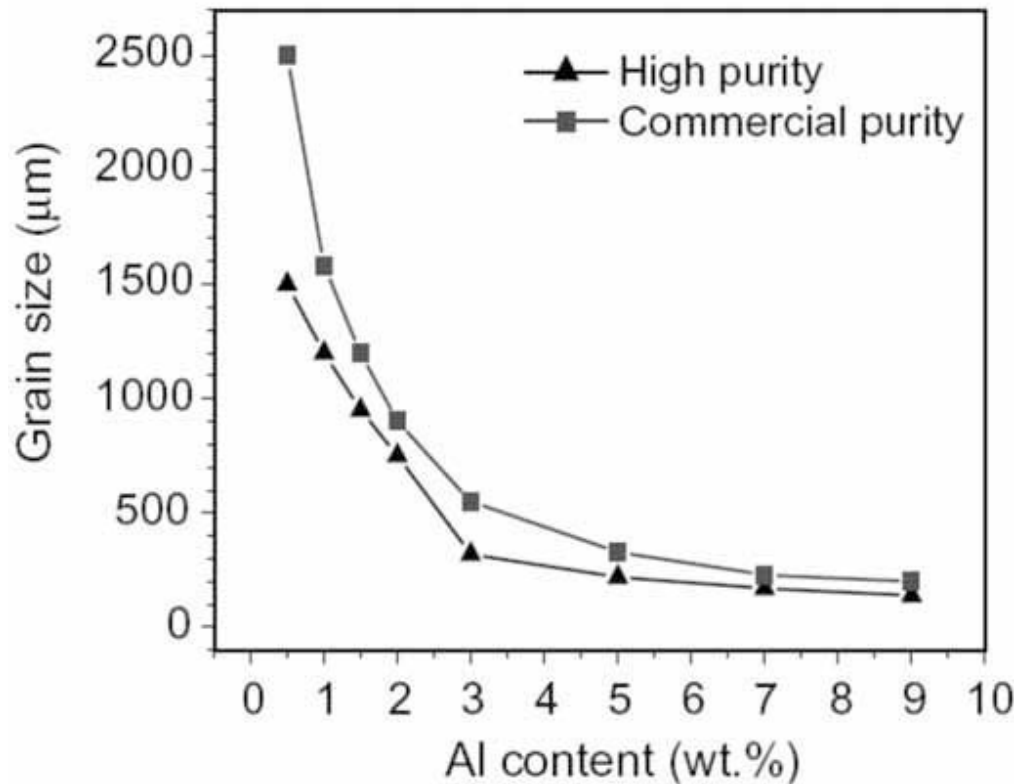
Fig. 2.7.11 Effect of source Mg purity on the grain size of Mg-Al alloys [Cao et. al., 2005].

2.7.3.4 Grain Refinement by Adding Other Additives

Environmental concerns and corrosion related issues arising from carbon inoculation and the Elfinal process warrant the development of alternative grain refiners for Mg-Al alloys. Over the past few years, a significant number of publications related to grain refinement of Mg-Al alloys have been produced. Some of the potential and effective Mg-Al grain refiners that have resulted from the research are strontium, Sr [Zeng et. al., 2006], [Liu et. al., 2008], boron, B [Suresh et. al., 2009], Al-Ti-B [Chen et. al., 2012], AlN [Fu et. al., 2009], calcium, Ca [Lee et. al., 2000], [Li et. al., 2005], [Elsayed et. al., 2009], manganese, Mn [Elsayed et. al., 2009], [Cao et. al., 2006], rare-earth elements like cerium, Ce [Liu et. al., 2009] and yttrium, Y   [Qiu et. al., 2009]. Grain refinement effect due to addition of these alloying elements to Mg-Al alloys are discussed in the subsequent sub-sections.

2.7.3.4.1 Strontium (Sr) Addition

Grain refinement of Mg-Al alloys using Sr has been extensively studied. Recent studies indicated that Sr is an effective grain refiner for Mg-Al alloys. It also acts as a good modifier for Si-containing Mg-Al alloys [Srinivasan et. al., 2006]. Strontium can be introduced in the Mg-Al melt in multiple forms, such as an Al-Sr master alloy, Mg-Sr master alloy or as pure Sr. Zeng et. al., 2006 added pure Sr to commercial AZ31B ingots while Yang et. al., 2007 introduced Sr as Al-10Sr and Mg-10Sr master alloys to AZ31. In all the cases referred here, it was found that a small addition (~ 0.1 wt.%) of Sr can effectively decrease the grain size of alloys. Yang et. al., 2007 found that the refinement efficiency of Mg-10Sr master alloy is higher than that of the Al-10Sr master alloy.

The refinement mechanism of Sr in Mg-Al alloys is attributed to solute enrichment in the liquid ahead of the growing interface restricting grain growth during solidification. Zeng et. al., 2006 established a relationship between grain size and GRF value of the AZ31 alloy at different addition levels of Sr. The relationship is shown in Fig. 2.7.12 [Zeng et. al., 2006]. From this relationship, it can be seen that the grain size decreased with increasing GRF values with Sr addition upto 0.1 wt.% which is the solid solubility limit of Sr in Mg. Decrease in grain growth of the alloy below the solid solubility limit of Sr in Mg is due to the constitutional undercooling generated by Al, Zn and Sr. The excess Sr atoms above the solubility limit formed $Mg_{16}(Al,Zn)_2Sr$ intermetallic particles which reduces the grain growth restriction effect of Sr. Zeng et. al., 2006 observed that increases in yield strength were consistent with the reductions in grain size of the AZ31 alloys with Sr addition as shown in Fig. 2.7.13 [Zeng et. al., 2006]. The yield strength increases followed the Hall-Petch relationship.
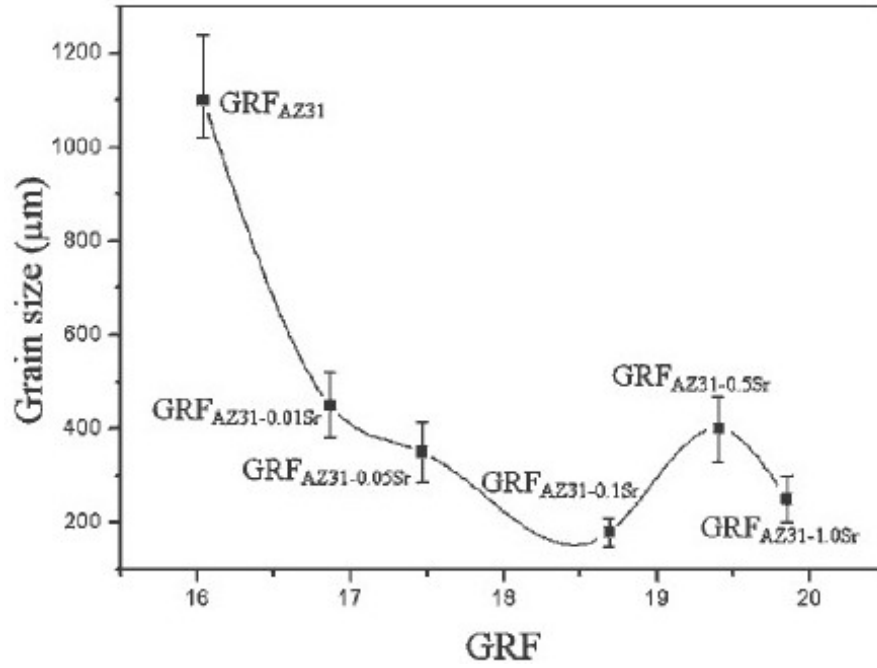
Fig. 2.7.12 Grain size vs GRF value of AZ31-Sr alloys [Zeng et. al., 2006].
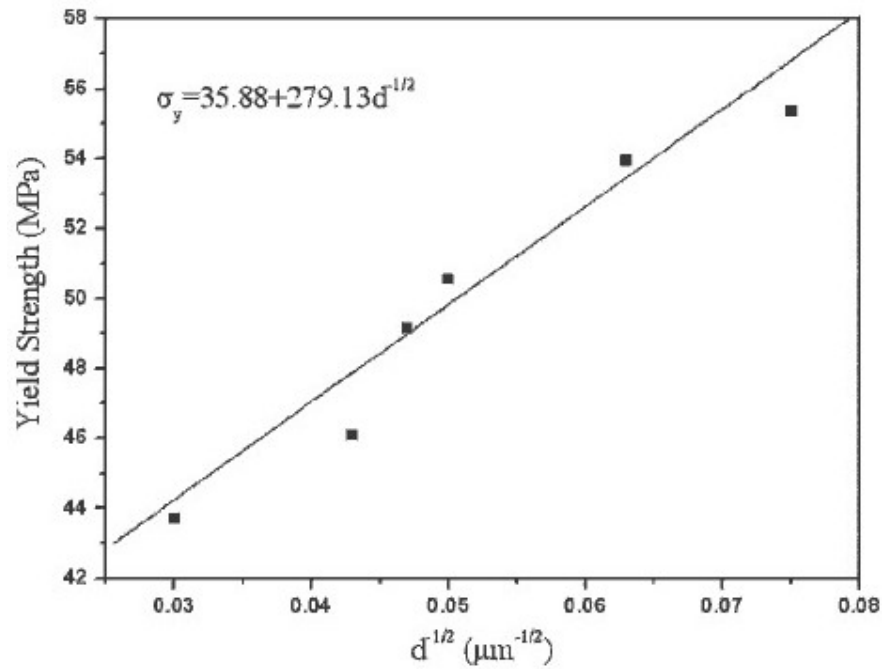
Fig. 2.7.13 Yield strength as a function of grain size for AZ31-Sr alloys [Zeng et. al., 2006].

Lee et. al. 2005 pointed out one of the major demerits of Sr in Mg-Al alloys with high Al content. The study, conducted to see the effect of Sr addition in low (3 wt.%) and high (9 wt.%) Al-containing binary Mg alloys, revealed significant grain refinement effect of Sr in low Al content alloy but the addition of Sr to high Al content alloy produced no significant grain refinement. It was suspected that Sr was poisoned at high concentration of Al. As the concentration of Al increased, the formation of Al_4Sr poisoned the grain refining effect of Sr.

2.7.3.4.2 Boron (B) Addition

Suresh et. al., 2009 studied the effect of B addition in the form of an Al-4B at 740°C on the grain size and mechanical properties of AZ91E alloy. The unrefined alloy had a grain size of 100 μm and with an addition of 0.008 wt.%, 0.02 wt.% and 0.032 wt.% B, the grain size of the alloy reduced to 70 μm, 45 μm and 30 μm, respectively. Further increased additions of B produced no significant changes in grain size. Along with the reduction in grain size, improved mechanical properties of the AZ91E alloy were also observed with the addition of B. Table 2.7.1 presents the mechanical properties of the as-cast AZ91 alloy with and without B addition.

Table 2.7.1 Mechanical Properties of As-cast AZ91 Alloy with B Addition
[Suresh et. al., 2009]

Alloy	BHN	0.2% YS (MPa)	UTS (MPa)	Elong. (%)
AZ91	61	95	180	3.3
AZ91 +0.008 wt.%B	67	102	197	3.9
AZ91+0.02 wt.%B	72	107	211	4.4
AZ91+0.032 wt.%B	77	110	226	4.8
AZ91+0.04 wt.%B	79	113	229	4.9

Combined SEM and EDS analyses revealed AlB_2 particles at the centre portions of grains as shown in Fig. 2.7.14 [Suresh et. al., 2009]. These AlB_2 particles are thought to be attributed to the grain refinement of the alloy acting as heterogeneous nucleation site for Mg grains. This assumption of grain refinement mechanism was further supported by the fact that both AlB_2 particles and α-Mg have similarity in crystallographic structure. Both of them have hexagonal crystal structure and their lattice parameters are also very close to each other (Mg: a= 0.3202 nm, c= 0.521 nm and AlB_2: a=0.30054 nm, c=0.32528 nm [Suresh et. al., 2009]). Despite reported significant success in reducing the grain size and increasing the mechanical properties of AZ91E

with B addition, the fading behaviour of B, which is a very important parameter in the industry, has not been studied.
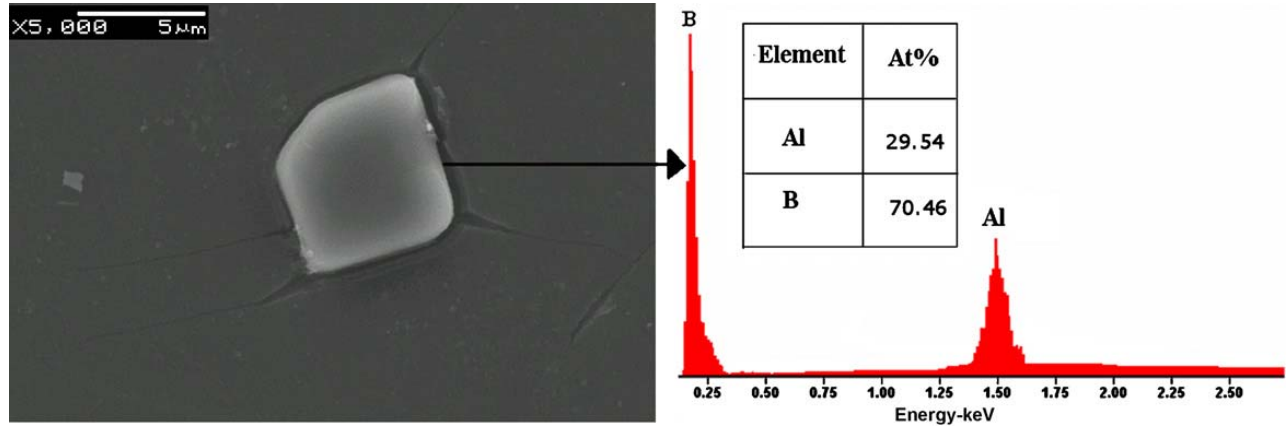
Fig. 2.7.14 SEM micrograph and EDS spectrum of 0.032 wt.% B added to AZ91 alloy [Suresh et. al., 2009].

2.7.3.4.3 Al-Ti-B Addition

Al-Ti-B master alloys are known to be the most effective type of grain refiner for Al alloys and it is also commercially available commonly in the form of Al-5Ti-1B (TiBor). Keeping this in mind, many researchers have tried this type of refiner for Mg-Al alloys. Xu-liang et. al., 2010 studied the efficiency of Al-5Ti-1B master alloy in AZ61 alloy. The master alloy was added to the melt at 730˚C and held for different times before pouring. The average grain size of the unrefined alloy was 400 μm which was reduced to 50 μm with an optimum addition level of 0.5 wt.% Al-5Ti-1B and for 30 minutes holding time. However, the grain size showed an increasing trend beyond 0.5 wt.% addition level and for holding times longer than 30 minutes. Along with the grain refinement effect, the addition of Al-5Ti-1B resulted in an increase in the mechanical properties of the AZ61 alloy. The average microhardness of the AZ61 alloy refined with the addition of 1 wt.% Al-5Ti-1B was 8% higher compared to the non-refined AZ61 alloy. A similar grain refinement effect of Al-5Ti-1B master alloy was observed for AZ91D alloy [Chen et. al., 2012]. In this case, the grain size of the unrefined AZ91D alloy was reduced from 422 μm (base alloy) to 79 μm with addition of 0.3 wt.% Al-5Ti-1B master alloy at 750˚C and holding the melt for 30 minutes. The grain size of the alloy tended to increase with increasing

addition levels exceeding 0.3 wt.%. An improvement in the mechanical properties of AZ91D alloys was also observed with addition of Al-5Ti-1B. Elsayed, 2010 added Al-5Ti-1B to AZ91E alloy and observed the similar grain refinement behaviour.

Similar to an Al-Ti-B master alloy, Liu et. al., 2009 used a Mg-50 wt.%TiB$_2$ master alloy as a grain refiner in AZ91D Mg alloys. The Mg-50%TiB$_2$ master alloy was added to the melt at 720°C and held for 10 minutes before pouring. The average grain size continually decreased with increasing Mg-50%TiB$_2$. The base AZ91D alloy had an average grain size of 240 μm and reduced to 124 μm, 64 μm and 50 μm with addition of 0.6 wt.%, 1.2 wt.% and 1.8 wt.% Mg-50 wt.% TiB$_2$, respectively. This established that TiB$_2$ particles had significant grain refinement in AZ91D alloy.

The grain refinement mechanism of Al-Ti-B master alloys in Mg-Al has been attributed to TiB$_2$ being an effective nucleant for Mg. In addition to the nucleation potency of TiB$_2$, some researchers [Chen et. al., 2012] assumed that grain growth restriction by Ti also contributes in reducing the grain size of Mg. The tendency of increasing grain size after exceeding certain addition level of Al-Ti-B to Mg-Al alloys was attributed to a saturation of TiB$_2$ particles within the melt and the TiB$_2$ agglomerating and settling resulting in a decrease in the effective substrate number under this condition [Chen et. al., 2012].

From all these studies it was established that Al-Ti-B refiners can effectively reduce the grain size of Mg-Al alloys with the main disadvantage being its poor fading behaviour. Fig. 2.7.15 shows the fading behaviour of Al-5Ti-1B in AZ91D+0.3 wt.% Al-5Ti-1B at 750°C [Chen et. al., 2012]. The grain size decreased with holding up to 30 minutes; beyond which, increasing holding time increased the grain size. It has been assumed that similar to excess addition of Al-Ti-B refiner, TiB$_2$ particles agglomerate and settle down after certain time period. This results in the decrease of nucleate substrate number and thus the increase of grain size.
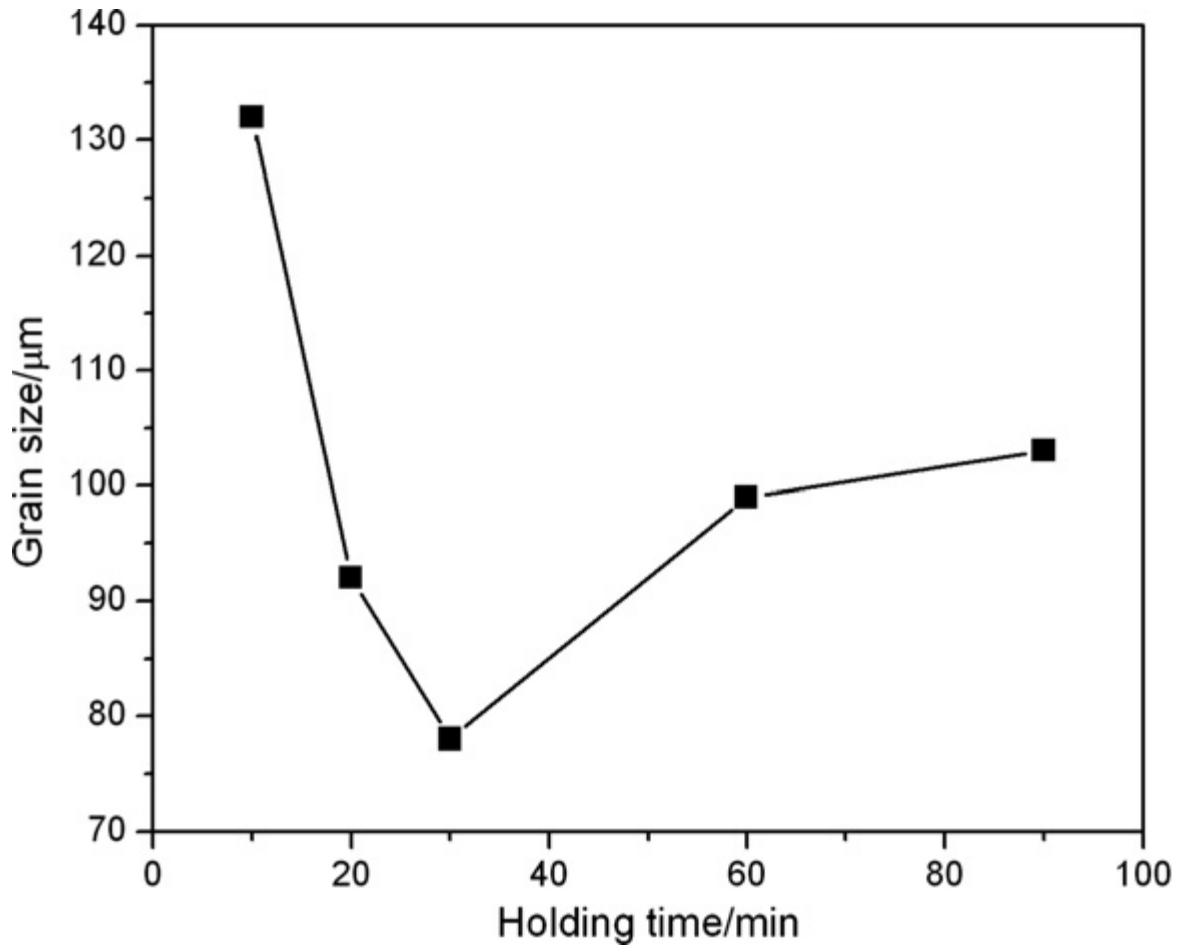
Fig. 2.7.15 Variation of grain size with holding time with Al-5Ti-1B addition to AZ91D [Chen et. al., 2012].

2.7.3.4.4 Aluminum Nitride (AlN) Addition

Aluminum nitride has a HCP crystal structure and the edge-to-edge matching model revealed that the inter-atomic spacing misfit and inter-planer spacing (d-value) mismatch between AlN and Mg at room temperature is 2.6% and is 2.67%, respectively [Fu et. al., 2009]. This crystallographic similarity has prompted researchers to investigate the effectiveness of AlN as grain refiner in Mg-Al alloys. Fu et. al., 2009 added AlN to Mg-3 wt.% Al and Mg-9 wt.% Al in the form of a Mg-AlN master alloy in the ratio of 1:1.5 by weight. At an addition temperature of 765°C a 0.5 wt.% addition of AlN in Mg-3 wt.% Al alloy reduced the alloy grain size from 450 μm to 120 μm. Fig. 2.7.16 demonstrates the change in microstructure with addition of AlN in Mg-3 wt.% Al alloy [Fu et. al., 2009]. No further reduction in grain size was observed for addition levels beyond 0.5 wt.%. At the same time, no change in grain size was observed for

holding the melt up to 120 min at 765˚C after adding 1 wt.% AlN. The grain refinement mechanism of AlN to Mg-Al alloys is not yet known.
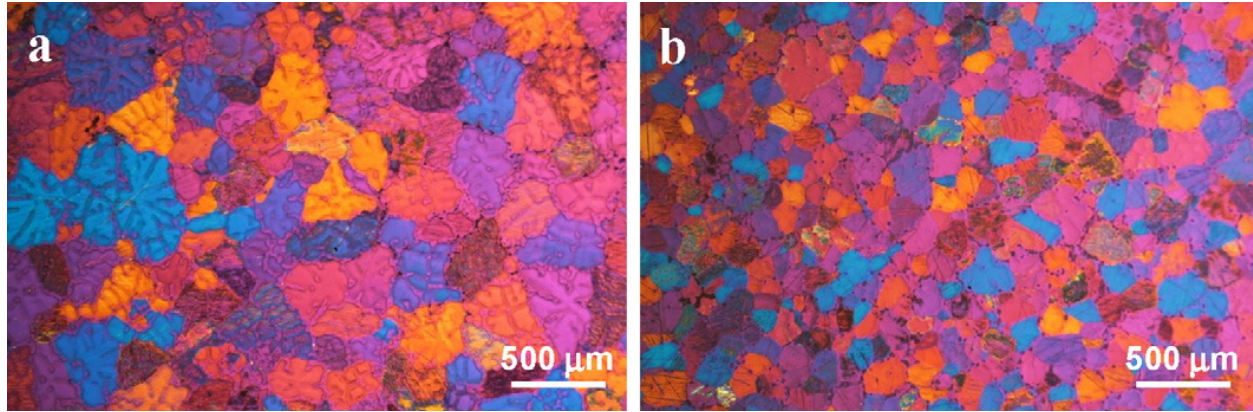
Fig. 2.7.16 Microstructure of Mg-3 wt.% Al sample held at 765˚C (a) without AlN (b) with AlN addition [Fu et. al., 2009].

2.7.3.4.5 Calcium (Ca) Addition

Calcium has a very high growth restriction factor of 11.94 in Mg, only second to Zr (Table 2.5.1). Hence Ca is thought to be a potential grain refiner for Mg-Al alloys. Calcium shows a significant grain refinement effect in pure Mg [Lee et. al. 2005]. However, the grain refinement efficiency of Ca in Mg-Al alloys is found to be contradictory. Li et. al., 2004 investigated the influence of small additions of Ca on the grain size, microstructure, hot tearing susceptibility and tensile properties of AZ91D alloy. Along with some grain refinement effect with addition of 0.1 to 1 wt.% Ca in AZ91D alloy, a substantial increase in hot tearing susceptibility coefficients (HSC) with rise in Ca content was also observed. Fig. 2.7.17 shows the effect of Ca content on the grain size and HSC for AZ91D alloy [Li et. al., 2004]. With an increase in Ca content there was an increase in Al_2Ca phase formation in the alloy which suppressed the formation of β-$Mg_{17}Al_{12}$. The formation of Al_2Ca phase is thought to be responsible for grain refinement (through grain growth restriction) as well as increase hot tearing susceptibility. The presence of Al_2Ca on the grain boundaries was assumed to be responsible for worsening some of the mechanical properties like the ultimate tensile strength and the elongation of the alloy.

43
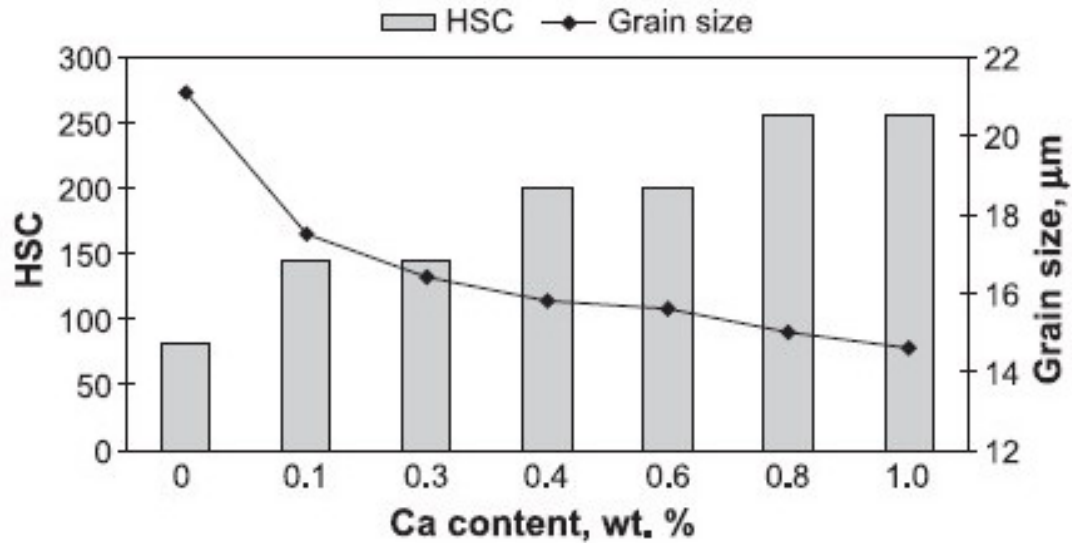
Fig. 2.7.17 Hot tearing susceptibility coefficient (HSC) and grain size of AZ91D alloy with various levels of Ca addition [Li et. al., 2004].

On the contrary, Elsayed et. al., 2009 observed that the addition Ca to AZ91D alloy resulted in grain coarsening of the alloy. With a change in the concentration of Ca from 0.5 wt.% to 1 wt.%, the grain size increased from 284 μm to 846 μm. Additional levels of Ca beyond 1 wt.% maintained the grain size between 600-800 μm. Fig. 2.7.18 shows the grain size effect of Ca addition in the alloy for various addition levels [Elsayed et.al. 2009]. The authors did not provide any reasoning for grain coarsening with Ca addition in AZ91D alloy. Although their observation of the increase of hot tearing susceptibility of the alloy with rise of Ca content is similar to the observation made by Li et. al., 2004. However, these conflicting results along with its detrimental effect on mechanical properties have made Ca not a very attractive grain refiner for Mg-Al alloys.
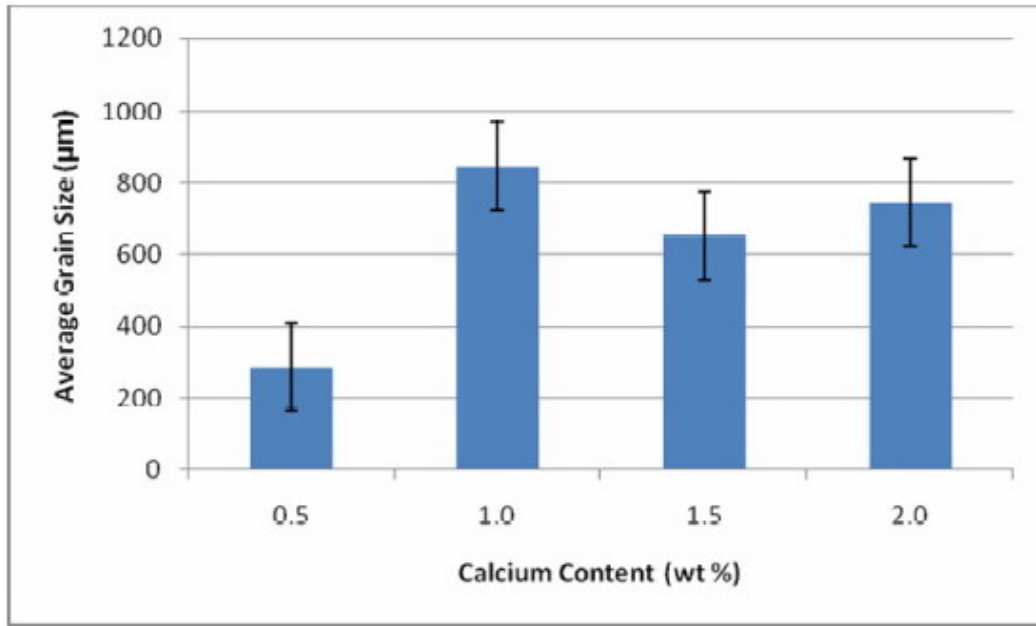
***Fig. 2.7.18 Average grain size of AZ91D alloy with various levels of Ca addition
[Elsayed et. al., 2009].***

2.7.3.4.6 Manganese (Mn) Addition

Most commercial Mg-Al alloys contain Mn as it plays a critical role as an iron remover in the alloy as discussed in section 2.1. From the discussion in section 2.7.2 it is also known that the presence of Mn is essential for effective grain refinement of Mg-Al alloys through the superheating process. However, the refinement effect is suppressed by the presence of excessive Mn. To clarify whether Mn can be used as a grain refiner for Mg-Al based alloys, a detailed study on the effect of Mn on grain size was conducted by Cao et. al., 2006. In this study four Mg alloys, binary Mg-3 wt.% Al, Mg-6 wt.% Al and Mg-9 wt.% Al made of high purity Mg (99.98 wt.%) and Al (99.999 wt.%) and a commercial purity AZ31 alloy were employed. The alloy melt was prepared at 730 ˚C under a protective cover gas (1.0 vol.% SF_6 in 49 vol.% dry air and 50 vol.% CO_2). The Mn was introduced in the alloys at different addition levels in the form of an Al-60 wt.% Mn splatter. An initial rapid decrease in grain size was observed after adding Mn to all three high purity binary alloys and further addition of Mn resulted in little further reduction in grain size. A significant drop in grain size was observed with high purity Mg-3 wt.% Al with a small addition (around 0.1 wt.%) of Mn. Obvious grain refinement was also achieved with commercial AZ31 alloy with addition of Al-60 wt.% Mn

splatter. The grain size dropped from 650 to 270 μm after addition of 0.2 wt.% Mn. The results of the study are shown in Fig. 2.7.19 [Cao et.al. 2006]. It was proposed that the hexagonal close-packed ε-AlMn phase present in the Al-60 wt.% Mn splatter acted as a nucleant for Mg grains. However, ε-AlMn intermetallics are stable only at temperatures above 840˚C, thus an obvious fading effect was observed for holding the melt for long time (2 hour) at the melt temperature of 730˚C.

(a)   (b)
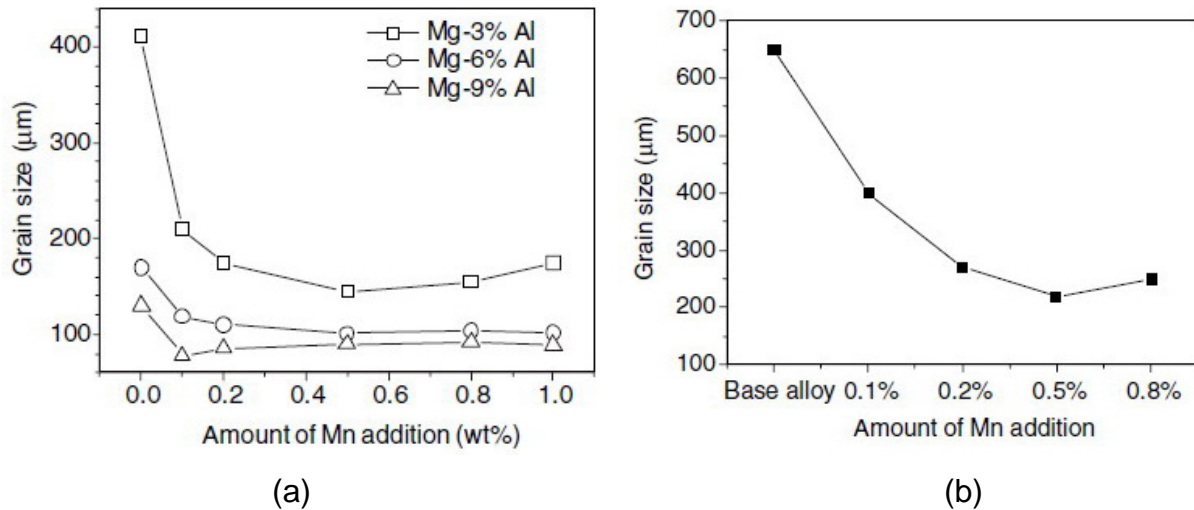
Fig. 2.7.19 Effect of Mn on average grain size of (a) high purity binary Mg-Al alloys and (b) AZ31 commercial alloy [Cao et. al., 2006].

In a separate study [Liu et. al., 2010], the role of Mn on the grain refining efficiency of AZ91D alloy after it was refined by Al_4C_3 was investigated. In this study a Mg-50 wt.% Al_4C_3 master alloy and commercial purity Mn additive ZS-Mn75 (produced by Sichuan Lande Industry Co. Ltd.) were added to commercial purity AZ91D alloy at 750˚C. The addition of 0.6 wt.% Al_4C_3 to commercial AZ91D alloys reduced the grain size of the alloy from 360 μm (for untreated alloy) to 210 μm. However, the combined addition of 0.6 wt.% Al_4C_3 and 0.27 wt.% Mn, 0.6 wt.% Al_4C_3 and 0.47 wt.% Mn and 0.6 wt.% Al_4C_3 and 0.67 wt.% Mn further reduced the grain sizes of the alloy to 130 μm, 132 μm and 138 μm respectively. Formation of Al-C-O-Mn-Fe-rich compounds with an Al-C-O-rich coating film were observed in grain centres. The particles formed through a reaction between Al_4C_3 and Al-Mn-Fe compounds were

believed to be the potential nucleating substrates for primary Mg of the AZ91D alloy treated by the combination of Al_4C_3 and Mn.

Elsayed et. al., 2009 studied the effect of Mn addition on the hot tearing susceptibility of AZ91D alloy. An increase in the hot tearing severity of the alloy was observed for the alloy when Mn content was above 0.5 wt.% in the alloy.

2.7.3.4.7 Addition of Rare Earth Elements

In recent years, grain refinement effect of rare earth elements (such as Ce, Y) on Mg-Al alloys has been studied. Liu et. al., 2009 examined the grain refinement effect of Ce on AZ91 alloy. In the same study, the effect of Ce addition combined with either Ca or Sr was also investigated. Master alloys such as Al-10 wt.% Ce, Al-30 wt.% Ca and Al-10 wt.% Sr were added to AZ91 Mg alloy (Mg-9 wt.% Al-0.8 wt.% Zn) at 700 ˚C. It was observed that the addition of 0.8 wt.% Ce to AZ91 alloy resulted in the reduction of the average grain size of the alloy from 107 μm (base alloy) to 36 μm. Further reductions in average grain size were observed with AZ91-0.8 wt.% Ce-0.2 wt.% Ca and AZ91-0.8 wt.% Ce-0.2 wt.% Sr alloys. The dendritic structure of AZ91-0.8 wt.% Ce became much finer and more uniform with further addition of either Ca or Sr. It was assumed that the grain refinement was mainly due to the impeding effect on grain growth of these elements on the primary α-Mg.

The grain refinement effect of Y on Mg alloys was studied by adding Y in the form of Mg-25.67 wt.% Y master alloy in Mg-5 wt.% Li-3 wt.% Al-2 wt.% Zn alloy [Cui et. al., 2011]. The addition of Y resulted in the formation of an Al_2Y phase which resulted in grain refinement through hindering grain growth. The smallest grain size of the alloy was produced with the addition of 0.8 wt.% Y to the alloy. At room temperature, the tensile properties of the alloy also improved with Y addition; tensile strength and ductility of the alloy reached peak value when Y addition were 0.8 wt.% and 1.2 wt.% respectively. Similar results of reduction in grain size and improvement in tensile properties were also reported when Y was added to AZ91D alloy in the form of Y-rich interalloy [Zhao et. al., 2009].

The addition of rare earth elements produce obvious grain refinement effect in Mg-Al alloys but the high cost of these elements deters their use on a large scale.

2.7.3.4.8 ZnO-A Potential Grain Refiner

In spite of success with previous refiners and refining processes discussed earlier in this chapter, there is no universally accepted refiner for Mg-Al alloys that is environmentally friendly, reliable and easy to apply [StJohn et. al., 2005]. As such, there is a need to develop effective and environmentally friendly grain refiners for Mg-Al alloys.

Fu et. al., 2008 examined ZnO as a potential grain refiner for pure Mg and Mg-3 wt.% Al. Using the edge-to-edge matching model (section 2.3.2), ZnO was found to have similar crystallographic parameters to pure magnesium. Various levels of ZnO powder were added to pure Mg (99.94 wt.%) and Mg-3 wt.% Al alloy at $720 \pm 5°C$ melt temperature. Significant grain size reductions from 1100 μm to 410 μm for pure Mg were observed with addition of 3 wt.% ZnO to pure Mg. The mean grain size of Mg-3 wt.% Al was reduced from 420 μm to 310 μm with 1 wt.% addition of ZnO to the alloy. The as cast microstructure of Mg-3 wt.% Al before and after addition of 1 wt.% ZnO are shown in Fig. 2.7.20 [Fu et. al. 2008]. When ZnO was introduced to molten Mg, part of ZnO was dissociated and which in turn, introduced Zn into the melt.

The grain refinement mechanism was attributed to the combined effects of grain growth restriction from Zn and heterogeneous nucleation of α-Mg by undissociated ZnO particles [Fu et. al. 2008].
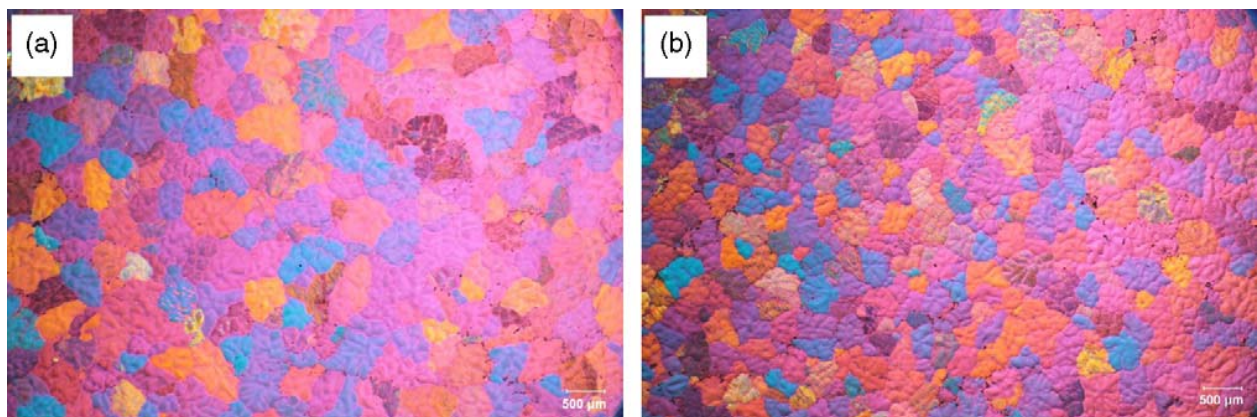
Fig. 2.7.20 Microstructure of Mg-3 wt.% Al alloy (a) base alloy (b) after 1 wt.% ZnO addition [Fu et. al., 2008].

Lee, 2011 carried out a preliminary study of ZnO in AZ91E alloy and found some encouraging results. With higher addition levels (2 wt.%) of ZnO to AZ91E alloy, he found 75% grain size reduction compared to the base alloy. There is a need to carry out a detailed study of the effect of ZnO addition on grain refinement in AZ91E and Mg-9 wt.% Al alloys.

In this research, an extensive study of the effect of ZnO in Mg alloys bearing 9 wt.% Al (AZ91E commercial alloys and Mg-9 wt.% Al binary alloy) has been carried out to specifically examine the effectiveness of ZnO as a potential grain refiner and to determine its refining mechanism. A separate study was conducted to investigate the effect of ZnO on permanent mold cast AZ91E alloys. The influence of ZnO on the grain size, microstructure, tensile properties and hardness at ambient temperature were studied to examine the grain refinement potential of ZnO.

Chapter 3: Experimental Procedure

This chapter begins with a flow chart describing the plan of study, followed by a discussion on the procedures carried out to perform the castings employed in this research. At the same time a detail description of materials used in this study, thermal analysis, microscopy, tensile testing, fractography, hardness and porosity testing is also presented.

3.1 EXPERIMENTAL PLAN

A schematic representation of the experimental plan is shown in Fig. 3.1.1.
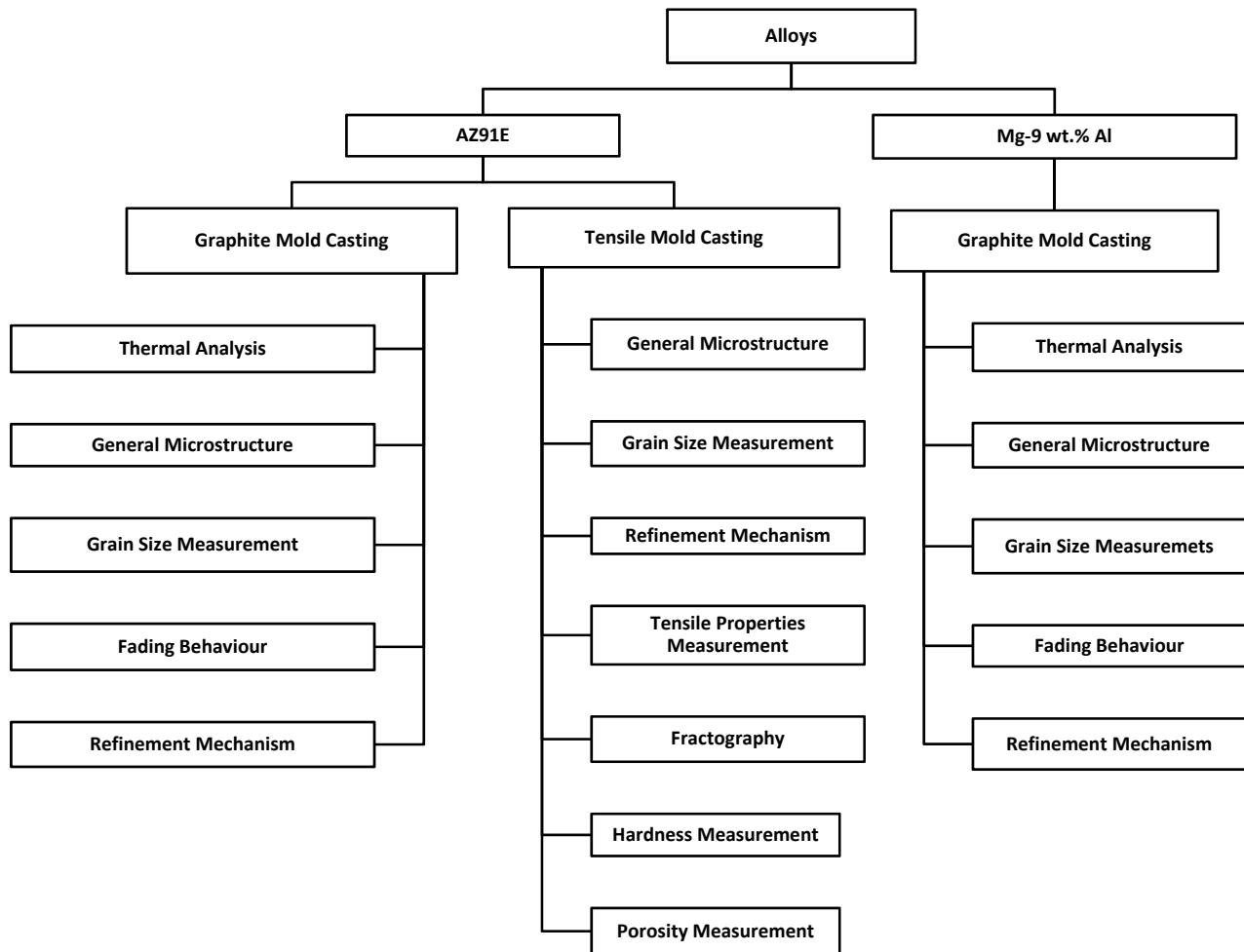
Fig. 3.1.1 Schematic representation of experimental plan.

3.2 MATERIAL

3.2.1 AZ91E ALLOY

Virgin ingots of AZ91E Mg alloy were one of the base materials used in this study. The chemical composition analysis of the AZ91E alloy (batch analysis from the supplier) is given in Table 3.2.1.

Table 3.2.1 Composition of AZ91E Alloy (wt.%)

Al	Zn	Mn	Ce	Cu	Fe	Fe/Mn	Ni	Mg
9.3	0.65	0.24	0.01	0.005	0.002	0.008	0.0009	Balance

3.2.2 Mg-9 wt.% Al BINARY ALLOY

The Mg-9 wt.% Al binary alloy was prepared using commercial purity Mg (99.8 wt.%) and Al (99.7 wt.%). The predetermined proportions of these materials were put into carbon steel crucibles and melted in an electric resistance melting furnace, the detailed procedure of which is described in the following sections.

3.2.3 ZnO GRAIN REFINER

The ZnO grain refiner used in this experiment was received as powder with a purity of 99% (particle size: < 1 μm). A representative SEM image of these particles is as shown in Appendix-A2.

3.3 GRAPHITE MOLD CASTING

Graphite molds were used for most of the castings in this study. Graphite molds capable of producing circular bottom castings of 40 mm/ 1.57 inch diameter and 50 mm/ 1.97 inch height were made from machining 70 mm/ 2.75 inch diameter graphite shafts. Images of a graphite mold used in this experiment are shown in Fig. 3.3.1.
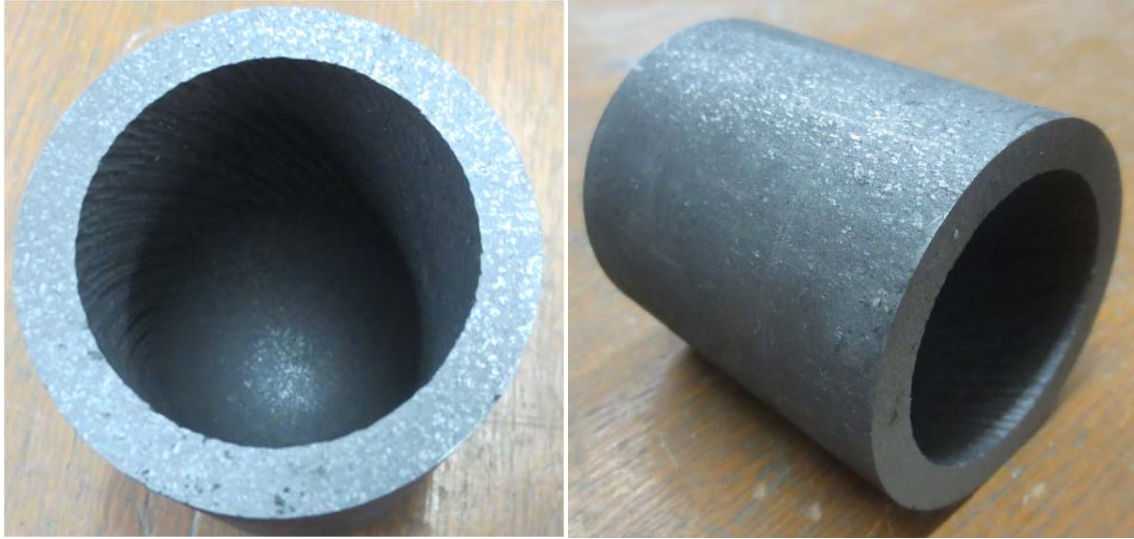
Fig. 3.3.1 Images of graphite molds from different angles.

Approximately 500 g of the base materials (both AZ91E and Mg-9 wt.% Al separately) were melted at 750 C / 1382 F set temperature in a steel crucible (diameter: 100 mm/ 3.94 inch and height: 150 mm/ 5.91 inch) using an electrical resistance furnace with CO_2 cover gas at the flow rate of 15 standard cubic feet per hour (SCFH) to protect melt from oxidation. The electric resistance furnace (PHS Kilns and Furnaces, Oakville, Ontario, Canada) used for this purpose was coupled with digital temperature controller.

ZnO was added as grain refiners to the alloys at different addition levels up to 3 wt.% ZnO of desired weight was wrapped into aluminum foils to prevent loose powders from scattering in the air during addition to the molten metal. ZnO was preheated at 250 C / 482 F to remove moisture. Temperature of the melt was measured using a K-type thermocouple probe connected with temperature meter (Omega, model DP i8). ZnO was added to the melt at 750 C / 1382 F and immediately stirred for 30 seconds with a coated (Foseco Dycote 36) propeller. After stirring, the material was held in the furnace for the duration of specific holding time (5 min or 60 min). Any oxide that formed on the top of the melt was skimmed before pouring using a low carbon spoon.

Three graphite molds were preheated at 750 C / 1382 F for 1 hour so that the molds are uniformly heated. The preheated molds were placed in the pouring platform immediately before pouring. Melt was then directly poured from the crucibles to the graphite molds at

$720^{\circ}C$ / $1328^{\circ}F$. Immediately after pouring; the molds were covered with steel plate to avoid oxidation. Steel plate used for mold covering was 3 mm / $\frac{1}{8}$ inch thick and had holes for thermocouple insertion. For rigidly holding the thermocouples, thermocouple holders were spot welded to the plates. Using set-screws and thermocouple holders, thermocouples were kept at fixed positions for all the castings during thermal data acquisitions. A schematic of the casting setup is shown in Fig. 3.3.2.
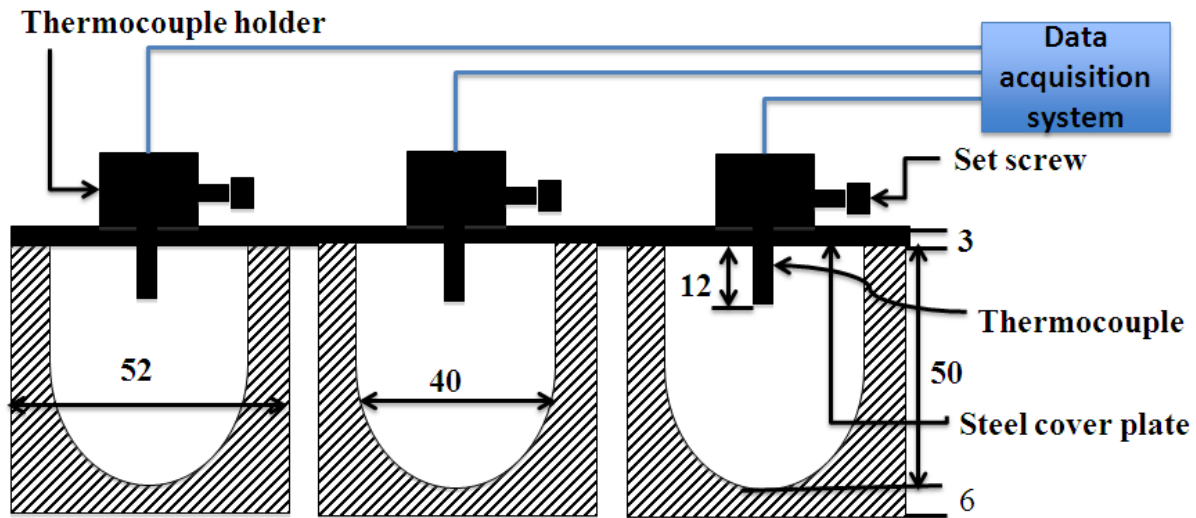
Fig. 3.2.2 Casting set-up in graphite mold (all dimensions are in mm).

Thermocouples in the steel cover plate were positioned as illustrated in the figure. The thermocouples were connected to the data acquisition systems (Daytronic System 10, DataPAC) for measuring thermal data during metal solidification. The data acquisition system was started prior to pouring the molten material into the graphite mold to ensure that the entire cooling curve was obtained. Thermal data were collected from all the three graphite mold castings for data accuracy. The castings were repeated for each condition.

Graphite mold cast samples were used to evaluate the effectiveness of ZnO as grain refiner through grain size measurement, fading effect, and microstructure through optical microscopy and SEM, with a view to gain an understanding of the grain refinement mechanism. All the graphite mold casting parameters used in this study are summarized in Table 3.3.1.

Pouring temperature was kept 720°C / 1328°F to match industry practice for Mg alloys. Addition levels were selected by observing trend of grain size reduction after using ZnO. The high mold temperature was selected to maintain low cooling rate during metal solidification process. Holding time of 1 hour (60 minute) was selected to investigate the occurrence of any fading effect after considerable longer time.

Table 3.3.1 Graphite Mold Casting Parameters

Parameter	Values
Addition level (wt.%)	AZ91E-0, 0.25, 0.5, 0.75, 1, 2, 3
	Binary alloy-0, 0.5, 1, 2, 3
Addition temp. (°C / °F)	750 / 1382
Holding time (min)	5, 60
Preheat temp. (°C / °F)	Graphite mold-750 / 1382
	Grain refiner-250 / 482
Pouring temp. (°C / °F)	720 / 1328

3.4 TENSILE MOLD CASTING

In this research, tensile mold castings were carried out to evaluate the tensile and other mechanical properties of AZ91E alloys with ZnO addition.

An ASTM B108-06 standard tensile mold made of H13 steel was used to prepare tensile specimens and is shown in Fig. 3.4.1. There were six thermocouple slots in the mold to measure the mold temperature. The mold was coated with Foseco Dycote 36 to ease casting ejection. Coating was done with compressed air spray gun at 30-40 kPa air pressure to ensure optimum application of coating.

Tensile mold was preheated in a gas fired furnace (Speedy-Melt, Mcenglevan, Danville, Illinois, USA). Temperature of the mold was measured by inserting K-type thermocouples in the mold slots and then connecting through thermal data acquisition system. Temperature at gauge point

(middle thermocouple slot of the mold) was maintained at $510 \pm 5°C$ / $950 \pm 9°F$ during pouring the material.

The melting and casting procedure used for tensile mold casting is similar to that of the graphite mold casting (section 3.3). The quantity of the virgin AZ91E alloy melted for each experiment was approximately 1200 g.
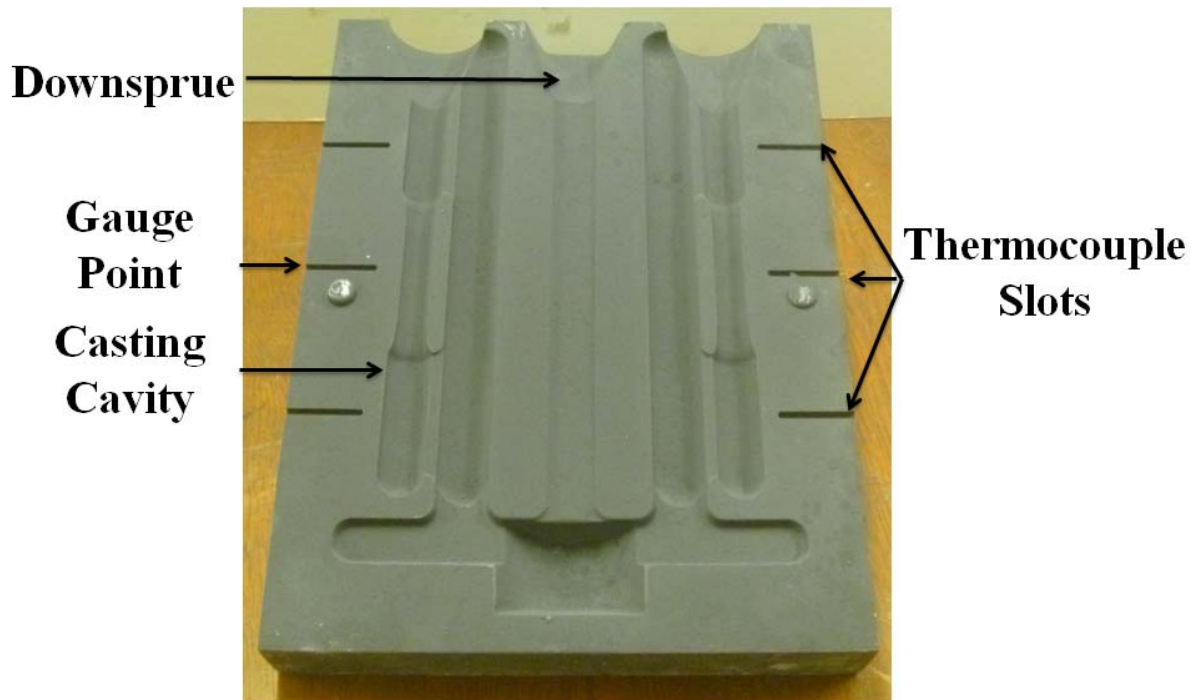
Fig. 3.4.1 ASTM B108-06 standard tensile mold.

Varying levels (0, 0.25, 0.5, 0.75, 1 and 3 wt.%) of ZnO were preheated to $250°C$ / $482°F$, added to the melt at $750°C$ / $1382°F$ and stirred with Foseco Dycote 36 coated steel propeller coupled with a hand drill for 30 seconds. After stirring, the melt was held in the furnace for 5 minutes. Similar to graphite mold casting (section 3.3) any oxide that formed on the top of the melt was skimmed before pouring.

The exact time for placing the preheated tensile mold in the pouring platform to maintain the temperature at gauge point at desired level ($510 \pm 5°C$ / $950 \pm 9°F$) during pouring, was

determined by trial and error. Molten material was directly poured from the crucible to the tensile mold at 720°C / 1328°F.

The cast samples were cooled in still air and removed from the tensile mold ten minutes after the pouring. Two tensile bar specimens were prepared for each pour, and one repeat pour was made. Thus, a total of four tensile bars were available for each condition shown in Table 3.4.1.

Table 3.4.1 Tensile Mold Casting Parameters

Parameter	Values
Addition level (wt.%)	0, 0.25, 0.5, 0.75, 1, 3
Addition temp. ($^{\circ}$C / $^{\circ}$F)	750 / 1382
Holding time (min)	5
Preheat temp. ($^{\circ}$C / $^{\circ}$F)	Tensile mold-510±5 / 950±9
	Grain refiner-250 / 482
Pouring temp. ($^{\circ}$C / $^{\circ}$F)	720 / 1328

Optimum grain refiner addition levels for tensile mold castings were determined from graphite mold casting experiments. Holding time was kept constant at 5 minute, as fading effect of ZnO in AZ91E was not observed in graphite mold casting for one hour (Section 4.2).

3.5 THERMAL ANALYSIS

Thermal analysis was carried out to record and quantify the solidification history of AZ91E and Mg-9 wt.% Al binary alloy for graphite mold casting. Data were collected at 5 readings per second for 10 minutes. Data gathered through data acquisition system (Daytronic System 10) was transferred to a computer and analyzed using Microsoft EXCEL$^{\circledR}$.

Cooling curves were generated from the temperature-time data and then analyzed to determine undercooling (UC), cooling rate (CR) and freezing range (FR) for each casting condition. The UC was measured as the decrease in temperature of the cooling curve near the beginning of solidification temperature, while CR was calculated as the rate of temperature drop from pouring

temperature to just above liquidus temperature. The FR was measured as the difference between the liquidus and solidus temperatures determined from the cooling curves. These three parameters are shown in Fig. 3.5.1 for a typical cooling curve of base AZ91E alloy obtained from this research.
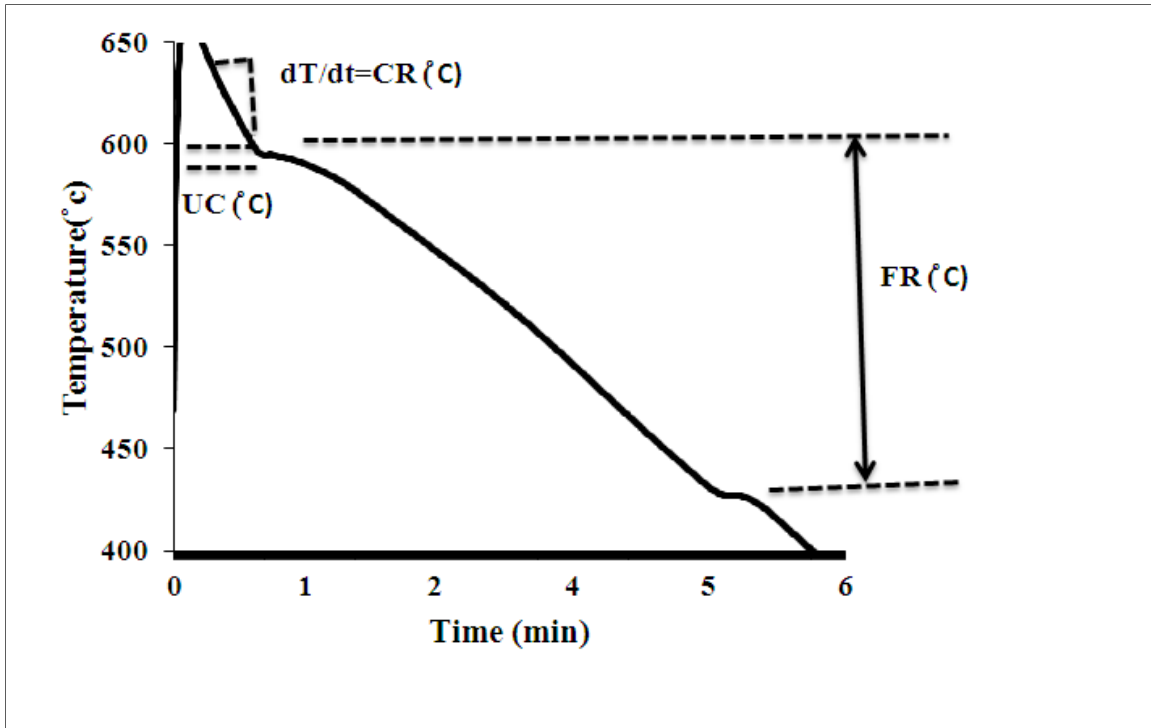
Fig. 3.5.1 Typical cooling curve of AZ91E alloy.

3.6 MICROSTRUCTURE ANALYSIS

For graphite mold castings (both AZ91E and Mg-9 wt.% Al alloys), samples were extracted from castings for optical microscopy (OM) and scanning electron microscopy (SEM). A schematic showing the test surface is as shown in Fig. 3.6.1. Also, a schematic of the permanent tensile mold and sampling area (for metallography, hardness and porosity) are shown in Fig. 3.6.2.

Graphite and permanent tensile mold castings were sectioned to get test samples. All the analyses were done on the test surfaces as indicated in Fig. 3.6.1 and Fig. 3.6.2. The sectioned cast samples were subject to solution heat treatment at 420˚C / 788˚F for 24 hours and air quenched to dissolve eutectic $Mg_{17}Al_{12}$ located at the grain boundary and better facilitate grain size measurement.

57
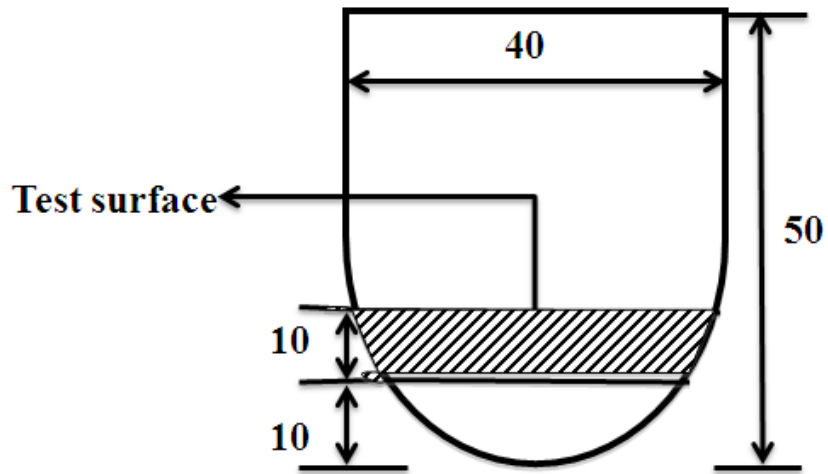
Fig. 3.6.1 Graphite mold castings indicating test surface (all dimensions are in mm).

Solutionized samples were ground successively using 120, 300, 600 and 1200 grit silicon carbide papers using water as lubricant in a grinding wheel of 150 rpm. Samples were held by hand and optimum pressure was applied. Samples were then polished by Lecloth in the same grinding wheel set up, successively using 5 µm Al_2O_3 for 3-4 minutes (in complimentary rotation), 3 µm diamond suspension for 3 minutes (in complimentary rotation) and finally 1 µm diamond suspension for 2 minutes (in contra rotation). After every polishing stage, the samples were cleaned by ethyl alcohol and dried with blast of compressed air.

Test surfaces of polished samples were analyzed using a JEOL JSM-6380LV scanning electron microscope (SEM) with backscattered electron detector (BSE) and the morphology of the alloys was observed. Energy dispersive X-ray (EDX) analysis was also performed to determine the chemical composition of the phases observed in the alloys. SEM fractography analysis was conducted on the tensile mold samples to analyze the fracture surfaces. The EDX point analysis was conducted in two areas on both matrix and β-phase and 10 point readings in each area were taken to find an average value. SEM operating conditions, i.e., voltage, magnification, working distance etc., are given in each SEM micrographs.
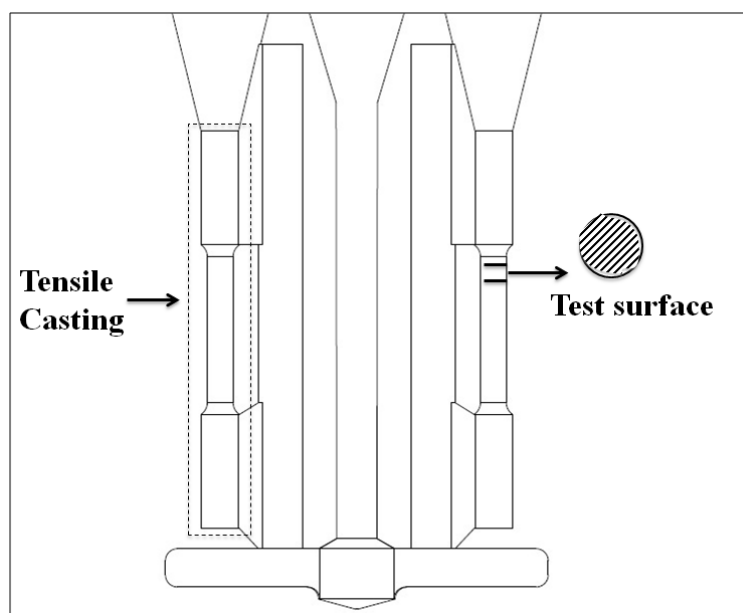
Fig. 3.6.2 Schematic showing the test surface of permanent tensile mold cast sample.

Optical microscopy (OM) was performed on the test surface of graphite and permanent tensile mold castings by using Buehler optical lab microscope in conjunction with Buehler OMNIMET® image analysis software. OM was used to characterize the microstructure and measuring the grain size of the alloys.

For OM, polished samples were etched with an etchant solution. Chemical composition of the etchant used is provided in Table 3.6.1. The samples were gently agitated in the etchant solution for 30 seconds and then quickly rinsed with ethyl alcohol and dried with compressed air.

Table 3.6.1 Chemical Composition of Etchant Solution

Chemicals	Quantity
Distilled water	10 ml
Acetic acid	10 ml
Ethanol	100 ml
Picric acid	6 gm

The linear intercept method was used to measure the grain sizes of the etched samples. A minimum of one hundred grain size readings were taken for grain size measurement of each sample.

3.7 TENSILE TESTING

Uniaxial tensile tests were conducted on the tensile bar samples at ambient temperature to determine the yield strength, ultimate tensile strength and elongation of the AZ91E alloys. A computer controlled universal material testing machine (United, Model- STM-50KN) was used at a nominal strain rate of 12 mm/min. An extensometer was attached to the gauge section to measure the tensile strain. Four samples of each alloy were tested to know the average final tensile properties (0.2% yield stress-YS, ultimate tensile stress- UTS and elongation) of the alloys. Fracture surface morphologies and microstructures of the fracture surface were observed along the tensile loading direction using SEM. An image of a tensile bar specimen is shown in Fig. 3.7.1.
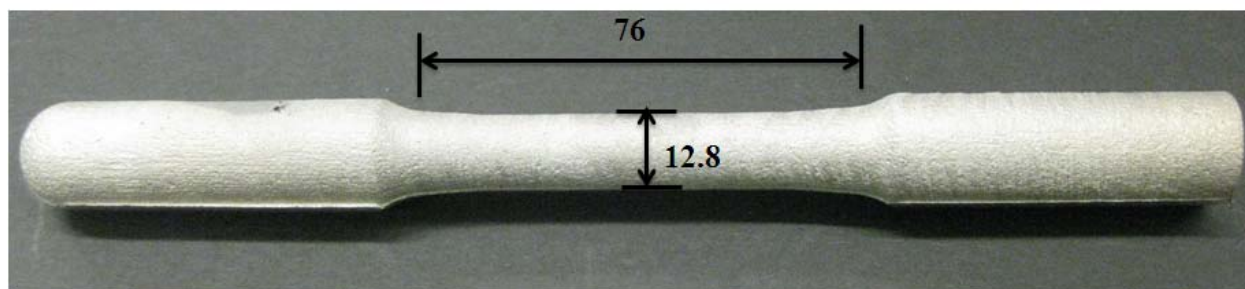
Fig. 3.7.1 Tensile bar specimen (all dimensions are in mm).

3.8 HARDNESS TESTING

Hardness measurements of as cast non-solutionized tensile mold samples of refined and unrefined AZ91E alloys were taken on test surface as shown in Fig. 3.6.2. Rockwell Hardness E (HRE) and Vickers microhardness measurements of the alloy matrix (HV) were carried out on the test surfaces for all the alloys. For HRE values, a minimum of 25 readings were taken on test surface of each sample using a Rockwell hardness testing machine (Universal). A 1/8″ steel ball indenter with 10 kg minor and 100 kg major load were used to create an indent on the surface. Vickers microhardness tester (Buehler) was used to collect HV values. HV values were obtained

as an average of 10 indentations on each sample of the alloys with 100 g applied load and dwell time of 15 seconds.

3.9 POROSITY MEASUREMENT

The porosity of the permanent tensile mold casting was measured using the Archimedes principle on the test surface (Fig. 3.6.2). Density of an object can be determined by using this principle. To determine the density, the mass of the cast samples was measured on a scale in the air. Mass of a container with water was also measured. The sample was then submerged in the container at the mid level by suspending it with a fishing wire and the weight in this condition was recorded. The volume of the sample was then calculated by the weight difference of the samples in the air and in submerged condition. The porosity of the sample was calculated using Equation 3.9.1 with known theoretical density of the sample [Ho, 2009]:

$$\% \text{ porosity} = \frac{100}{\rho_s}\left(\rho_s - \frac{M_m\rho_w}{M_{m+w}-M_w}\right) \qquad\qquad \text{Equation 3.9.1.}$$

where ρ_s is the theoretical density of the sample (g/cm^3), M_m is the mass of the sample (g), ρ_w is the density of water at room temperature (0.9982 g/cc) and M_{m+w} is the mass of water with sample.

Chapter 4: Results and Discussion

This chapter closely follows the experimental procedures described in the previous chapter. In every section, an analysis follows the presentation of results. Graphite mold data for grain refinement, fading effects, refinement mechanism and thermal analysis are presented for the AZ91E alloy, followed by similar data for the Mg-9 wt.% Al alloy (section 4.1-4.9). The tensile casting results are then presented (section 4.10-4.11). Finally, the tensile samples are analyzed for porosity (section 4.12).

4.1 GRAIN REFINEMENT OF AZ91E ALLOY (GRAPHITE MOLD)

Optical micrographs of as-cast and solutionized AZ91E alloy samples produced in graphite mold castings are shown in Fig. 4.1.1. The as-cast AZ91E, shown in Fig. 4.1.1-a consists of two distinct phases of α-Mg and β-$Mg_{17}Al_{12}$. The grain structure is highly dendritic in nature. After solution heat treatment, the β-$Mg_{17}Al_{12}$ is dissolved and the grain boundaries are clearly visible as shown in Fig. 4.1.1-b. The average grain size of the base AZ91E alloy was 217 μm. With 0.5 wt.% and 0.75 wt.% ZnO addition, the average grain sizes of the alloy were 126 μm and 108 μm, respectively (Fig. 4.1.1-c and Fig. 4.1.1-d). The average grain sizes of the alloys with different levels of ZnO addition for 5 minutes holding time are summarized in Fig. 4.1.2 and Table 4.1.1. With increasing ZnO addition, the grain size of the alloys gradually decreased, up to

---

† Most of the data presented in this chapter has been accepted or submitted for publication in peer reviewed journals.

1. Saha, S., Ravindran, C., "Grain Refinement of AZ91E and Mg-9 wt.% Al Binary Alloys Using Zinc Oxide," International Journal of Metalcasting, Accepted on May 13, 2014
2. Saha, S., Ravindran, C., "Effects of Zinc Oxide Addition on the Microstructure and Mechanical Properties of AZ91E Mg Alloy." International Journal of Metalcasting, Submitted on July 12, 2014

an addition level of 0.75 wt.% ZnO. Beyond 0.75 wt.% addition of ZnO (up to 3 wt.%) there was no significant change in grain size suggesting maximization of the potency of ZnO at 0.75 wt.% ZnO in AZ91E alloy. The slight increase in grain size beyond 1 wt.% ZnO is not significant if we consider the error bars. The possible reason for maximization of the potency of ZnO addition in AZ91E at 0.75 wt.% addition is that with ZnO addition beyond 0.75 wt.% a balance is reached where increasing the number of nuclei is countered by increase in latent heat released and further reduction in grain size is not possible [Easton et. al., 2001], [Liu et. al., 2004].
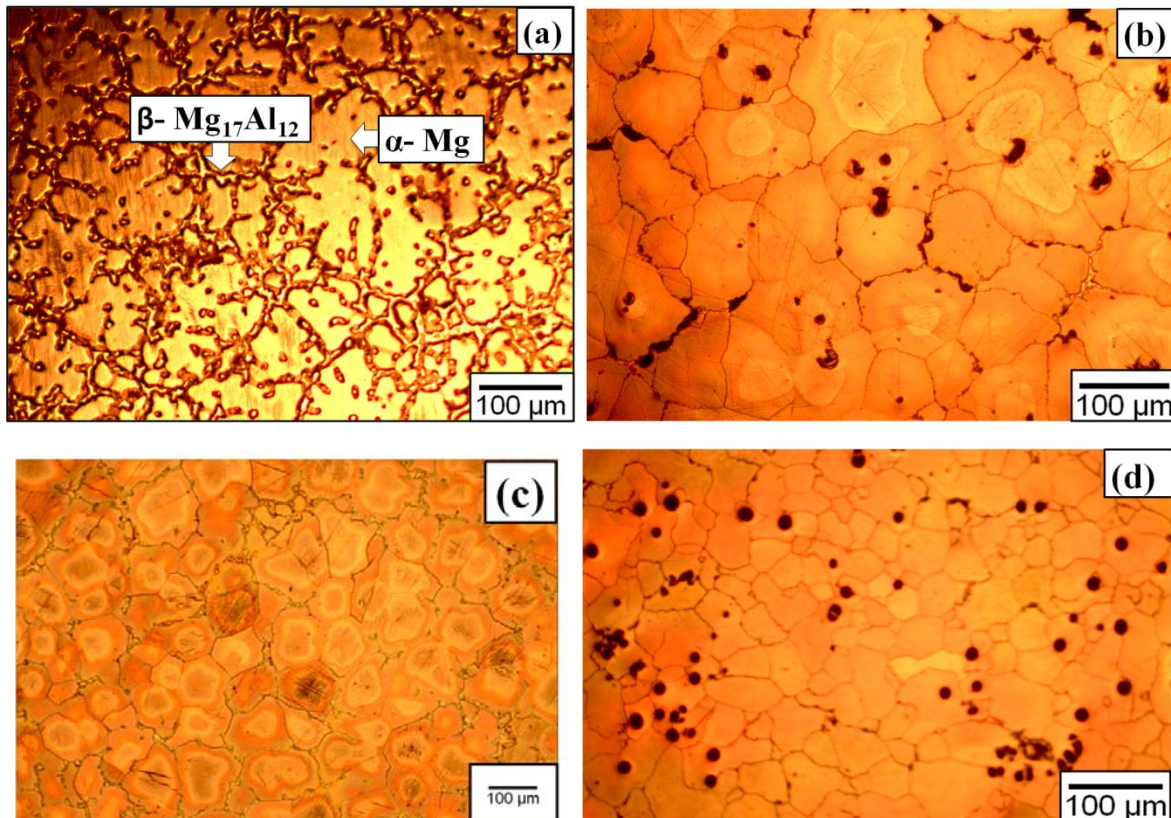
Fig. 4.1.1. Optical micrograph of (a) as cast base AZ91E alloy; after solutionized for 24 hours at 420°C/788°F and etched (b) base alloy (average grain size 217 µm) (c) AZ91E+0.5 wt.% ZnO (average grain size 126 µm) (d) AZ91E+0.75 wt.% ZnO (average grain size 108 µm).
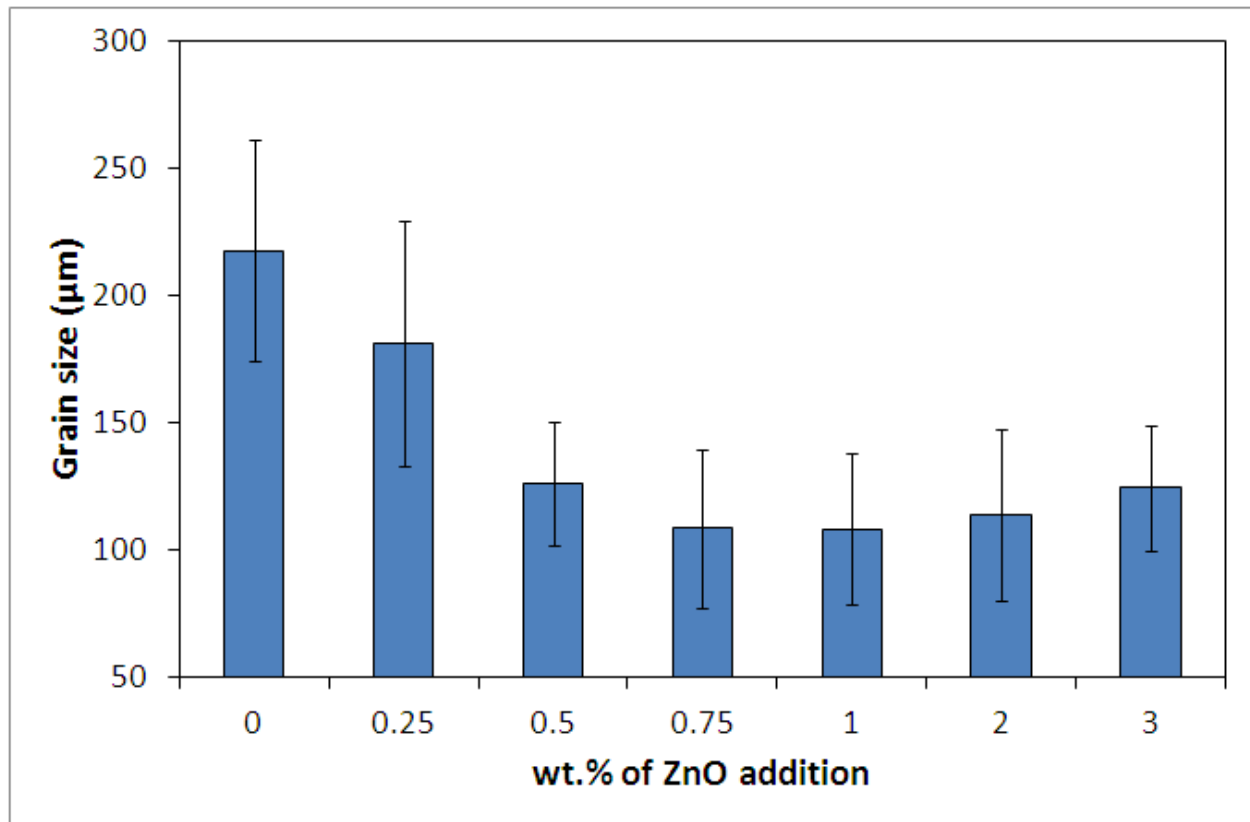
Fig. 4.1.2. Average grain size of AZ91E alloy with various ZnO addition levels.

Table 4.1.1. Grain Size of AZ91E Alloy at Different Addition Levels of ZnO
(Graphite Mold)

Addition Level (wt.%)	Grain Size (µm)	Std. Dev. (+/-)	Change (%)
0	217	43.71	-
0.25	181	48.20	16.58↓
0.5	126	24.06	41.93↓
0.75	108	31.32	50.23↓
1	108	29.40	50.23↓
2	114	33.72	47.46↓
3	124	24.53	42.85↓

4.2 FADING IN AZ91E ALLOY (GRAPHITE MOLD)

During grain refinement, holding the melt for a long time after the addition of the grain refiner before pouring, usually leads to develop coarse grain structure, instead of otherwise fine grain structure. This loss of refinement is termed as fading which is usually attributed to either dissolution or settling (or both) of nucleating particles during long holding [Chakraborty et. al., 2005]. A strong resistance to loss of grain refiner efficiency with holding of the melt at elevated temperature for extended periods of time is an important characteristic of a good grain refiner [Schumacher et. al., 1998]. The fading behaviour of ZnO in AZ91E alloy was examined by comparing 5 and 60 minutes after adding 0.5 wt.% ZnO and same 5 and 60 minutes after adding 3 wt.% ZnO. The results are shown in Fig. 4.2.1. No significant fading was observed and this is consistent with the observations of Fu et. al.,2008 using pure Mg with ZnO. The grain sizes at different conditions are shown in Table 4.2.1. The grain size remained constant at approximately 125 μm.
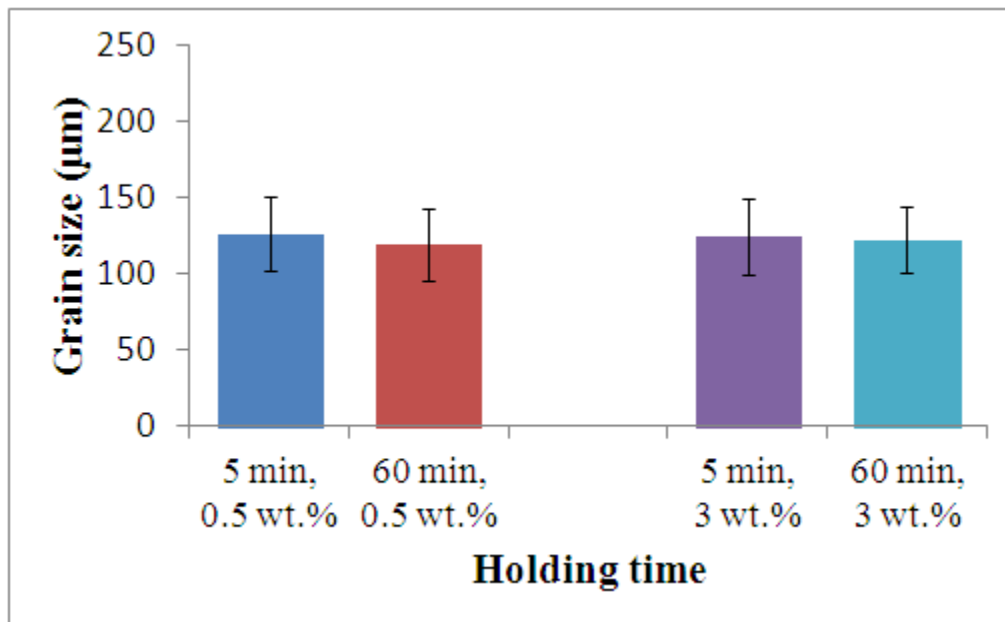
Fig. 4.2.1. Fading effect of ZnO in AZ91E at different holding times and addition levels.

Table 4.2.1. Grain Size of AZ91E Alloy at Different Addition Levels of ZnO and Holding Time

Addition Level (wt.%)	Holding Time (Min.)	Grain Size (μm)	Std. Dev. (+/-)	Change (%)
0.5	5	126	24.06	-
	60	119	23.35	5.55↓
3	5	124	24.53	-
	60	122	22.00	1.61↓

4.3 MECHANISM OF GRAIN REFINEMENT IN AZ91E ALLOY (GRAPHITE MOLD)

SEM analysis of AZ91E enabled an understanding of refinement mechanism of ZnO. It has been identified by other researchers [Zhang et. al., 2005], [Campbell, 1993] that a good lattice match between nucleating solid and grain refiner will promote heterogeneous nucleation. Both Mg and ZnO have excellent crystallographic similarity as discussed in subsection 2.3.2. With such crystallographic similarities it was expected that ZnO particles would act as heterogeneous nuclei for Mg.

SEM image of AZ91E alloy with 3 wt.% ZnO is shown at low and higher magnification in Fig. 4.3.1-a and 4.3.1-b. Fig. 4.3.1-a shows a particle towards the center of the grain (indicated by arrow). The EDX in Fig. 4.3.1-c clearly indicated the Zn and O peaks. Thus it can be assumed that ZnO provided as heterogeneous nucleation site for α-Mg.
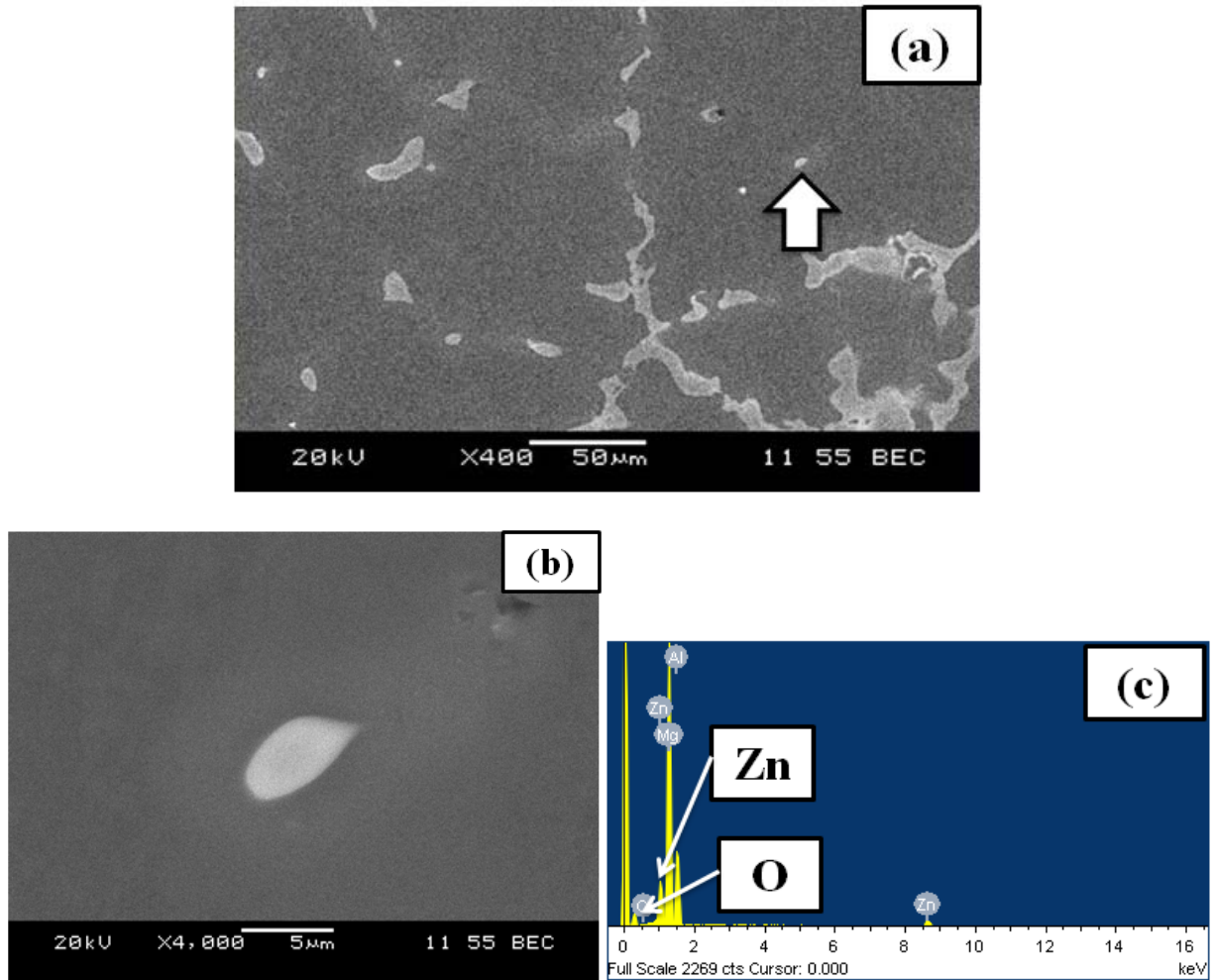
Fig. 4.3.1. SEM image of AZ91E with 3 wt.% of ZnO (a) at low magnification and (b) at higher magnification and (c) corresponding EDX image of particle shown in (b).

4.4 THERMAL ANALYSIS OF AZ91E ALLOY (GRAPHITE MOLD)

The cooling curves for the base AZ91E alloy and AZ91E with 0.5 wt.% ZnO are shown in Fig. 4.4.1. By analyzing the cooling curves, it was found that the base AZ91E alloy had an undercooling of $0.4°C$ / $0.7°F$ for primary phase nucleation. The undercooling was measured as the decrease in temperature of the cooling curve just after solidification beginning temperature ($\sim 595°C$ / $1103°F$). With the addition of ZnO, no undercooling was observed in the generated cooling curves further suggesting that the refinement mechanism was primarily heterogeneous nucleation by ZnO.
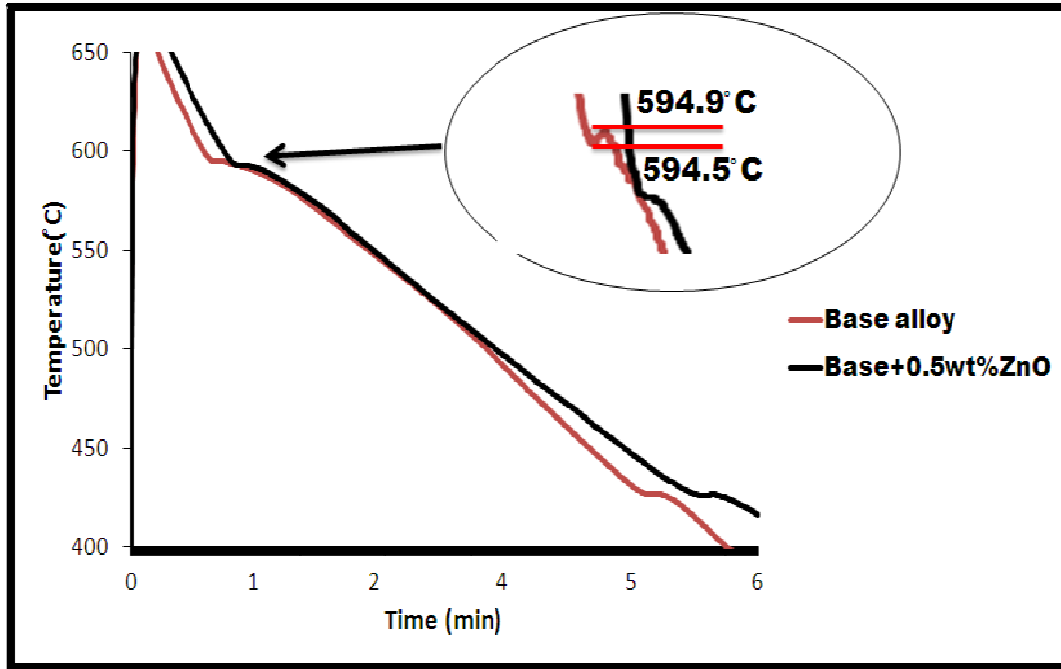
Fig. 4.4.1. Cooling curve of base AZ91E alloy and AZ91E with 0.5 wt.% ZnO. Enlarged region as indicated is shown in the inset.

The freezing range (FR) of the alloys with different levels of ZnO is presented in Table 4.4.1. The FR was measured as the difference between the liquidus and solidus temperatures determined from the cooling curves. For base AZ91E alloy, FR was 166.8 C / 300.2 F, whereas after 3 wt.% addition of ZnO FR was 169.5 C / 305.1 F. These increased FR with ZnO addition is an indication that the ZnO is changing the solidification behaviour of the alloy.

Along with an increase in FR with the increase of ZnO addition, the solidus temperature decreased as shown in Fig. 4.4.2. A similar trend was also observed by Wang et. al., 2002 while adding different addition levels of Zn in Mg-Al alloys. As such, the trends may be attributed to increased solute level in the alloy with increasing addition of ZnO to the alloy. This trend of increased Zn solute with addition of ZnO to AZ91E prompted an investigation of the effect of ZnO on binary Mg-9 wt.% Al. Since AZ91E already contains about 0.65 wt.% Zn, the effect of solute Zn from ZnO in AZ91E during solidification process will be difficult to differentiate. By using Mg-9 wt.% Al, the effect of solute Zn from ZnO can be very easily determined which will give an account of the effect of ZnO in AZ91E alloy. Cooling rate throughout the experiments

was kept constant at 1.77±0.08˚C/s. Cooling curves of AZ91E alloy at different addition levels of ZnO is provided in Appendix-A3.

Table 4.4.1. Freezing Range of AZ91E Alloy at Different Addition Levels of ZnO

wt.% of ZnO	FR (˚C/˚F)	Std. Dev.(+/-)
0	166.8/300.2	2.14
0.25	166.6/299.9	1.29
0.5	166.8/300.2	0.23
0.75	168.6/303.5	0.91
1	168.5/303.3	1.41
2	171.0/307.8	0.83
3	169.5/305.1	1.27
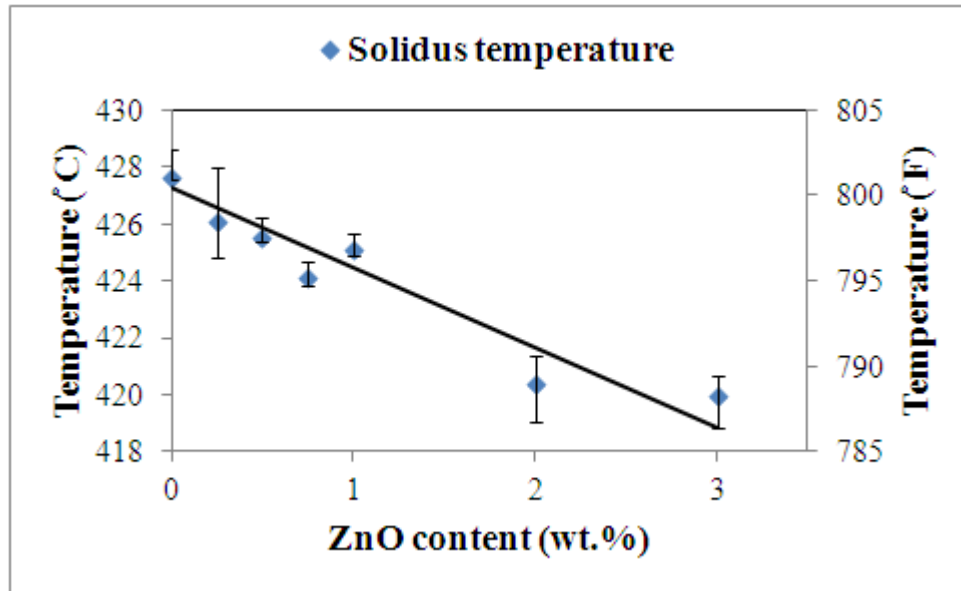
Fig. 4.4.2. Solidus temperature of AZ91E with ZnO content.

4.5 GRAIN REFINEMENT IN Mg-9 wt.% Al ALLOY (GRAPHITE MOLD)

The optical microscopy of solution treated base Mg-9 wt.% Al alloy and with 1 wt.% ZnO addition is shown in Fig. 4.5.1(a-b). All the casting parameters were kept the same as the conditions used for the AZ91E castings. Optical microscopy of the Mg-9 wt.% Al alloys revealed that the average grain size of the base Mg-9 wt.% Al binary alloy was 288 µm which was approximately 24% larger than that of AZ91E alloy. This was likely due to the combined effect of Zn and Mn in the AZ91E alloy. Previous research has shown that both Zn [Fu et. al., 2008] and Mn [Elsayed et. al., 2009] have a grain refining effect on Mg-Al alloys.
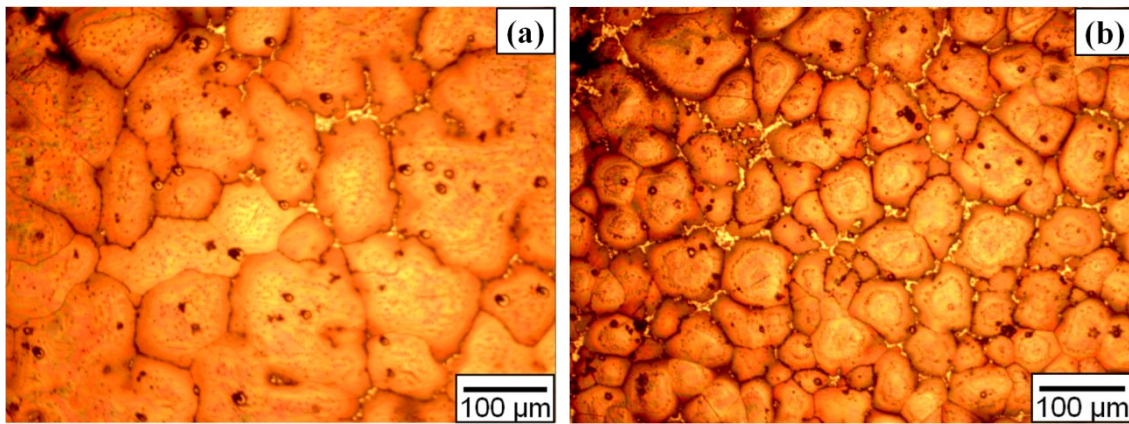
Fig. 4.5.1. Microstructure of Mg-9 wt.% Al binary alloy after solution heat treatment (a) base alloy (average grain size-288 µm) (b) with 1 wt.% ZnO addition (average grain size-121 µm).

Mg-9 wt.% Al binary alloy castings with 0.5, 1, 2 and 3 wt.% of ZnO were produced. The average grain size of Mg-9 wt.% Al with different addition levels of ZnO are shown in Fig. 4.5.2 and the results are summarized in Table 4.5.1. A similar grain refinement trend to that of AZ91E (Fig. 4.1.2) was observed for Mg-9 wt.% Al alloy. Maximum grain size reduction was found at 3 wt.% addition of ZnO (93 µm), although beyond 0.5 wt.% addition of ZnO (121 µm) the grain size reduction was not very significant suggesting maximization of the potency of ZnO at 0.5 wt.% ZnO in Mg-9 wt.% Al binary alloy. The possible reason for maximization of grain refinement potency of ZnO in Mg-9 wt.% Al binary alloy at 0.5 wt.% addition is considered to be similar to that of the addition of ZnO in AZ91E alloy in graphite mold casting (Section 4.1).
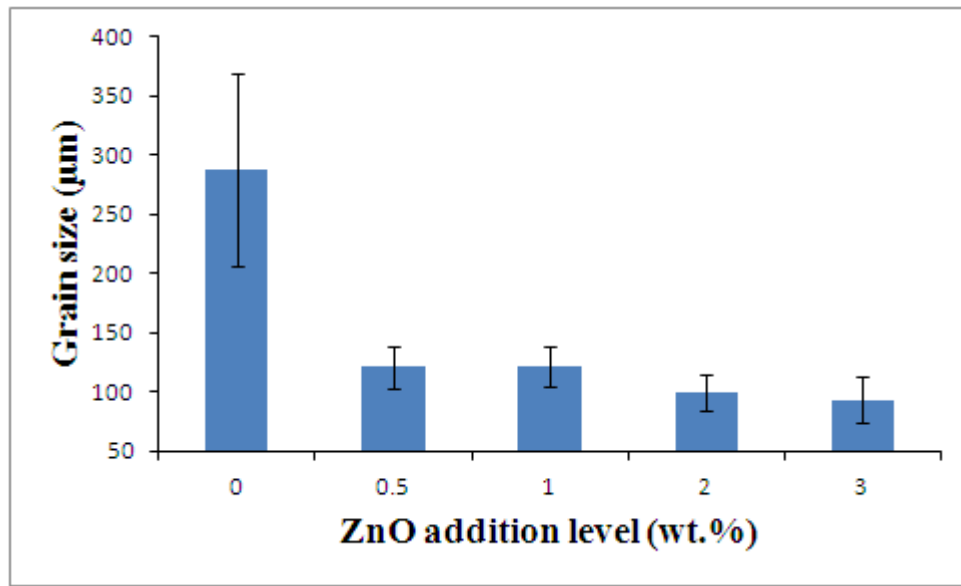
Fig. 4.5.2. Average grain size of Mg-9 wt.% Al binary alloy with various levels of ZnO addition.

Table 4.5.1. Grain Size of Mg-9 wt.% Al Alloy at Different Addition Levels of ZnO

Addition Level (wt.%)	Grain Size (µm)	Std. Dev. (+/-)	Change (%)
0	288	81.09	-
0.5	121	17.38	57.99↓
1	121	16.66	57.99↓
2	100	15.38	65.28↓
3	93	19.32	67.70↓

For complete reduction of ZnO to Zn, the Zn concentration with 0.5 wt.% addition of ZnO to AZ91E (initially containing 0.65 wt.% Zn) would be higher than the same addition to binary Mg-9 wt.% Al (equivalent to 0.4 wt.% Zn). In this experiment, the mean average grain sizes with 0.5 wt.% ZnO addition to AZ91E and Mg-9 wt.% Al were similar at 126 µm and 121 µm respectively. This suggests that the grain refinement achieved by the ZnO particle addition is greater than that gained by an equivalent addition of Zn solute [StJohn et. al., 2013].

4.6 FADING IN Mg-9 wt.% Al ALLOY (GRAPHITE MOLD)

The fading behaviour of ZnO in Mg-9 wt.% Al alloy was examined by comparing 5 and 60 minutes after adding 0.5 wt.% ZnO and same 5 and 60 minutes after adding 3 wt.% ZnO. The results are summarized in Table 4.6.1 and graphically shown in Fig. 4.6.1. The average grain sizes at 0.5 wt.% ZnO addition after 5 minutes and 60 minutes were 121 μm and 126 μm respectively. With 3 wt.% ZnO addition average grain sizes after 5 minutes and 60 minutes were 93 μm and 103 μm respectively. No significant fading was observed which is consistent with the results of AZ91E alloy (Fig. 4.2.1).

Table 4.6.1. Grain Size of AZ91E Alloy at Different Addition Levels of ZnO and Holding Time

Addition Level (wt.%)	Holding Time (Min.)	Grain Size (μm)	Std. Dev. (+/-)	Change (%)
0.5	5	121	17.38	-
	60	126	21.10	4.13↑
3	5	93	19.32	-
	60	103	25.28	10.75↑
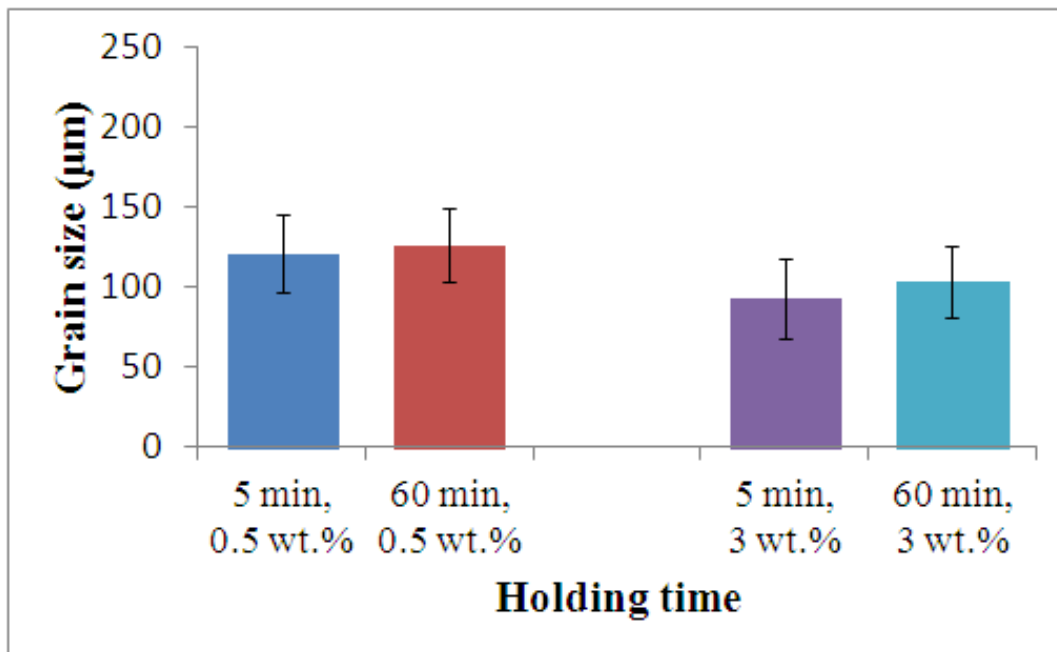
Fig. 4.6.1. Fading effect of ZnO in Mg-9 wt.% Al binary alloy at different holding times and addition levels.

4.7 MECHANISM OF GRAIN REFINEMENT IN Mg-9 wt.% Al ALLOY (GRAPHITE MOLD)

The SEM and corresponding EDX results of base Mg-9 wt.% Al are shown in Fig. 4.7.1. The sample consisted of α-Mg matrix (Point A in Fig. 4.7.1) and β- $Mg_{17}Al_{12}$ (Point B in Fig. 4.7.1).
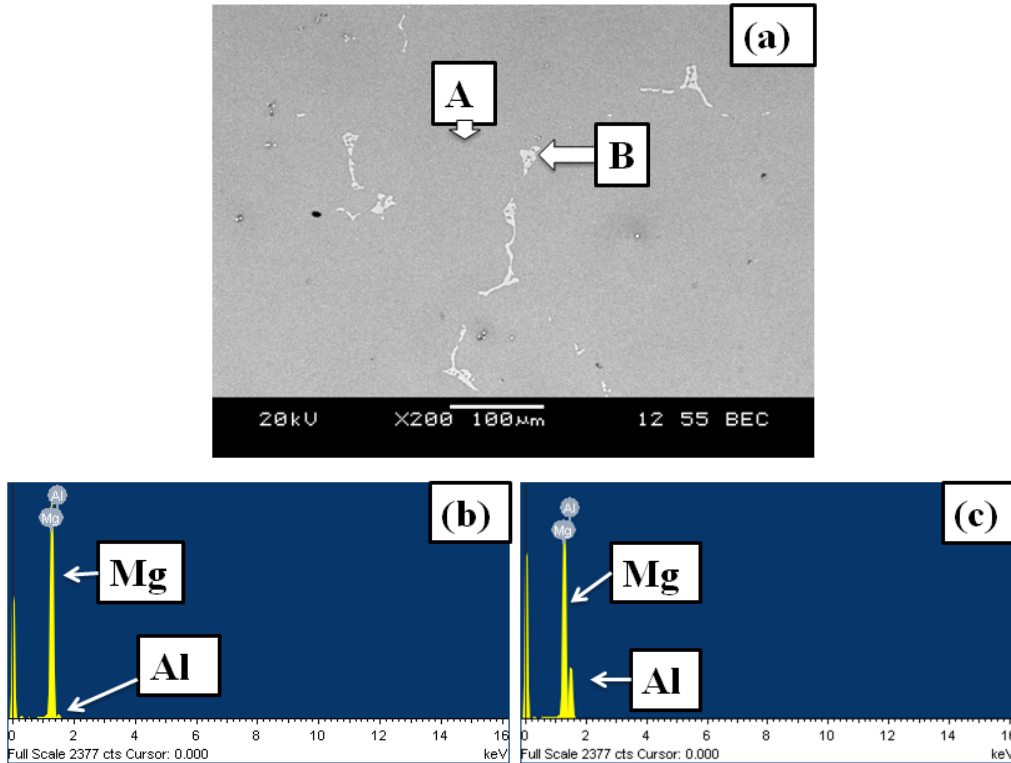
Fig. 4.7.1. (a) SEM image of base Mg-9 wt.% Al showing α-phase and β-phases (b-c) shows the EDX analysis of point-A and point-B respectively.

With increased ZnO addition, the β-phase was found to be increasingly enriched with Zn solute as shown in Fig. 4.7.2. This Zn solute is thought to have been liberated from ZnO because it reacted with Mg according to Equation 4.7.1 [Fu et. al., 2008]. Thermodynamic data of this chemical reaction is provided in Appendix-A4.
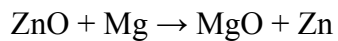
$$ZnO + Mg \rightarrow MgO + Zn \hspace{4cm} \text{Equation 4.7.1}$$

Therefore, since only a small amount of added ZnO particles act as nucleating sites, it is possible that some ZnO may have dissociated, which in turn, introduced Zn into the melt.

Fig. 4.7.2 shows SEM image and corresponding Zn element maps of base Mg-9 wt.% Al and with 1 wt.%, 2 wt.% and 3 wt.% of ZnO addition, respectively. It is evident from the image that with an increased ZnO content in Mg-9 wt.% Al, increased Zn solute is observed (in Fig. 14-b some background noises can be seen though Zn is absent). This supports results from thermal analysis suggesting increased FR and decreased solidus temperature with ZnO addition. Increased divorcing of intermetallic phases with additions of ZnO is also clearly visible, which is indicative of increased Zn solute presence and effective grain refining capability of ZnO [Dahle et. al., 2001].
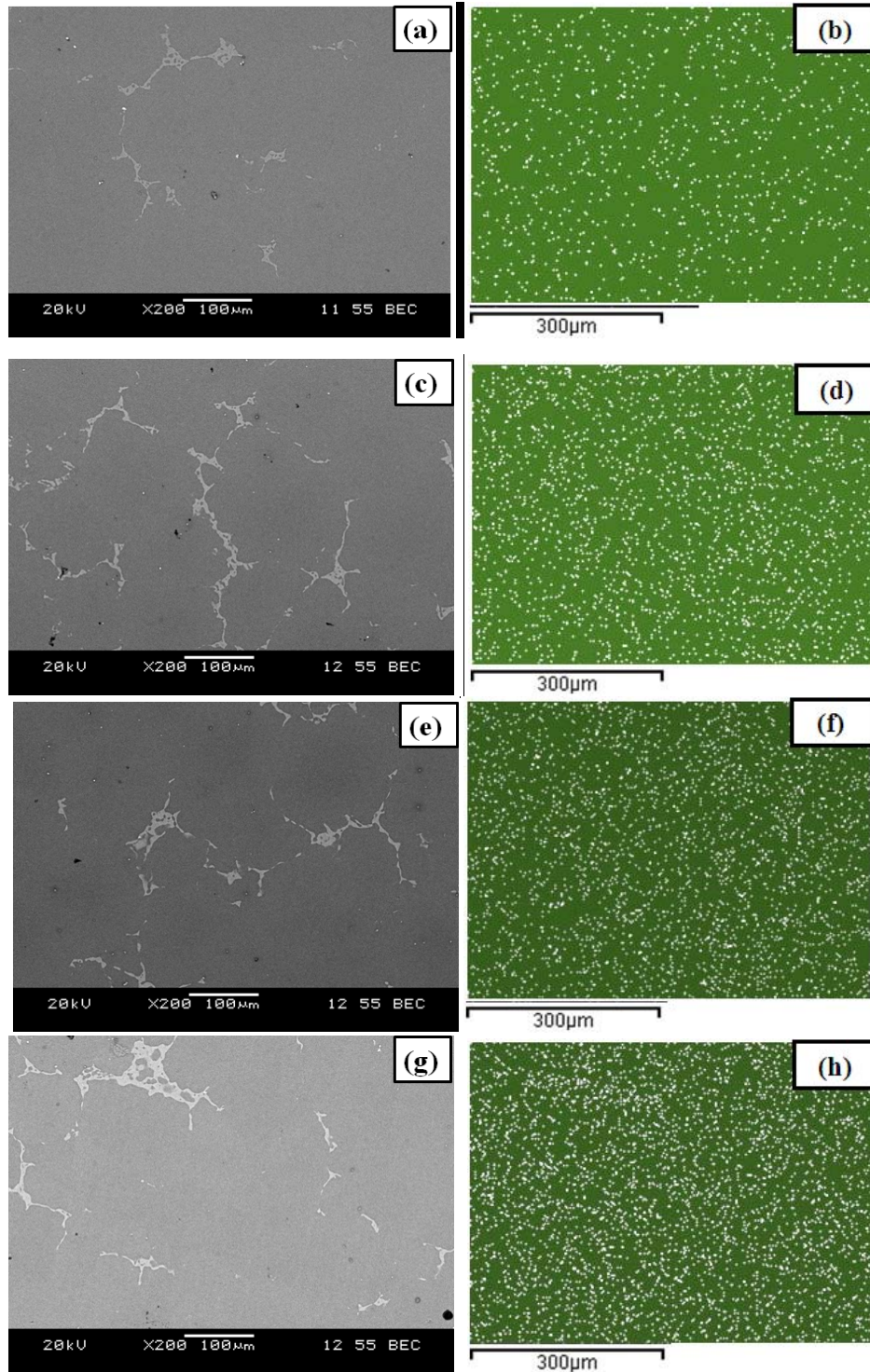
Fig. 4.7.2. SEM image and corresponding Zn element map of (x200) of Mg-9 wt.% Al with (a-b) no addition of ZnO, (c-d) 1 wt.% ZnO addition, (e-f) 2 wt.% ZnO addition (g-h) 3 wt.% ZnO addition.

Fig. 4.7.3 shows the SEM and EDX results of Mg-9 wt.% Al with 2 wt.% addition of ZnO. The bright white spots seen embedded within the $Mg_{17}Al_{12}$ indicate enriched Zn. Zn has a relatively very high growth restriction factor of 5.31 in Mg (Table 2.5.1). This high growth restriction factor likely restricted the α-Mg grain growth by generating constitutional undercooling in solid-liquid interface, thus limiting the size of the grain [Lee et. al., 2000].
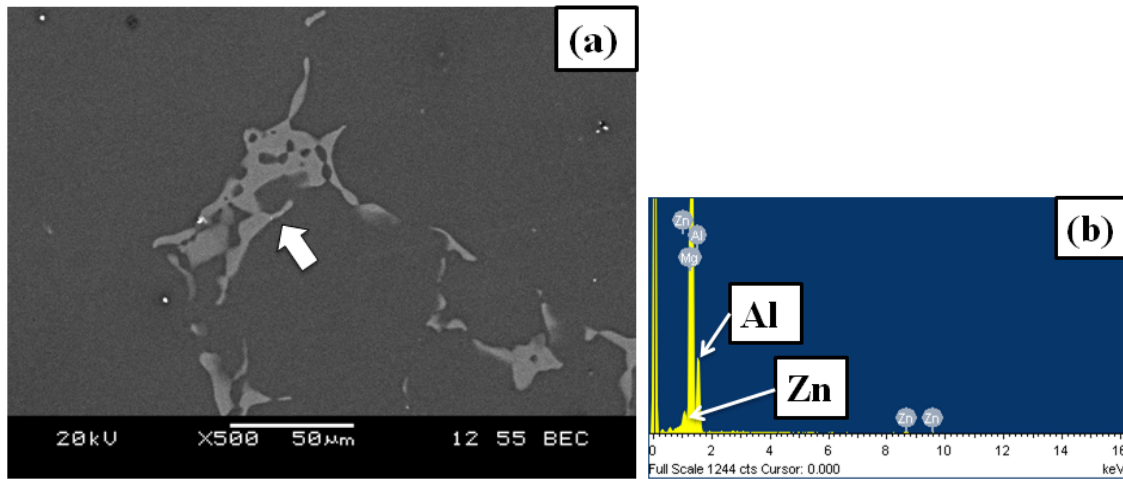
Fig. 4.7.3. Mg-9 wt.% Al with 2 wt.% ZnO (a) SEM image and (b) EDX results at location indicated by arrow.

4.8 THERMAL ANALYSIS OF Mg-9 wt.% Al ALLOY (GRAPHITE MOLD)

Thermal analysis of Mg-9 wt.% Al alloy with ZnO addition revealed the same characteristics to that of AZ91E alloy. By analyzing the generated cooling curves, no undercooling was observed with the addition of ZnO for all addition levels (cooling curves of Mg-9 wt.% Al alloy at different addition levels of ZnO are provided in Appendix-A5). The freezing range (FR) of the alloys with different levels of ZnO measured from the cooling curves is presented in Table 4.8.1. For base Mg-9 wt.% Al alloy, FR was 160.0°C (288°F), whereas after 3 wt.% addition of ZnO FR was 171.3°C (308.4°F). An increased FR with ZnO addition indicates the similar change in solidification behaviour to that of AZ91E alloy.

Along with an increase in FR with the increase of ZnO addition, the solidus temperature decreased as shown in Fig. 4.8.1. This decreased trend of solidus temperature is also similar to AZ91E alloy (Fig. 4.4.2). Similar thermal behaviours for AZ91E and Mg-9 wt.% Al alloys of

ZnO reinforces that the grain refining mechanism of ZnO for both the alloys appears to be via two routes:- 1) ZnO act as a nucleating site and 2) ZnO reacts with Mg according to Equation 4.7.1 increasing Zn solute in the melt providing growth restriction.

Table 4.8.1. Freezing Range of Mg-9 wt.% Al Alloy at Different Addition Levels of ZnO

wt.% of ZnO	FR (°C/°F)	Std. Dev.(+/-)
0	160.0/288.0	2.9
0.5	166.1/299.0	1.9
1	167.2/300.9	1.78
2	169.4/304.9	1.45
3	171.3/308.4	1.27
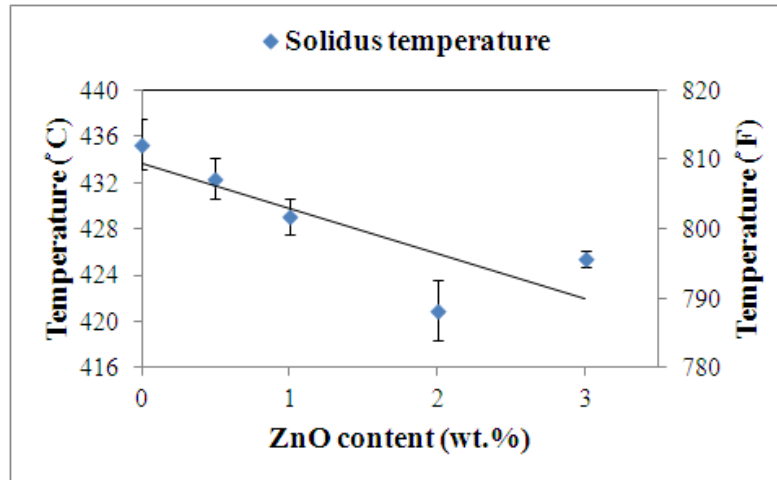
Fig. 4.8.1. Solidus temperature of Mg-9 wt.% Al with ZnO content.

4.9 GRAIN REFINEMENT OF AZ91E ALLOY (PERMANENT TENSILE MOLD)

Optical micrographs of as-cast and solutionized AZ91E alloy samples are shown in Fig. 4.9.1. The as-cast AZ91E (Fig. 4.9.1-a), consists of two distinct phases of α-Mg and β-$Mg_{17}Al_{12}$ as was in graphite mold (Fig. 4.1.1-a). The grain structure is highly dendritic in nature. After solution heat treatment, the β-$Mg_{17}Al_{12}$ is dissolved and the grain boundaries are clearly visible as shown in Fig. 4.9.1-b. The average grain size of the base was 133 μm. The etched surface of

AZ91E + 0.5 wt.% ZnO with grain size of 79 μm is shown in Fig. 4.9.1-c. A significant reduction of grain size as compared to the base AZ91E alloy (Fig. 4.9.1-b) was observed. The average grain size at 0.75 wt.% ZnO was 72 μm. The average grain sizes, measured using optical microscope, at different levels of ZnO addition are summarized in Fig. 4.9.2 and Table 4.9.1. The percentage decrease in grain sizes was comparable to those observed in graphite mold castings (Table 4.1.1). With increasing ZnO addition, the grain size gradually decreased, up to an addition level of 0.75 wt% ZnO. However, beyond 0.5 wt.% addition of ZnO (up to 3 wt.%) no significant change in grain size was observed. The slight increase in grain size beyond 0.75 wt.% ZnO is not significant considering the error bars. The possible reason for maximization of grain refinement potency of ZnO in AZ91E alloy was discussed in section 4.1.
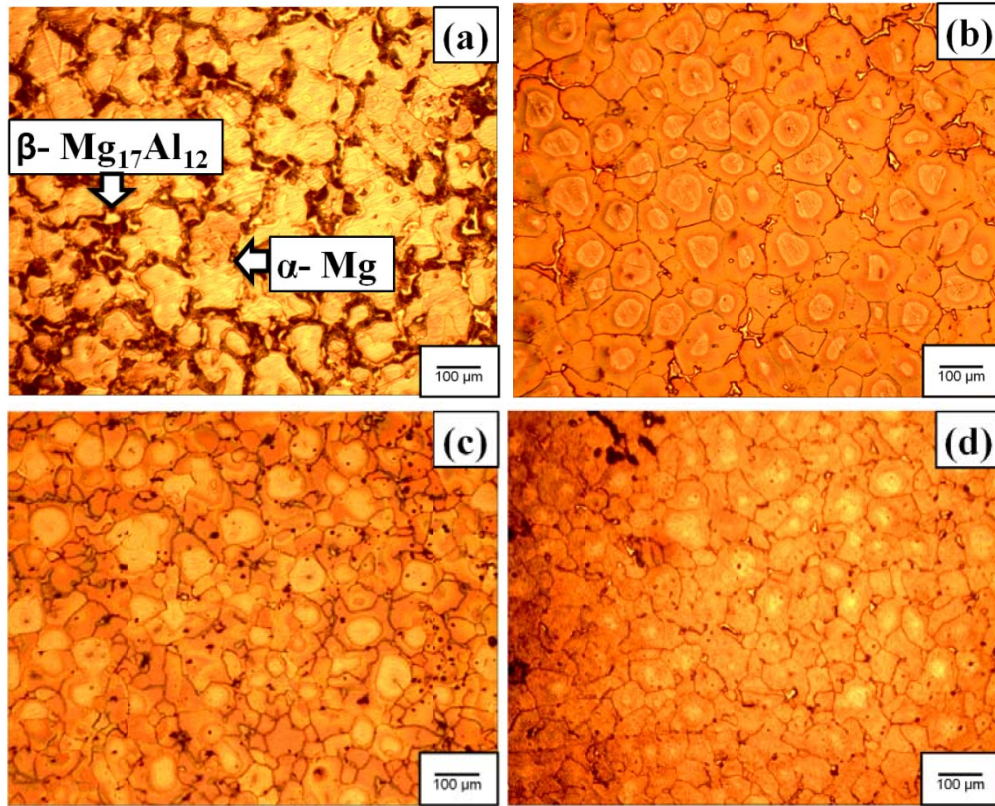
Fig. 4.9.1. Optical micrograph of (a) as cast base AZ91E alloy (b) base alloy after solution heat treatment at 420 C for 24 hours and etching (average grain size 133 μm) (c) AZ91E+0.5 wt.% ZnO (average grain size 79 μm) (d) AZ91E+0.75 wt.% ZnO (average grain size 72 μm).

Table 4.9.1. Grain Size of AZ91E Alloy at Different Addition Levels of ZnO (Permanent Tensile Mold)

Addition Level (wt.%)	Grain Size (μm)	Std. Dev. (+/-)	Change (%)
0	133	23.69	-
0.25	112	17.58	15.79↓
0.5	79	16.77	40.60↓
0.75	72	15.94	45.86↓
1	76	16.38	42.85↓
3	80	14.88	39.85↓
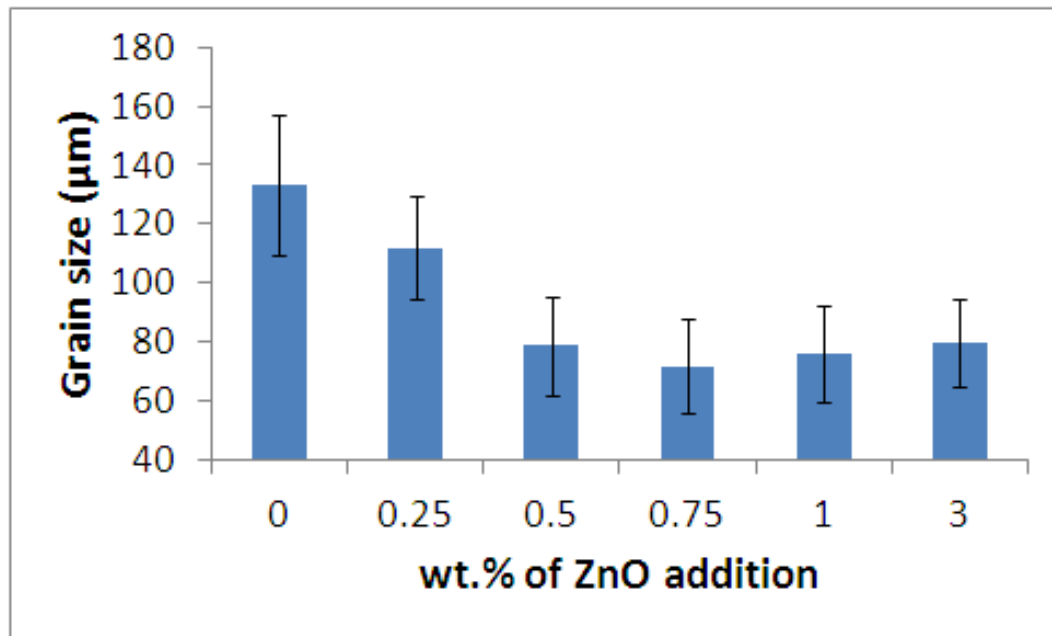
Fig. 4.9.2. Average grain size of AZ91E alloy with increasing levels of ZnO addition in permanent tensile mold casting.

4.10 MECHANISM OF GRAIN REFINEMENT IN AZ91E ALLOY (PERMANENT TENSILE MOLD)

The SEM and corresponding EDX results of base AZ91E alloy in permanent mold casting are shown in Fig. 4.10.1. The sample consisted of α-Mg matrix (Point A in Fig. 4.10.1) and Zn enriched β- intermetallics (Point B in Fig. 4.10.1).
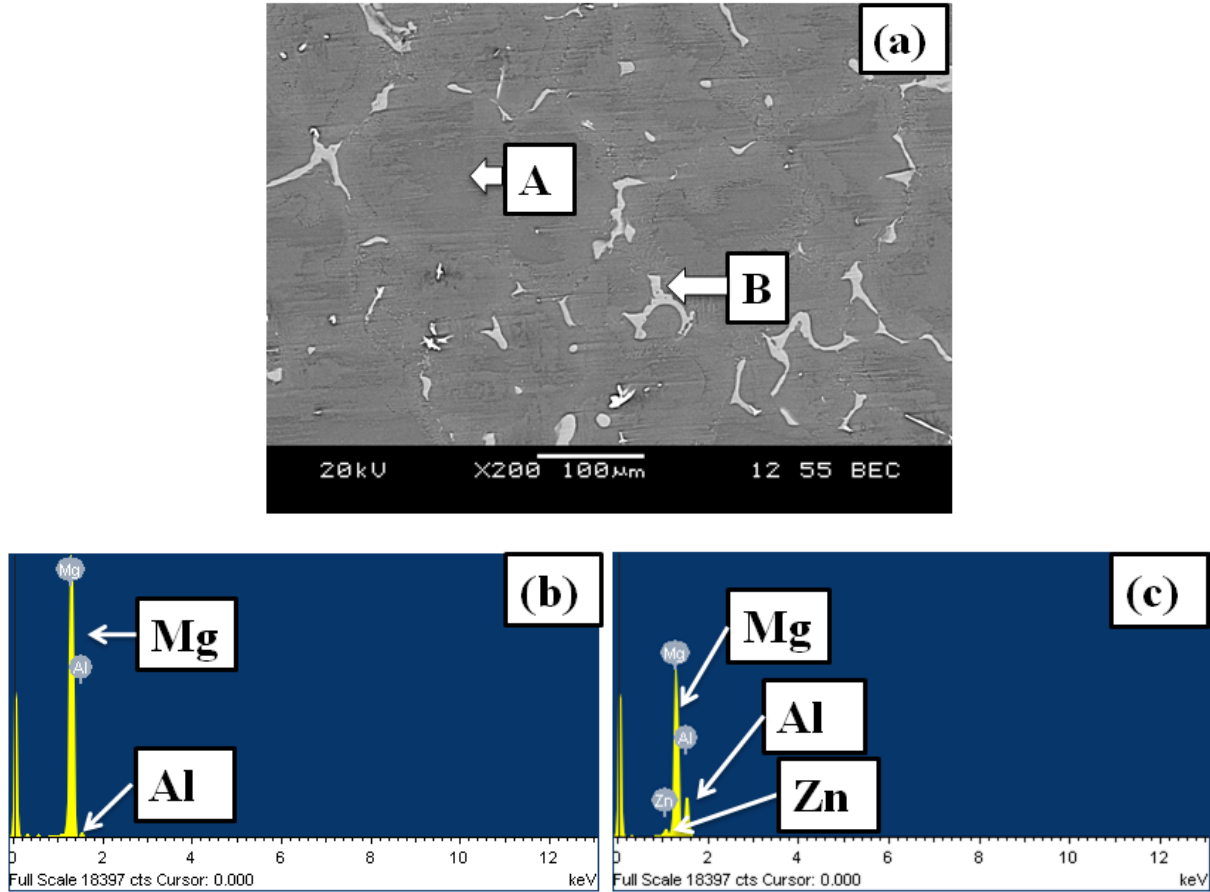
Fig. 4.10.1. (a) SEM image of base AZ91E alloy showing α-phase and β-phase (b-c) shows the EDX analysis of point-A and point-B respectively.

An SEM image of AZ91E+3 wt.% ZnO alloy with particles towards the center of a grain (indicated by arrow) is shown in Fig. 4.10.2. A magnified view of the particle indicated in Fig. 4.10.2-a is shown in Fig. 4.10.2-b. The corresponding EDX (Fig. 4.10.2-c) showed Zn and O peaks which can be assumed that ZnO acted as heterogeneous nucleation site for α-Mg.
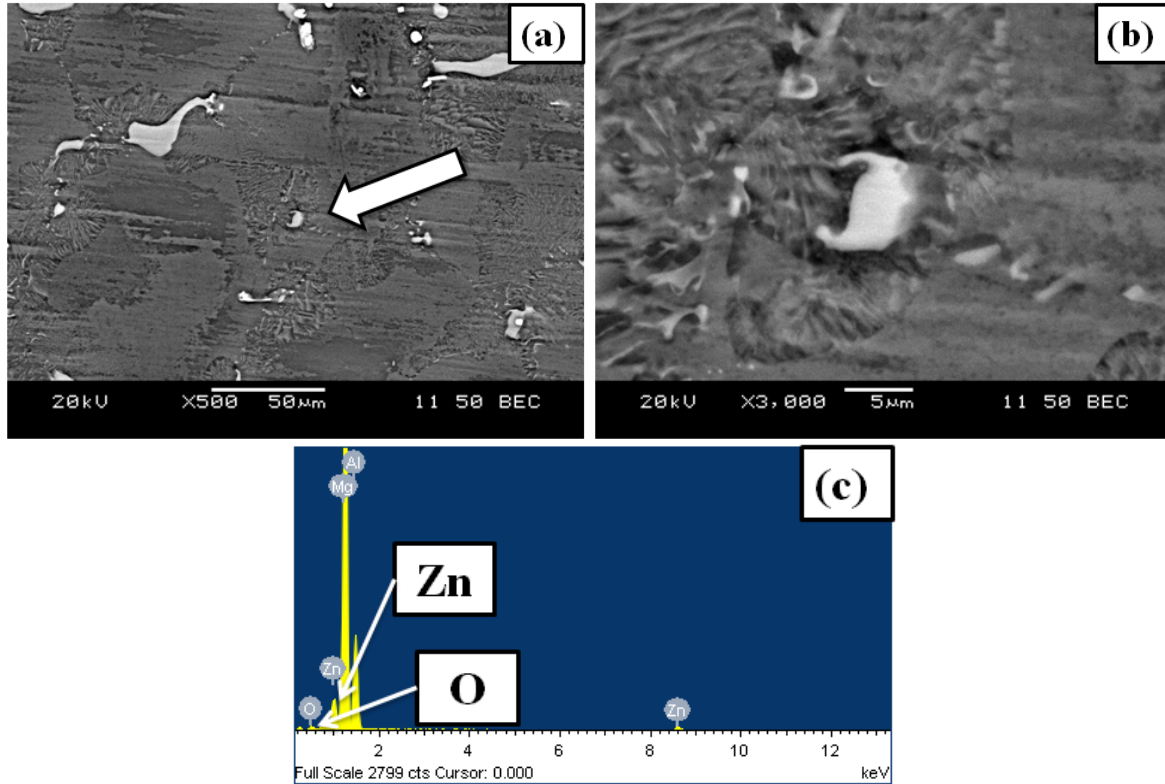
Fig. 4.10.2. SEM image of AZ91E alloy with 3 wt.% ZnO (a) at low magnification (b) at higher magnification and (c) corresponding EDX image of particle shown in (b).

With increasing ZnO addition, the β-phase was found to be increasingly enriched with Zn solute as can be seen from Fig. 4.10.3 and Table 4.10.1. Fig. 4.10.3 shows SEM images and corresponding Zn element maps of base AZ91E alloy and AZ91E alloy with 3 wt.% of ZnO addition, respectively. The Zn content in the alloys obtained through EDX point analysis is presented in Table 4.10.1. The overall Zn content in the alloys found through EDX area analysis is shown in Fig. 4.10.4. The overall Zn content in the base alloy and with addition of 3 wt.% ZnO were 0.7 wt.% and 1.8 wt.% respectively. It is evident from the images that with ZnO addition in AZ91E alloy, increased Zn solute is observed in both matrix and β-phases. This Zn solute is thought to have been liberated from ZnO because it reacted with Mg according to Equation 4.7.1 similar to that in the case of graphite mold casting. Increased divorcing of intermetallic phases with additions of ZnO is also visible, which is indicative of increased Zn solute presence [Dahle et. al., 2001]. The high growth restriction factor of Zn in Mg (Table 2.5.1)

effectively restricted the growth of α-Mg grain. It is known that the resulting constitutional undercooling in solid-liquid interface limited the size of the grain [Lee et. al., 2000].
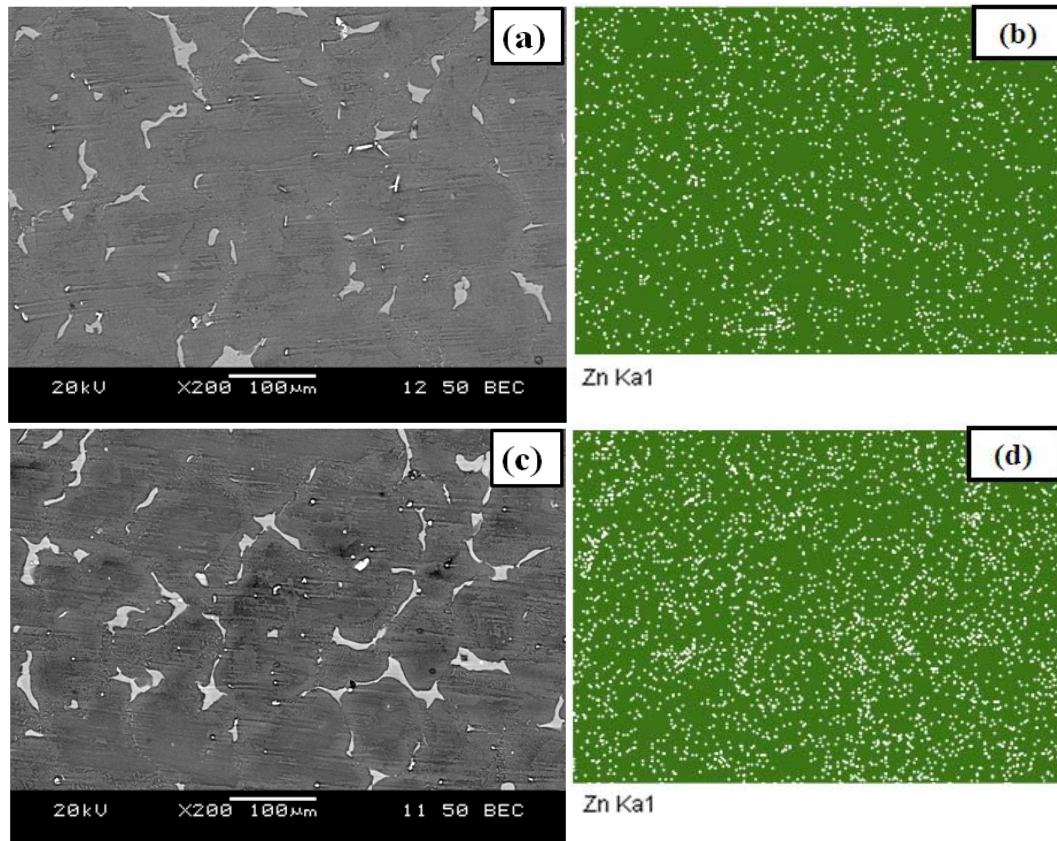
Fig. 4.10.3. SEM image and corresponding EDX map of AZ91E alloy with (a-b) no addition of ZnO and (c-d) 3 wt.% ZnO addition.

Table 4.10.1. Average Zn Content (wt.%) of AZ91E Alloy Castings Obtained Through EDX Point Analysis at Various ZnO Addition Levels

Addition Level (wt.%)	Average Zn Content (wt.%)	
	Matrix	β-Phase
0	0.64 ± 0.05	2.5 ± 0.16
3	1.62 ± 0.18	5.8 ± 0.26
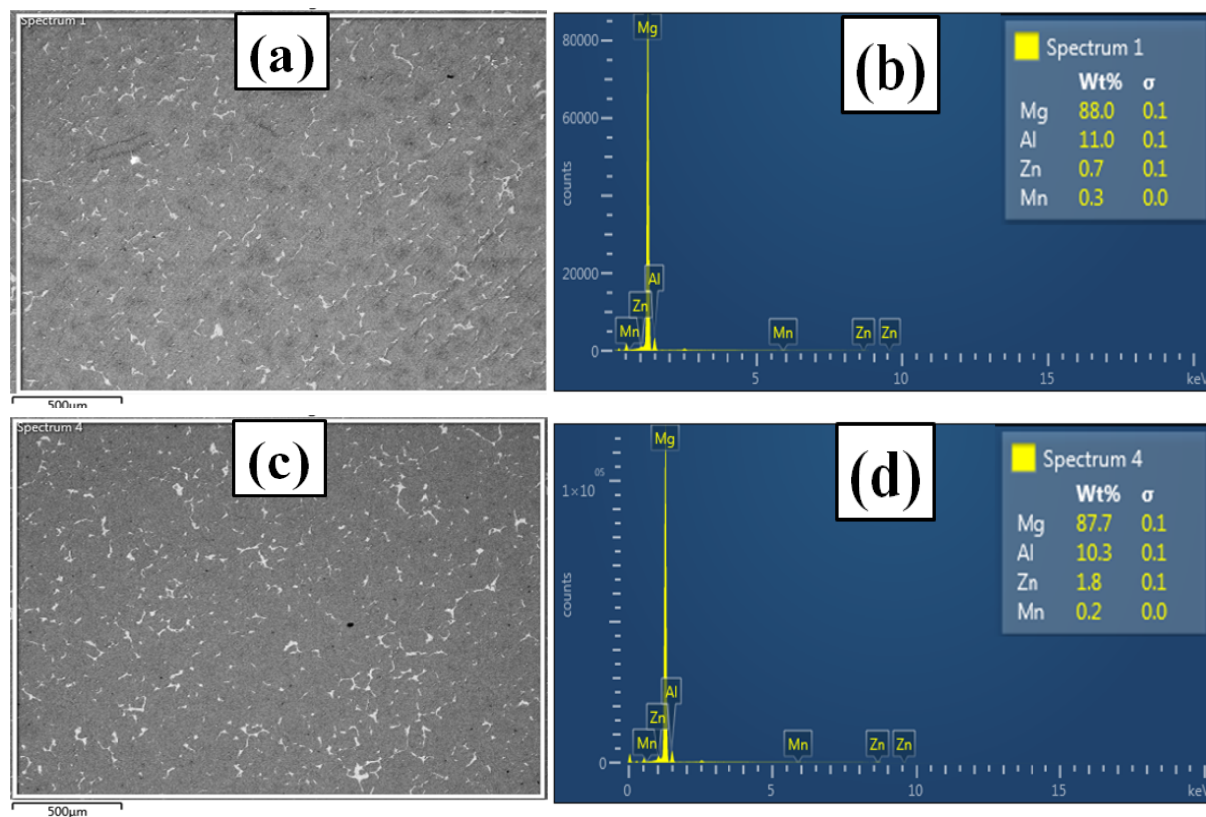
Fig. 4.10.4. SEM image and corresponding EDX analysis of AZ91E alloy with (a-b) no addition of ZnO and (c-d) 3 wt.% ZnO addition.

A small amount of added ZnO particles acted as nucleating sites while the remaining ZnO may have dissociated, into Zn and MgO according to the chemical reaction shown in Equation 4.7.1. The presence of MgO in the alloys refined with ZnO is evident from the SEM image and corresponding EDX analysis as shown in Fig. 4.10.5. The melt appeared to oxidize to a greater extent with increasing ZnO addition. These analysis in permanent tensile mold casting further confirmed our assumptions of the grain refining mechanism of ZnO in 9 wt.% Al containing Mg alloys (as discussed in section 4.8), appears to be via two routes: - 1) ZnO act as a nucleating site and 2) Zn liberated during ZnO dissolution enabled grain growth restriction.
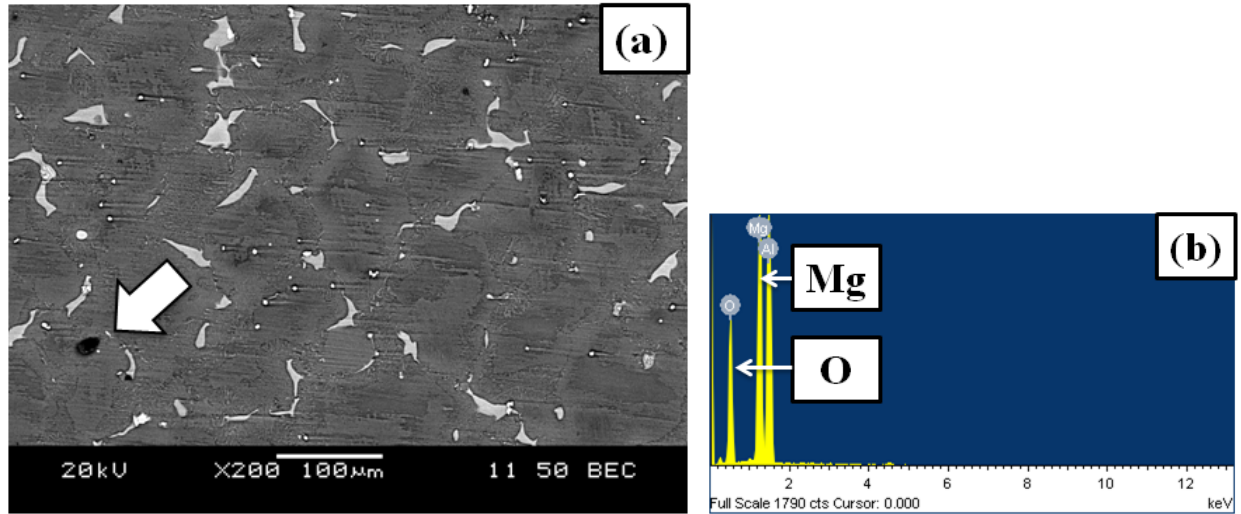
Fig. 4.10.5. SEM image and corresponding EDX analysis of AZ91E alloy with 3 wt.% ZnO showing the presence of MgO.

4.11 EFFECTS OF ZnO CONTENT ON MECHANICAL PROPERTIES OF AZ91E ALLOY (PERMANENT TENSILE MOLD)

4.11.1 TENSILE PROPERTIES

The tensile properties (0.2% offset yield strength, YS, ultimate tensile strength, UTS and elongation of the as-cast alloys tested at room temperature) are shown in Table 4.11.1 and Fig. 4.11.1. The YS, UTS and elongation of base AZ91E alloy was found to be 101 MPa, 154 MPa and 3.05% respectively. With increasing ZnO addition, the YS of the alloys continuously increased. The YS with 3 wt.% ZnO addition was 116 MPa which was around 15% higher than the base alloy. From the base alloy to 0.5 wt.% ZnO addition, the UTS and elongation increased. The UTS and elongation of AZ91E with 0.5 wt.% ZnO were 172 MPa and 5.49% respectively. The maximum UTS value (177 MPa) was found at 3 wt.% ZnO addition (15% higher than that of the base alloy). The elongation beyond 0.5 wt.% addition continuously decreased. The elongation with 3 wt.% ZnO addition was 4.3%. Finer grain sizes associated with ZnO addition likely increased the strength of the alloys. In addition thinner and more divorced Zn enriched β-intermetallic phases were observed with increased ZnO addition. Finely distributed β-phase possibly improved alloy strengthening compared to the base alloy which has continuous brittle β-intermetallic phases. Solid solution strengthening of the alloys, due to increased Zn solute with increased ZnO addition, is considered to be responsible for reduction of

84

the elongation beyond 0.5 wt.% of ZnO accompanied by an increase in tensile strength. In addition, the higher ZnO levels possibly introduced more oxides causing a reduction in elongation.

Table 4.11.1Tensile Properties of AZ91E Alloy with ZnO Addition

Addition Level (wt.%)	0.2% YS			UTS			Elongation		
	MPa	Std. Dev. (+/-)	Change (%)	MPa	Std. Dev. (+/-)	Change (%)	%	Std. Dev. (+/-)	Change (%)
0	101	3.85	-	154	3.31	-	3.05	0.11	-
0.25	107	5.17	5.9↑	158	20.12	2.6↑	4.94	0.47	61.9↑
0.5	110	3.09	8.9↑	172	14.17	11.7↑	5.49	0.57	80.0↑
0.75	111	1.34	9.9↑	170	7.57	10.4↑	4.79	0.40	57.0↑
1	113	1.25	11.9↑	175	12.57	13.6↑	4.59	0.59	50.5↑
3	116	8.35	14.9↑	177	8.32	14.9↑	4.30	0.36	40.9↑
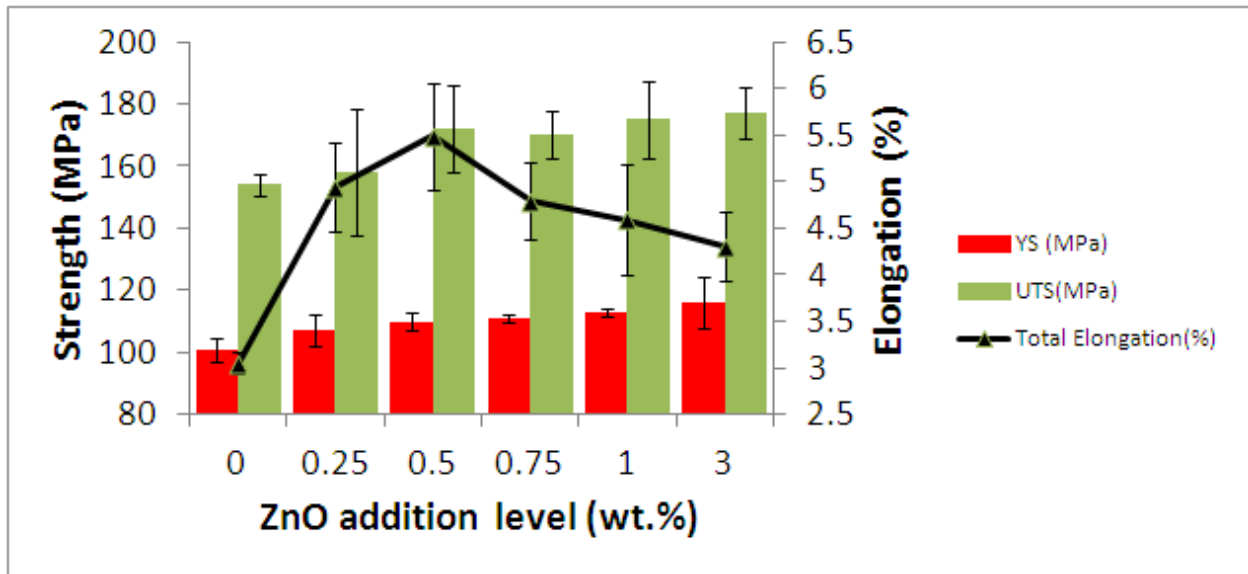
Fig. 4.11.1. Tensile properties of AZ91E alloy with various levels of ZnO addition.

The variation of yield strength with grain size according to the Hall-Petch relation plotted in Fig. 4.11.2 according to equation 4.11.1. The yield strength and the corresponding grain sizes are presented in Table 4.11.2

$$YS = 351.09d^{-1/2} + 72.05 \ (MPa) \qquad\qquad\qquad \text{Equation 4.11.1}$$
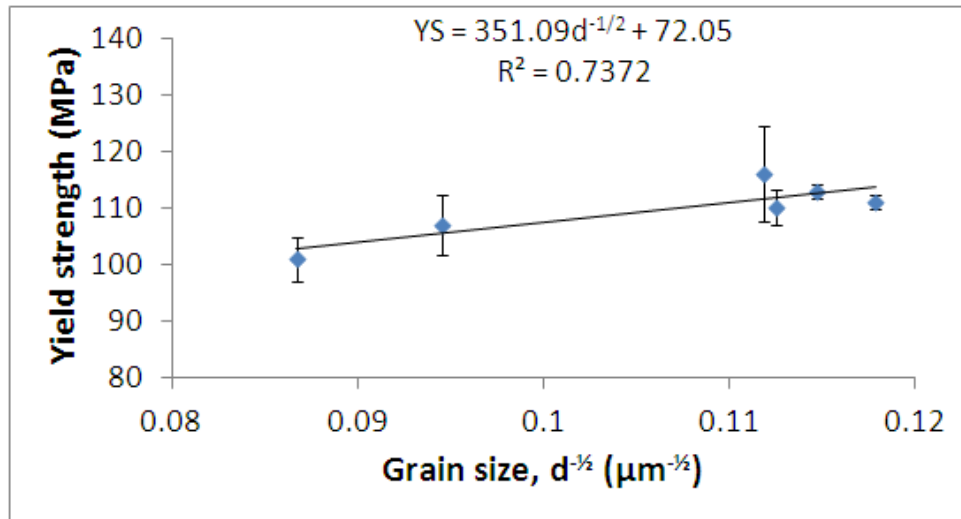
Fig. 4.11.2. Average YS of AZ91E alloy at different grain sizes.

Table 4.11.2. 0.2% YS of AZ91E Alloy at Different Grain Sizes

Grain Size (µm)		0.2% YS (MPa)
d (µm)	$d^{-1/2}$ $(µm)^{-1/2}$	
133	0.087	101
112	0.094	107
79	0.113	110
72	0.118	111
76	0.115	113
80	0.111	116

4.11.2 FRACTOGRAPHY

Samples for fracture analysis were prepared from the tested tensile specimens to gain a better understanding of the failure mode of the refined and unrefined AZ91E alloys. SEM images of the fractured tensile samples of (a) AZ91E, (b) AZ91E with 0.5 wt.% addition and (c) AZ91E with 3 wt.% addition of ZnO are shown in Fig. 4.11.3. Tensile fracture of Mg alloys at room temperature is usually brittle where cleavage is the principal fracture mode [Lu et. al., 2000]. Fig. 4.11.3-a reveals that the fracture surface of the base AZ91E alloy composed of large cleavage planes and cleavage steps (indicated by "1") and cleavage rivers with large crystal like morphology. Some secondary cracks (indicated by "2") can also be seen. From all these characteristics it can be assumed that the failure is cleavage fracture matching the low ductility (3.05%) of the alloy (Fig. 4.11.1). On the other hand Fig. 4.11.3-b with AZ91E+0.5 wt.% ZnO shows a finer microstructure with some secondary cracks and a few small cleavage planes. With further addition of ZnO the ductility of the alloy is decreased as can be seen from Fig. 4.11.3-c with 3 wt.% addition of ZnO. However, the fracture surface is dominant by many shallow dimples indicating more ductile (5.49%) type fracture.
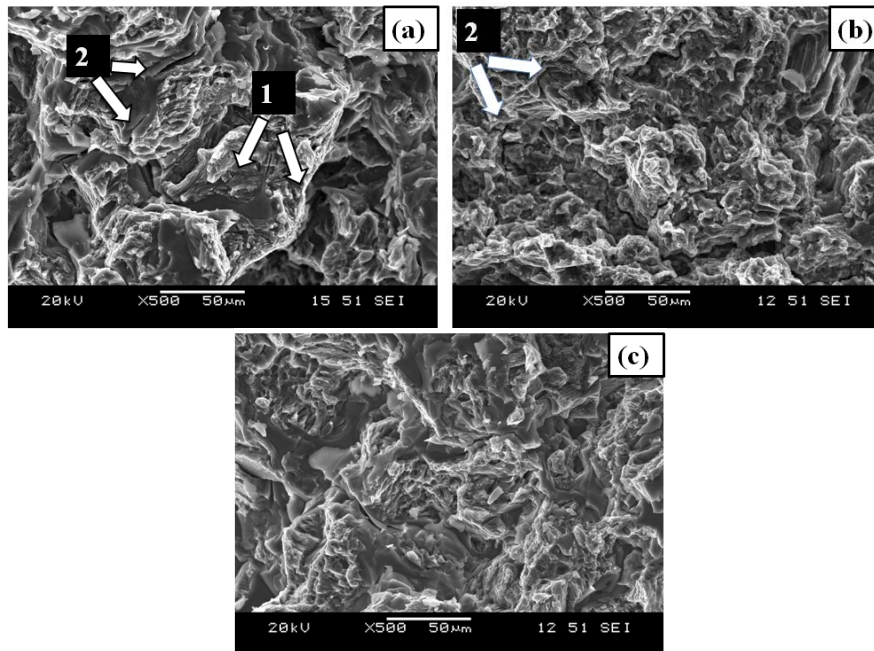
Fig. 4.11.3. SEM images of fracture surface of AZ91E alloy with (a) no addition of ZnO and (b) 0.5 wt.% ZnO addition (c) 3 wt.% ZnO addition. (1) Cleavage steps (2) Secondary crack.

In the base AZ91E alloy, the α-matrix is surrounded by hard and brittle β-phase along the grain boundaries which weaken the boundaries. It can be assumed that when load is applied, microcracks are readily initiated and propagated along the grain boundaries. This made the fracture surface more brittle in nature [Suresh et. al., 2011] (Fig. 4.11.3-a). The AZ91E alloy refined by ZnO has a finer microstructure and thinner, more divorced β-phase as compared to the base alloy. This may have helped in improving the strength of the grain boundaries. It is assumed that the cracks developed due to tensile loading, frequently pass through the matrix along with the grain boundaries resulting in a fracture surface showing more ductile character (Fig. 4.11.3-b).

4.11.3 HARDNESS

The effects of ZnO addition on the hardness of AZ91E alloy were studied in permanent tensile mold castings. The average Rockwell hardness values (HRE) and microhardness (HV) values of the matrix of AZ91E with different levels of ZnO addition are summarized in Table 4.11.3.

Table 4.11.3. Hardness of AZ91E Alloy with ZnO Addition

Addition Level (wt.%)	Rockwell Hardness E Test			Vickers Hardness Test		
	Hardness (HRE)	Std. Dev. (+/-)	Change (%)	Microhardness (HV)	Std. Dev. (+/-)	Change (%)
0	57	6.04	-	58	6.53	-
0.25	57	3.97	0	61	8.14	5.2
0.5	58	8.84	1.8	64	9.81	10.3
0.75	60	7.70	5.3	65	5.22	12.1
1	63	5.85	10.5	67	9.46	15.5
3	65	3.70	14.0	72	5.82	24.1

The average Rockwell hardness values (HRE) of AZ91E alloys with ZnO addition are shown in Fig. 4.11.4. With increasing ZnO addition, the HRE of the alloys also had an increasing trend. The hardness of the base AZ91E alloy was 57 HRE. Zinc oxide addition upto 0.5 wt.% showed no significant change in HRE. Addition levels beyond 0.5 wt.% showed an increase of 14% over that of the base alloy.
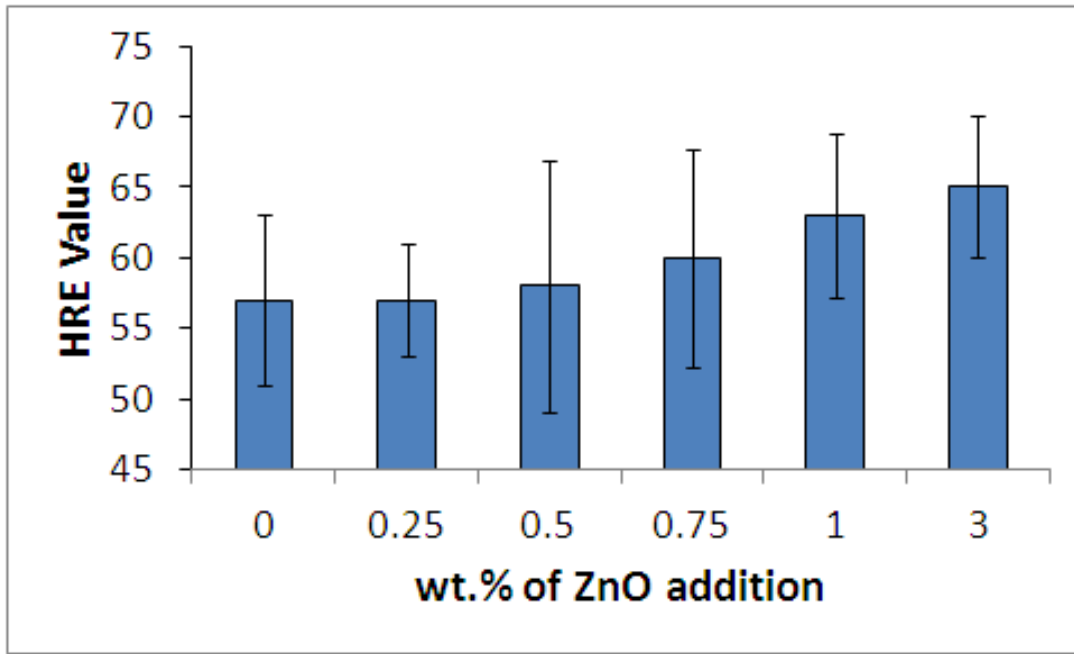
Fig. 4.11.4. Average HRE of AZ91E alloy with ZnO addition.

The microhardness (HV) values of the matrix of AZ91E with different levels of ZnO addition are shown in Fig. 4.11.5. The microhardness of the base alloy was 58 HV. With 0.25 and 0.5 wt.% ZnO additions the microhardness values were 61 HV and 64 HV respectively. The average hardness of the alloy matrix at 3 wt.% addition of ZnO was 72 HV (24% higher than the base alloy matrix).

Smaller grains result in larger grain boundary area. The larger grain boundary area can better impede dislocation motion compared to a coarse grain structure resulting in increased alloy strength [Cao et. al., 2006]. The increase in hardness and microhardness of the alloy with ZnO addition may also be related to solid solution strengthening of the matrix.
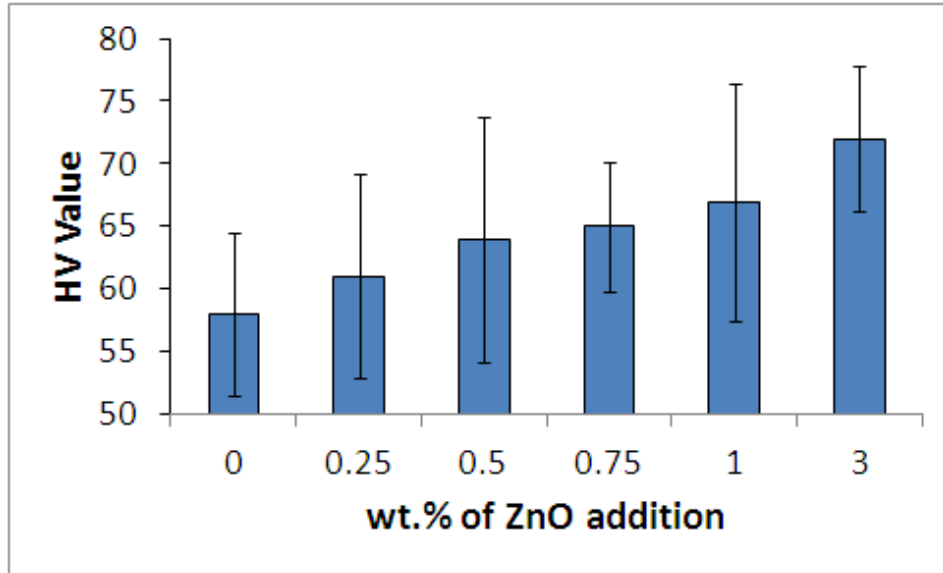
Fig. 4.11.5. Average microhardness of AZ91E alloy with ZnO addition.

4.12 POROSITY

The average porosity (%) levels of all the castings used in this study were less than 2.5% as shown in Table 4.12.1 and Fig. 4.12.1. The low porosity levels indicate that the mechanical properties obtained in this study represented sound castings.

Table 4.12.1. Average Porosity (%) Levels of AZ91E Alloy at Different Addition Levels of ZnO

Addition Level (wt.%)	Porosity (%)	Std. Dev. (+/-)
0	1.6	0.63
0.25	2.15	0.32
0.5	2.23	0.20
0.75	1.6	0.35
1	1.58	0.65
3	1.01	0.22
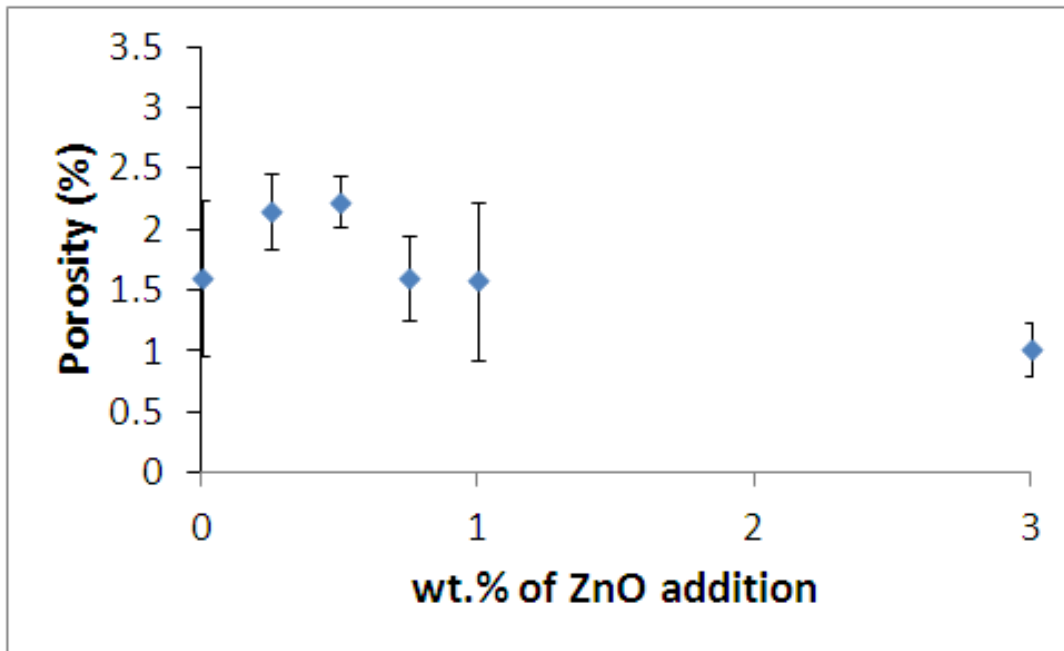
Fig. 4.12.1. Average porosity (%) of AZ91E alloy with ZnO addition.

4.13 CHAPTER SUMMARY

The grain refinement effect of ZnO was significant in both AZ91E and binary Mg-9 wt.% Al alloys. The effect persisted upto 1 hour of holding time. Addition of ZnO improved the mechanical properties of AZ91E alloy.

Chapter 5: Conclusions

This study was conducted with a view to examine the effectiveness of ZnO as a potential grain refiner for AZ91E and Mg-9 wt.% Al binary alloys as well as to determining its refining mechanism. The influence of ZnO on the grain size, hardness, and tensile properties at ambient temperature were studied. This study showed that ZnO is a reliable, effective and economical grain refiner for both AZ and binary alloys.

The conclusions drawn from this study are as follows:

Graphite Mold Casting

1.   For AZ91E alloy, maximum grain size reduction (50%) was found at 0.75 wt.% addition of ZnO (108 μm) and for Mg-9 wt.% Al binary alloy maximum reduction (68%) was found at 3 wt.% addition of ZnO (93 μm).
2.   No fading effect was observed for upto 1 hour of holding time for the 3 wt.% ZnO in both AZ and binary alloys. Grain size was found to remain constant during this period.
3.   Grain refinement was attributed heterogeneous nucleation due to ZnO and grain growth restriction of Zn (which was liberated during ZnO dissociation) on α-Mg matrix.

Tensile Mold Casting

1.   A grain size reduction of almost 44% was achieved with a small (0.5 wt.%) addition of ZnO. The base alloy had a grain size of 133 μm. Optimum grain size reduction of the AZ91E alloy was achieved using 0.5 wt.% ZnO addition resulting in grain size of 75 μm.
2.   Grain refinement was attributed to heterarogeneous nucleation due to ZnO. Further, Zn liberated during ZnO dissolution appears to have enabled grain growth restriction.
3.   Addition of ZnO improved the tensile properties of the AZ91E alloy. For the base alloy, the YS, UTS and elongation were 101 MPa, 154 MPa and 3.05% respectively. The highest YS and UTS of the alloy were found at 3 wt.% addition of ZnO which were 116 MPa and 177 MPa respectively. These values were 15% higher than that of the base alloy. The maximum elongation was 5.49% observed using 0.5 wt.% ZnO addition.

4.   SEM observations of tensile fracture surfaces revealed mainly cleavage type fracture for the base AZ91E alloy. With 0.5 wt.% addition of ZnO, the fracture surfaces were dominated by shallow dimples along with small cleavage planes which were more quasi-cleavage in nature, indicating higher ductility in alloys refined with ZnO.

5.   With ZnO addition, the Rockwell hardness and Vickers microhardness of the alloys increased. With 3 wt.% ZnO addition the HRE and HV of the alloys were higher than the base alloy by 14% and 24% respectively.

Chapter 6: Recommendations for Future Work

The current study showed the potential of ZnO as a grain refiner for Mg alloys containing 9 wt.% Al. Further investigation is required to investigate some additional features in order to explore the total opportunity that can be gained from this grain refiner in an industrial set up.

1. Optimization of casting parameters (addition temperature, holding time, addition method) to reduce the reduction of ZnO in Mg alloys melt.
2. Study the post-recycle effect of Mg alloys refined by ZnO on grain size and mechanical properties.
3. Study the effects of ZnO particle size on the grain refinement and mechanical properties of Mg alloys.
4. Effect on mechanical properties with ZnO refined Mg alloys at service temperatures (e.g. 180-200°C) for automotive engine block components.

Appendices

Appendix-A1: Mg-Al Phase Diagram
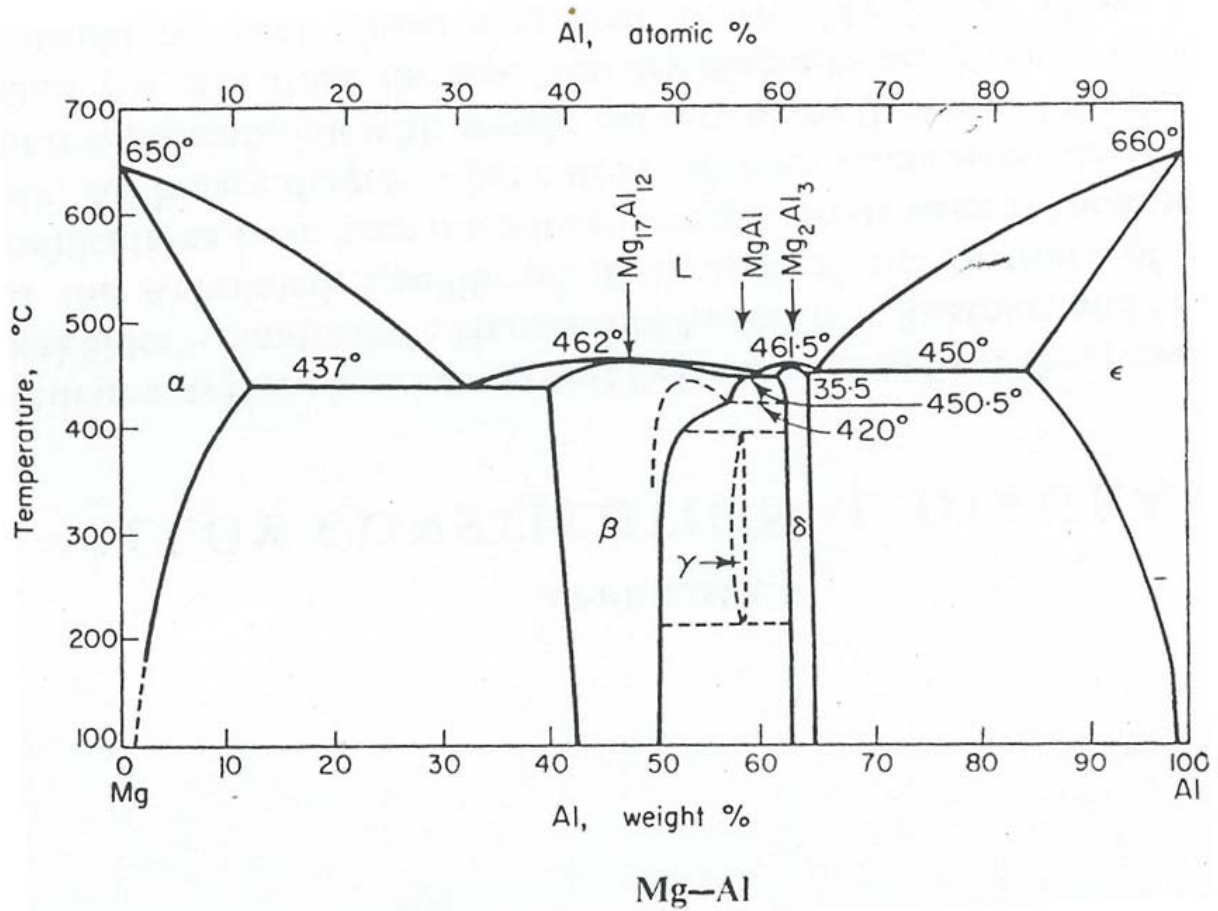
Fig. A.1 Mg-Al phase diagram [Emely, 1966].

Appendix-A2: SEM Image of ZnO
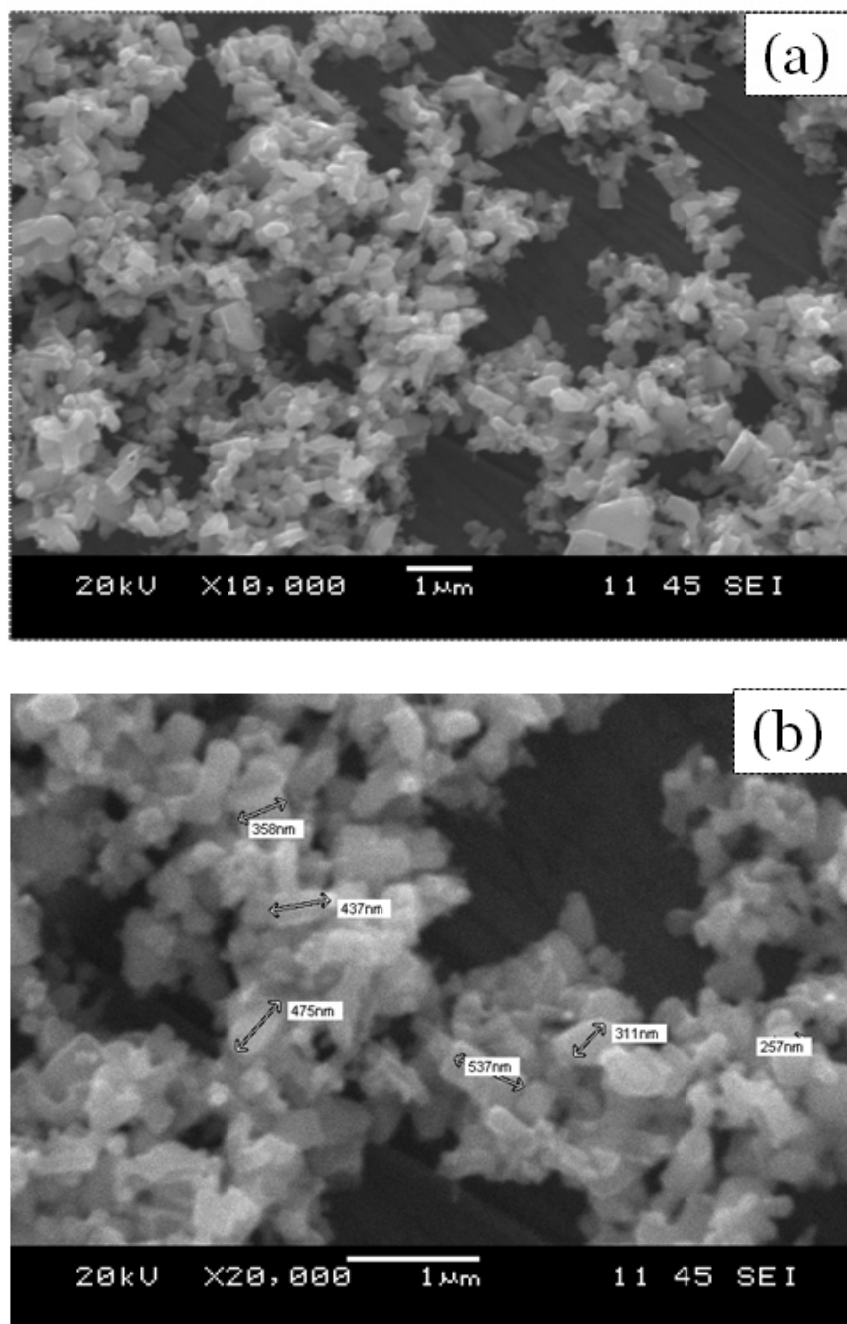
Fig. A.2 (a) Representative SEM image of ZnO (b) showing dimensions of individual ZnO particle.

Appendix-A3: Cooling Curves of AZ91E+X wt.% ZnO
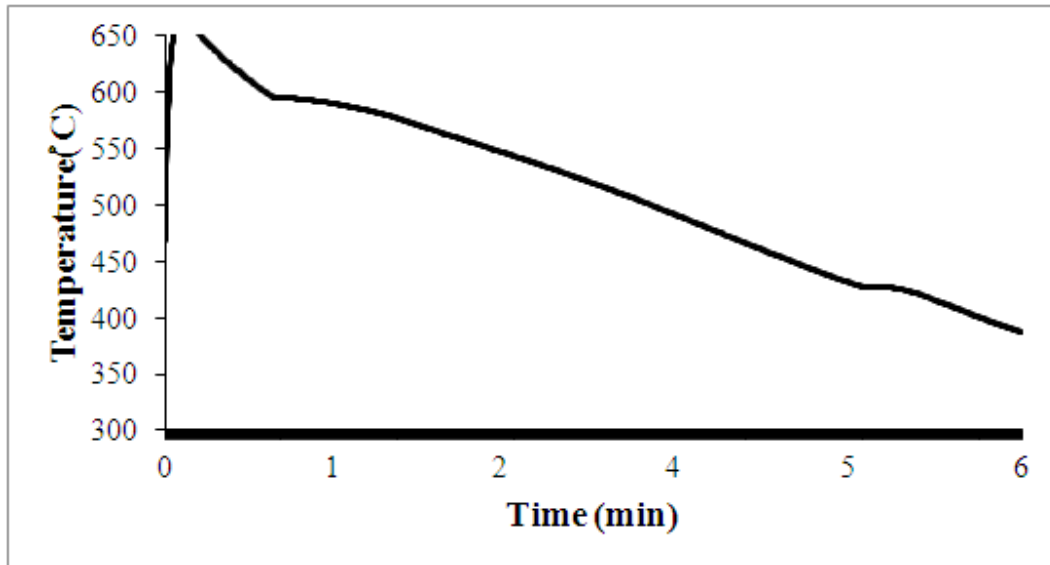
Fig. A.3.1. Cooling curve of base AZ91E alloy.
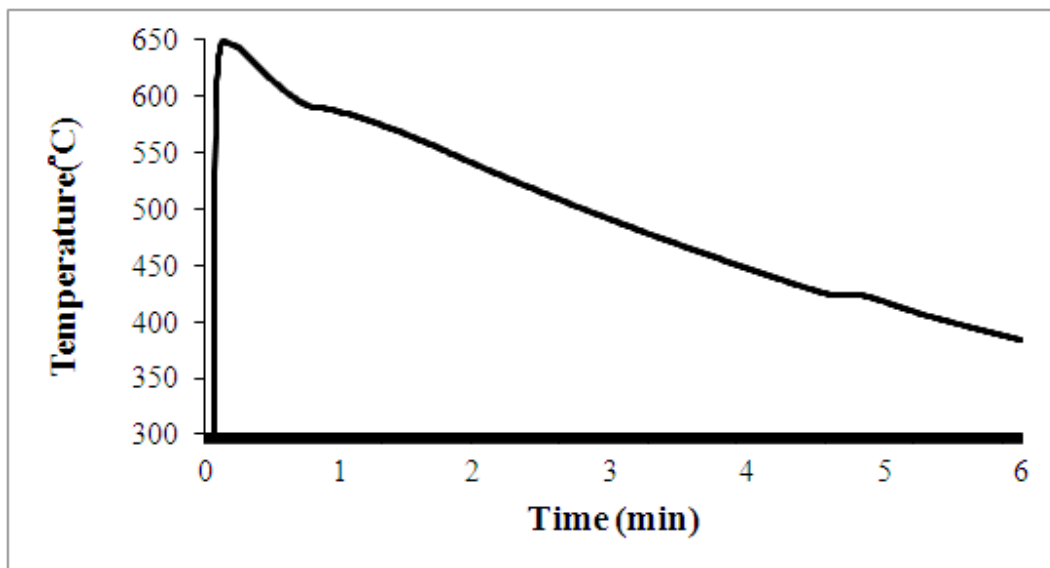
Fig. A.3.2. Cooling curve of base AZ91E + 0.25 wt.% ZnO alloy.
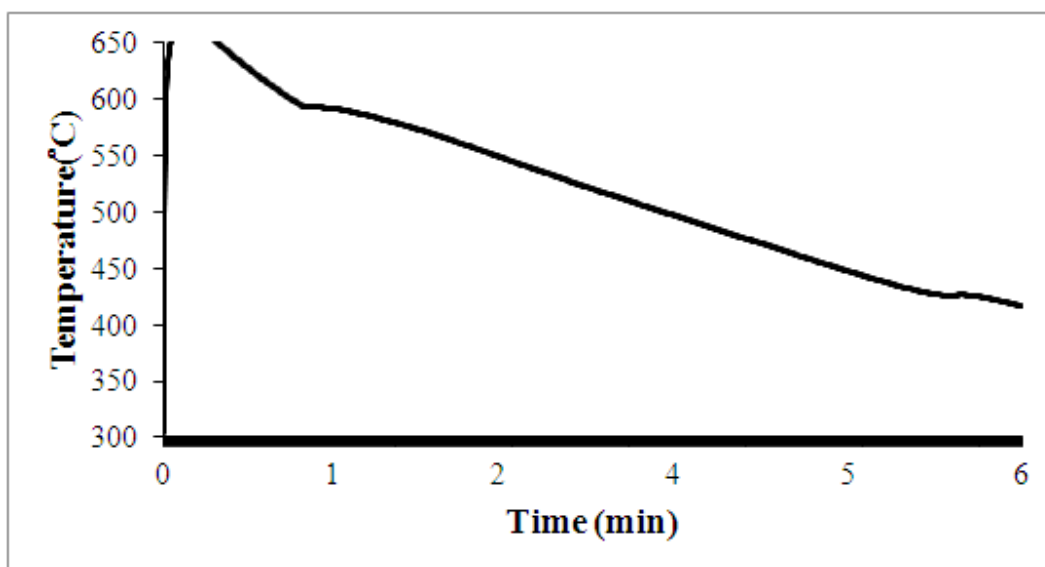
Fig. A.3.3. Cooling curve of base AZ91E + 0.5 wt.% ZnO.
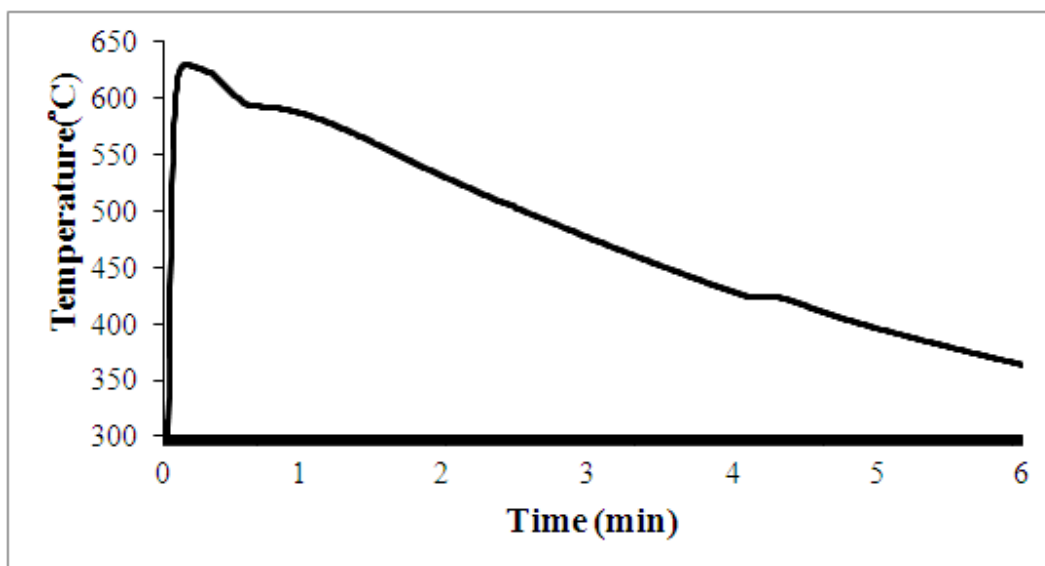
Fig. A.3.4. Cooling curve of base AZ91E + 0.75 wt.% ZnO.
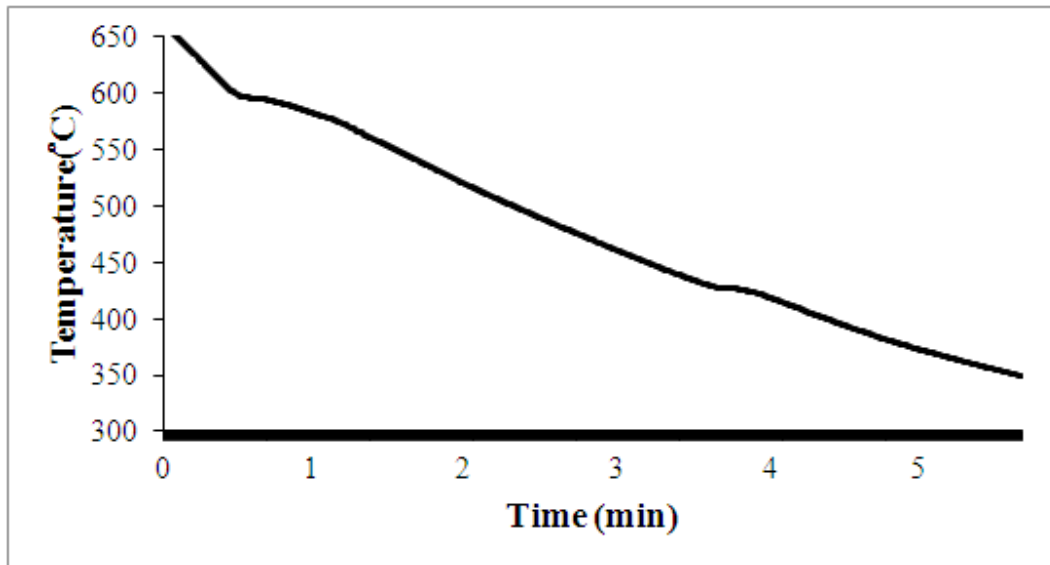
Fig. A.3.5. Cooling curve of base AZ91E + 1 wt.% ZnO.
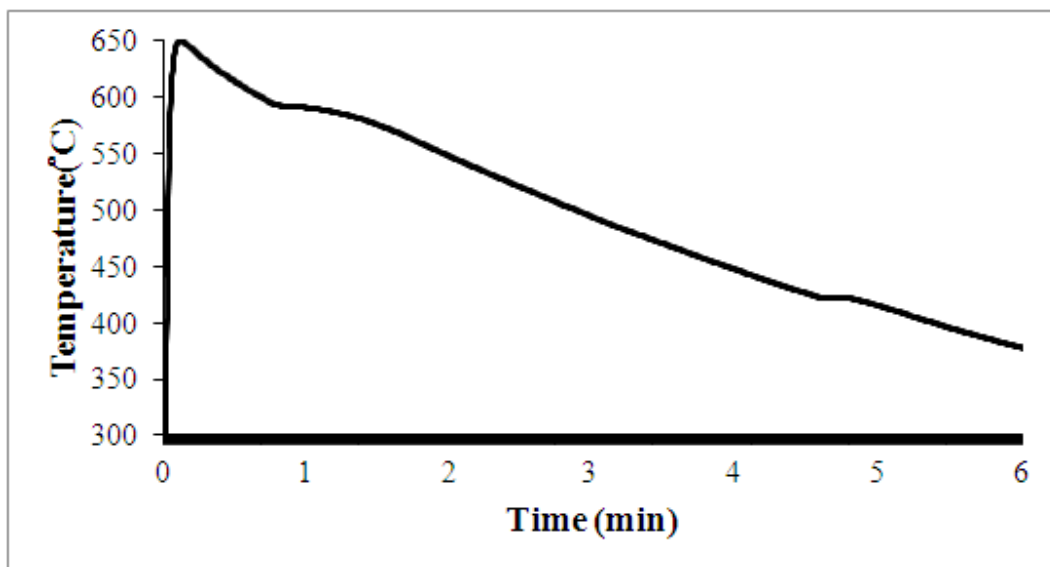
Fig. A.3.6. Cooling curve of base AZ91E + 2 wt.% ZnO.
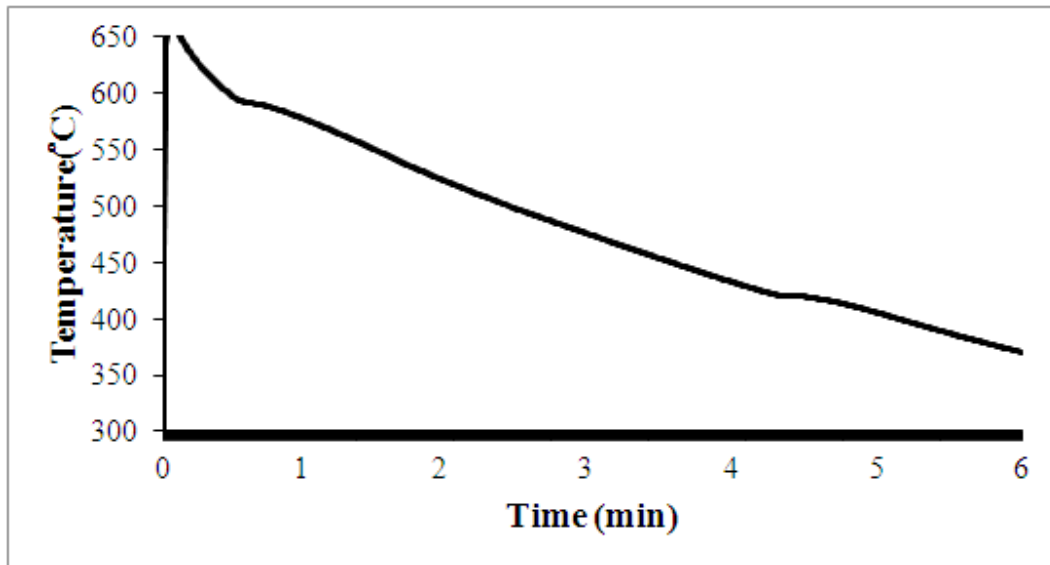
Fig. A.3.7. Cooling curve of base AZ91E + 3 wt.% ZnO.

Appendix-A4: Free Energy Calculations

The stability and equilibrium of a process or chemical reaction can be determined through thermo-chemical calculation. A negative value of the change in energy (ΔG) implies the process or chemical reaction is spontaneous and in forward direction. ΔG (also known as "driving force") can be determined using Gibbs-Helmholtz equation [Kubaschewski, 1967]:

$$\Delta G^\circ = \Delta H^\circ - T\Delta S^\circ \qquad\qquad\qquad \text{Equation A4.1}$$

where

ΔG is the free energy of formation

ΔH is the heat of formation

ΔS is the entropy of reaction

Equation A4.1 was used to find the spontaneity and stability of the following reaction

$$ZnO + Mg \rightarrow MgO + Zn \qquad\qquad\qquad \text{Equation 4.7.1}$$

A sample calculation for determining ΔG is described below. All the thermodynamic data are collected from Kubaschewski, 1967.

Table A3.1. Heats of Formation, Standard Entropies of Different Substances

Substance	$-\Delta H^\circ_{298}$ (Kcal/mole)	S°_{298} (cal. Deg^{-1}.mole^{-1})
\<MgO\>	143.7±0.2	6.55±0.15
\<Mg\>	0	7.77±0.1
\<Zn\>	0	9.95±0.05
\<ZnO\>	83.2±0.3	14.4±0.1

< >   Solid

$\Delta G^\circ \quad = (\sum\Delta H_{products} - \sum\Delta H_{reactents}) - (\sum S_{products} - \sum S_{reactants})T$

$\quad\quad = (\text{-}) \, 60500\text{-}5.67T \text{ cal/mole}$

Hence, ΔG at ZnO addition temperature (750°C/ 1023 K) is -66.3 kcal / mole.

Appendix-A5: Cooling Curves of Mg-9 wt.% Al+X wt.% ZnO
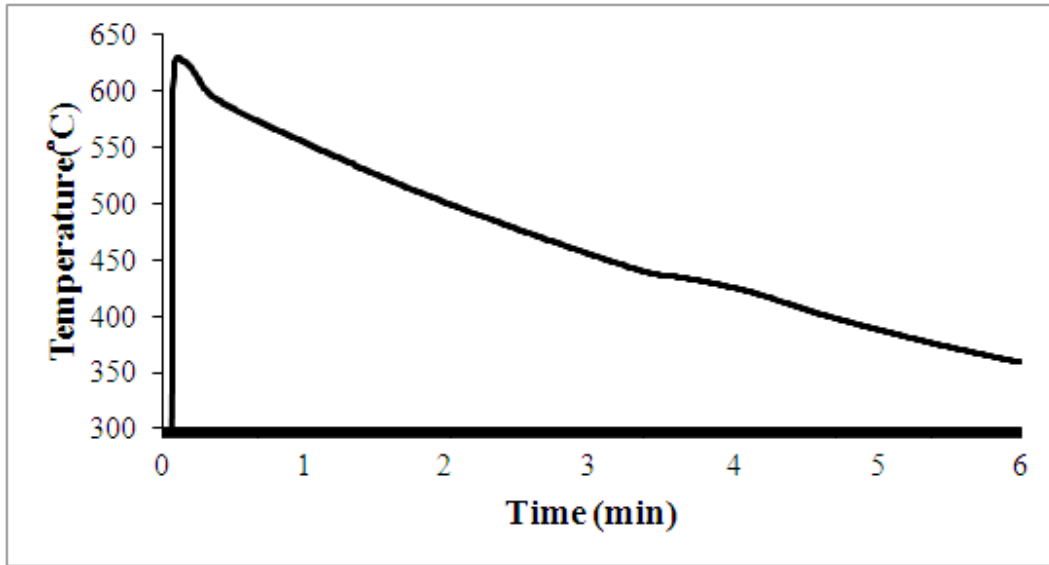
Fig. A.5.1. Cooling curve of base Mg-9 wt.% Al.
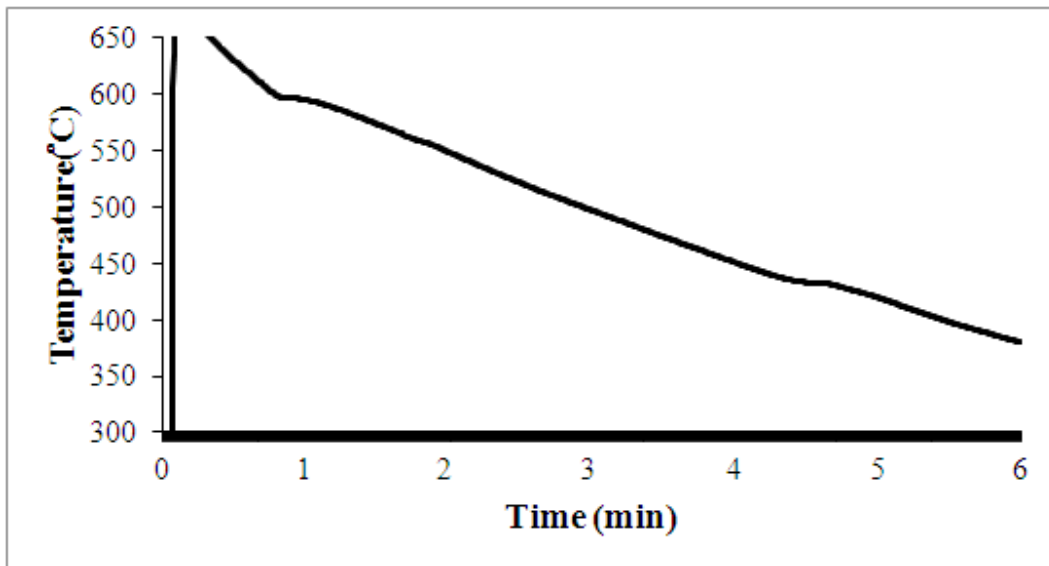
Fig. A.5.2. Cooling curve of base Mg-9 wt.% Al + 0.5 wt.% ZnO.
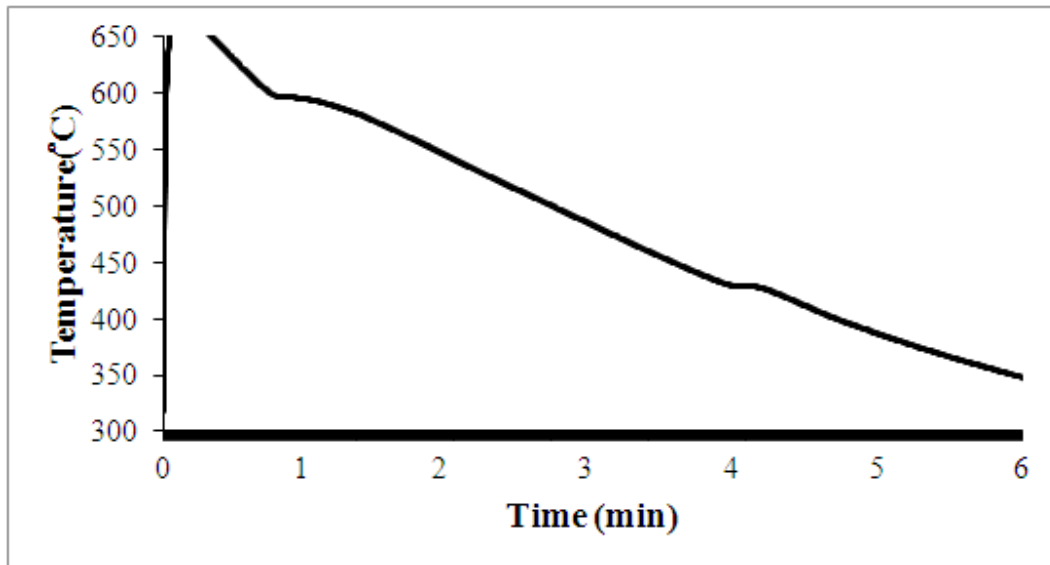
Fig. A.5.3. Cooling curve of base Mg-9 wt.% Al + 1 wt.% ZnO.
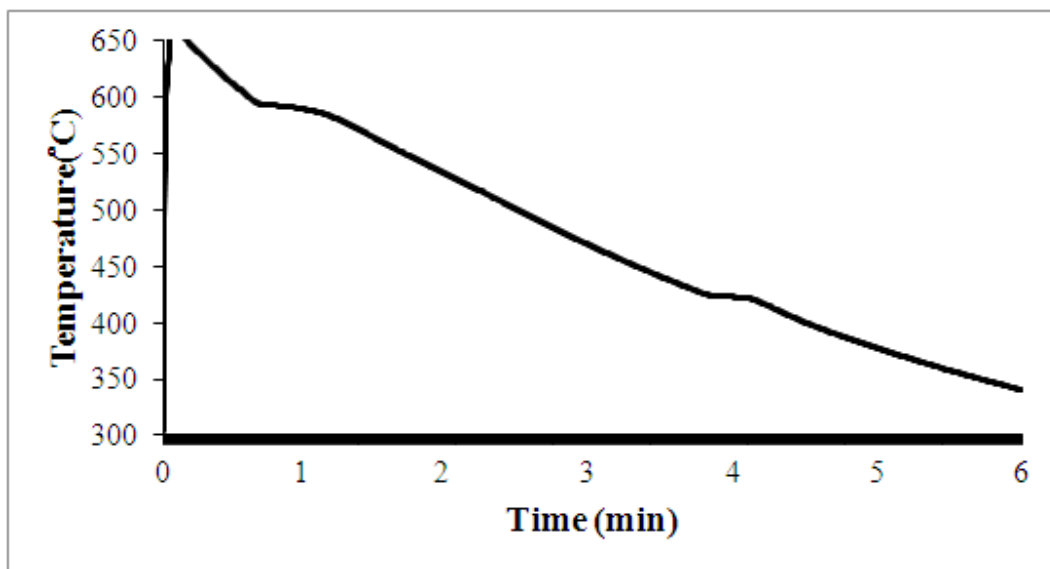
Fig. A.5.4. Cooling curve of base Mg-9 wt.% Al + 2 wt.% ZnO.

\
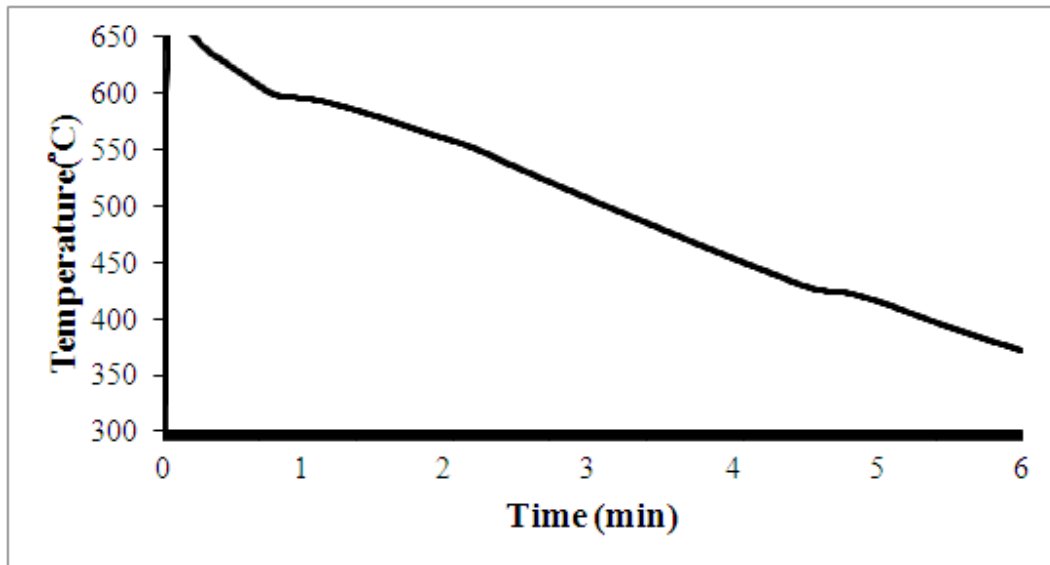
Fig. A.5.5. Cooling curve of base Mg-9 wt.% Al + 3 wt.% ZnO.

References

1. Aghayani, M.K., Niroumand, B., "Effects of Ultrasonic Treatment on Microstructure and Tensile Strength of AZ91 Magnesium Alloys," *Journal of Alloys and Compounds,* Vol. 509, pp. 114-122 (2011).

2. Askeland, D.R., Fulay, P.P., Wright, W.J., "The Science and Engineering of Materials," Global Engineering, 2010.

3. ASM Handbook Committee, "ASM Metals Hand Book-Properties and Selection: Nonferrous Alloys and Special Purpose Materials," ASM International, Vol. 2, 1992.

4. Avedesian, M.M., Baker, H., "Magnesium and Magnesium Alloys," ASM International, 1999.

5. Bamberger, M., "Structural Refinement of Cast Magnesium Alloys," *Materials Science and Technology,* Vol. 17, pp. 15-24 (2001).

6. Campbell, J., "Castings," Butterworth-Heinimann, Woburn, M.A., 1993.

7. Cao, P., Qian, M., StJohn, D.H., "Effect of Iron on Grain Refinement of High-Purity Mg-Al Alloys," *Scripta Materialia,* Vol. 51, pp. 125-129 (2004).

8. Cao, P., Qian, M., StJohn, D.H., "Native Grain Refinement of Magnesium Alloys," *Scripta Materialia,* Vol. 53, pp. 841-844 (2005).

9. Cao, P., Qian, M., *StJohn,* D.H., "Effect of Manganese on Grain Refinement of Mg-Al Based Alloys," *Scripta Materialia,* Vol. 54, pp. 1853-1858 (2006).

10. Cao, P., Qian, M and StJohn, H., "Mechanism for Grain Refinement of Magnesium Alloys by Superheating," *Scripta Materialia,* Vol. 56, pp. 633-636 (2007).

11. Celotto, S., "TEM Study of Continuous Precipitation in Mg-9 wt.% Al-1 wt.% Zn Alloy," *Acta Materialia,* Vol. 48, pp. 1775-1787 (2000).

12. Chakraborty, M., Vinod Kumar, G.S., Murty, B.S., "Poisoning and Fading Phenomena in the Grain Refinement of Al and Its Alloys," *Transactions of the Indian Institute of Metals,* Vol. 58, No. 4, pp. 661-670 (2005).

13. Chen, T.J., Jiang, X.D. Ma, Y., Li, Y.D., Hao, Y., "Grain Refinement of AZ91D Magnesium Alloys by SiC," *Journal of Alloys and Compounds,* Vol. 496, pp. 218-225 (2010).

14. Chen, T.J., Ma, Y., Lv, W.B., Li, Y.D., "Grain Refinement of AM60B Magnesium Alloy by SiC Particles," *Journal of Material Science,* Vol. 45, pp. 6732-6738 (2010).

15. Chen, T.J., Jiang, X.D., Ma, Y., Wang, R.Q., Hao, Y., "Grain Refinement of AZ91D Magnesium Alloy by MgCO$_3$," *Materials Research,* Vol. 14(1), pp. 124-133 (2011).

16. Chen, T.J., Wang, R.Q., Ma, Y., Hao, Y., "Grain Refinement of AZ91D Magnesium Alloy by Al-Ti-B Master Alloy and Its Effect on Mechanical Properties," *Materials and Design,* Vol. 34, pp. 637-648 (2012).

17. Cui, C., Wu, L., Wu, R., Zhang, J., Zhang, M., "Influence of Yttrium on Microstructure and Mechanical Properties of As-Cast Mg-5Li-3Al-2Zn Alloy," *Journal of Alloys and Compounds,* Vo. 509, pp. 9045-9049 (2011).

18. Dahle, A.K., Lee, Y.C., Nave, M.D., Schaffer, P.L., StJohn, D.H., "Development of The As-Cast Microstructure in Magnesium-Aluminum Alloys," *Journal of Light Metals,* Vol. 1, pp. 61-72 (2001).

19. D'Elia, F., "A Study on Grain Refinement and Hot Tearing in Permanent Mold Cast Aluminum Alloys," Ryerson University, Toronto, M.A.Sc. Thesis, 2009.

20. Dieter, G.E., "Mechanical Metallurgy," McGraw-Hill, Third ed., 1986.

21. Easton, M.A., StJohn, D.H., "A Model of Grain Refinement Incorporating Alloy Constitution and Potency of Heterogeneous Nucleation Particles," *Acta Materialia,* Vol. 49, pp. 1867-1878 (2001)

22. Easton, M.A., Schiffl, A., Yao, J.Y., Kaufmann, H., "Grain Refinement of Mg-Al (-Mn) Alloys by SiC Additions," *Scripta Materialia,* Vol. 55, pp. 379-382 (2006).

23. Elsayed, A., Lee, K., Ravindran, C., "Effect of Ca and Mn Additions on the Castability and Mechanical Properties of AZ91D Mg Alloy Permanent Mold Castings," *AFS Transactions,* Vol. 117, pp. 659-672 (2009).

24. Elsayed, A., "Novel Grain Refinement of AZ91E Magnesium Alloy and the Effect on Hot Tearing During Solidification," Ryerson University, Toronto, M.A.Sc. Thesis, 2010.

25. Elsayed, A., Lun Sin, S., Ravindran, C.R., "Finding and Removing Inclusions in Magnesium Alloys," *Advanced Materials and Process,* , pp. 15-19 (2014).

26. Emley, E.F., "Principles of Magnesium Technology," Pergamon Press, London, 1966.

27. Flemings, M.C., "Solidification Processing," McGraw-Hill, USA, 1974.

28. Fu, H.M., Qiu, D., Zhang, M.X., Wang, H., Kelly, P.M., Taylor, J.A., "The Developments of a New Grain Refiner for Magnesium Alloys Using Edge-to-Edge Model," *Journal of Alloys and Compounds,* Vol. 456, pp. 390-394 (2008).

29. Fu, H.M., Zhang, M.X., Qiu, D., Kelly, P.M., Taylor, J.A., "Grain Refinement by AlN Particles in Mg-Al Based Alloys," *Journal of Alloys and Compounds,* Vol. 478, pp. 809-812 (2009).

30. Gao, S.Y., Cui, J.Z., Li, Q.C., Zhang, Z.Q., "The Research on The Effect of $MgCO_3$ on Grain Refinement in AZ31 Magnesium Alloys," *Mat.-wiss.u. Werkstofftech,* Vol. 41, Issue 8, pp. 652-656 (2010).

31. Gruzleski, J.E., "Microstructure Development during Metal Casting," American Foundrymen's Society Inc, Illinois, 2000.

32. Ho, S.S.C., "Lost Foam Castings of Periodic Cellular Materials with Aluminum and Magnesium Alloys," University of Toronto, M.A.Sc. Thesis, 2009.

33. Huang, Y., Kainer, K. U., Hort, N., "Mechanism of Grain Refinement of Mg-Al Alloys by SiC Inoculation," *Scripta Materialia,* Vol. 64, pp. 793-796 (2011).

34. Jin, Q., Eom, J.P., Lim, S.G., Park, W.W., You, B.S., "Grain Refining Mechanism of a Carbon Addition Method in a Mg-Al Magnesium Alloy," *Scripta Materialia,* Vol. 49, pp. 1129-1132 (2003).

35. Kelly, P.M., Zhang, M.X., "Edge-to-Edge Matching- the Fundamentals," *Metallurgical and Materials Transactions,* Vol. 37A, pp. 833-839 (2006).

36. Kubaschewski, O., Evans, E.LL., Alcock, C.B., "Metallurgical Thermochemistry" Pergamon Press Ltd., London, 1967.

37. Lee, Y.C., Dahle, A.K., St.John, D.H., "The Role of Solute in Grain Refinement of Magnesium," *Metallurgical and Materials Transactions A,* Vol. 31A, pp. 2895-2906 (2000).

38. Lee, K., "A Study on Grain Refinement of AZ91E Magnesium Alloy with Al-5TiB$_2$, Al-Al$_4$C$_3$ and ZnO Additions," Ryerson University-Toronto, M.A.Sc. Thesis, (2011).

39. Li, P., Tang, B., Kandalova, E.G., "Microstructure and Properties of AZ91D Alloy with Ca Additions," *Materials Letters,* Vol. 59, pp. 671-675 (2005).

40. Li, M.J., Tamura, T., Miwa, K., "Microstructure Formation and Grain Refinement of Mg-Based Alloys by Electromagnetic Vibration Technique," *Transaction of Nonferrous Metals Society of China,* Vol. 20, pp. 1192-1198 (2010).

41. Liu, Y., Liu, X., Xiufang, B., "Grain Refinement of Mg-Al Alloys with Al$_4$C$_3$-SiC/Al Master Alloy," *Materials Letters,* Vol. 58, pp. 1282-1287 (2004).

42. Liu, X., Osawa, Y., Takamori, S., Mukai, T., "Microstructure and Mechanical Properties of AZ91 Alloy Produced with Ultrasonic Vibration," *Materials Science and Engineering A,* Vol. 487, pp. 120-123 (2008).

43. Liu, S.F., Liu, L.Y., Kang, L.G., "Refinement Role of Electromagnetic Stirring and Strontium in AZ91 Magnesium Alloys," *Journal of Alloys and Compounds,* Vol. 450, pp. 546-550 (2008).

44. Liu, S.F., Li, B., Wang, X.H., Su, W., Han, H., "Refinement Effect of Cerium, Calcium and Strontium in AZ91 Magnesium Alloy," *Journal of Material Processing Technology,* Vol. 209, pp. 3999-4004 (2009).

45. Liu, S., Zhang, Y., Han, H., Li, B., "Effect of Mg-TiB$_2$ Master Alloy on the Grain Refinement of AZ91D Magnesium Alloy," *Journal of Alloys and Compounds, V*ol. 487, pp. 202-205 (2009).

46. Liu, S., Zhang, Y., Han, H., "Role of Manganese on the Grain Refining Efficiency of AZ91D Magnesium Alloys Refined by Al$_4$C$_3$," *Journal of Alloys and Compounds,* Vol. 491, pp. 325-329 (2010).

47. Lu, Y.Z., Wang, Q.D., Ding, W.J., Zeng, X.Q., Zhu, Y.P. "Fracture Behavior of AZ91 Magnesium Alloy," *Material Letters,* Vol. 44, pp. 265-268 (2000).

48. Lu, L., Dahle, A.K., StJohn, D.H., "Grain Refinement Efficiency and Mechanism of Aluminum Carbide in Mg-Al Alloys," *Scripta M*a*terialia,* Vol. 53, pp. 517-522 (2005).

49. Mordike, B.L., Ebert, T., "Magnesium Properties-Applications-Potential," *Materials Science and Engineering A,* Vol. 302, pp. 37-45 (2001).

50. Motegi, T., "Grain-Refining Mechanisms of Superheat-Treatment of and Carbon Addition to Mg-Al-Zn Alloys," *Materials Science and Engineering A,* Vol. 413-414, pp. 408-411 (2005).

51. Murty, B.S., Kori, S.A., Chakrabory, M., "Grain Refinement of Aluminum and Its Alloys by Heterogeneous Nucleation and Alloying," International *Materials Reviews,* Vol. 47, No. 1, pp. 3-28 (2002).

52. Nimityongskul, S., Jones, M., Choi, H., Lakes, R., Kou, S., Li, X., "Grain Refinement Mechanisms in Mg-Al Alloys with Al$_4$C$_3$ Microparticles," *Materials Science and Engineering A,* Vol. 527, pp. 2104-2111 (2010).

53. Pearson, W.B., "A Handbook of Lattice Spacings and Structures of Metals and Alloys," Pergamon press, Oxford, United Kingdom, 1964.

54. Qian, M., Cao, P., "Discussion on Grain Refinement of Magnesium Alloys by Carbon Inoculation," *Scripta Materrialia,* Vol. 52, pp. 415-419 (2005).

55. Qiu, D., Zhang, M.X., "Effect of Active Heterogeneous Nucleation Particles on the Grain Refining Efficiency in An Mg-10 wt% Y Cast Alloys," *Journal of Alloys and Compounds,* Vol. 488, pp. 260-264 (2009).

56. Ramirez, A., Qian, M., Davis, B., Wilks, T., "High-intensity Ultrasonic Grain Refinement of Magnesium Alloys: Role of Solute," *International Journal of Cast Metals Research,* Vol. 22, No. 1-4, pp. 260-263 (2009).

57. Robert, T., Noguez, M.E., Salas, G., Montejano, S., "Influence of Grain Refinement on Some Mechanical Properties of Non Ferrous Cast Alloys," *Acta Metall. Mater*, Vol. 40, No. 4, pp. 771-777 (1992).

58. Schumacher, P., Greer, A.L., Worth, J., Evans, P.V., Kearns, M.A., Fisher, P., Green, A.H., "New Studies of Nucleation Mechanisms in Aluminum Alloys: Implications for Grain Refinement Practice," *Material Science and Technology,* Vol. 14, pp. 394-404 (1998).

59. Srinivasan, A., Pillai, U.T.S., Swaminathan, J., Das, S.K., Pai, B.C., "Observations of Microstructural Refinement in Mg-Al-Si Alloys Containing Strontium," *Journal of Materials Science,* Vol. 41, pp. 6087-6089 (2006).

60. StJohn, D.H., Qian, M., Easton, M.A., Cao, P., Hildebrand, Z. "Grain Refinement of Magnesium Alloys," *Metallurgical and Materials Transactions A,* Vol. 36A, pp. 1669-1679 (2005).

61. StJohn, D.H., Cao, P., Qian, M., Easton, M.A., "A New Analytical Approach to Reveal the Mechanism of Grain Refinement," *Advanced Engineering Materials,* Vol. 9, No. 9, pp. 739-746 (2007).

62. StJohn, D.H., Easton, M.A., Qian, M., Taylor, J.A., "Grain Refinement of Magnesium Alloys: A Review of Recent Research, Theoretical Developments, and Their Application," *Metallurgical and Materials Transactions A,* Vol. 44A, pp. 2935-2949 (2013).

63. Suresh, M., Srinivasan, A., Ravi, K.R., Pillai, U.T.S., Pai, B.C., "Influence of Boron Addition on the Grain Refinement and Mechanical Properties of AZ91 Mg Alloy," *Materials Science and Engineering A,* Vol. 525, pp. 207-210 (2009).

64. Suresh, M., Srinivasan, A., Pillai, U.T.S., Pai, B.C., "The Effect of Charcoal Addition on the Grain Refinement and Ageing Response of Magnesium Alloy AZ91,"*Material Science and Engineering A,* Vol. 528, pp. 8573-8578 (2011).

65. Tammura, Y., Haitani, T., Yano, E., Motegi, T., Kono, N., Sato, E., "Grain Refinement of High-Purity Mg-Al Alloy Ingots and Influences of Minor Amounts of Iron and Manganese on Cast Grain Size," *Materials Transactions,* Vol. 43, N0. 11, 2784-2788 (2002).

66. Vinotha, D., Raghukandan, K., Pillai, U.T.S., Pai, B.C., "Grain Refining Mechanisms in Magnesium Alloys-An Overview," *Transactions of the Indian Institute of Metals,* Vol. 62, Issue 6, pp. 521-532 (2009).

67. Wang, Y., Wang, Q., Wu, G., Zhu, Y., Ding, W., "Hot Tearing Susceptibility of Mg-9Al-xZn Alloy," *Material Letters,* Vol. 57, pp. 929-934 (2002).

68. Xu-liang, M., Xiang, W., Xin-lin, L., Lei, Y., "Effect of Al5Ti1B Master Alloy on Microstructures and Properties of AZ61 Alloys," *Trans. Nonferrous Met. Soc.*, Vol. 20, pp. 397-401 (2010).

69. Yang, M., Pan, F., Cheng, R., Tang, A., "Comparation about Efficiency of Al-10Sr and Mg-10Sr Master Alloys to Grain Refinement of AZ31 Magnesium Alloys," *Journal of Materials Science,* Vol. 42, pp. 10074-10079 (2007).

70. Yano, E., Tamura, Y., Motegi, T., Sato, E., "Effect of Carbon Powder on Grain Refinement of an AZ91 Magnesium Alloy," *Materials Transactions,* Vol. 44, No. 1, pp. 107-110 (2003).

71. Zeng, X., Wang, Y. Ding, W., Luo, A.A., Sachdev, A.K., "Effect of Strontium on the Microstructure, Mechanical Properties and Fracture Behavior of AZ31 Magnesium Alloys," *Metallurgical and Materials Transactions A,* Vol. 37A, pp. 1333-1341 (2006).

72. Zhang, M.X., Kelly, P.M., Qian, M., Taylor, J.A., "Crystallography of Grain Refinement in Mg-Al Based Alloys," *Acta Materialia,* Vol. 53, pp. 3261-3270 (2005).

73. Zhao, Z., Chen, Q., Wang, Y., Shu, D., "Microstructure and Mechanical Properties of AZ91D Alloy with Y Addition," *Material Science and Engineering A, V*ol. 515, pp. 152-161 (2009).